Spring 4-30-2018

The Stability and Control of Stochastically Switching Dynamical Systems

Russell C. Jeter
Georgia State University

THE STABILITY AND CONTROL OF STOCHASTICALLY SWITCHING DYNAMICAL SYSTEMS

by

RUSSELL CLARKE JETER

Under the Direction of Dr. Igor Belykh

ABSTRACT

Inherent randomness and unpredictability is an underlying property in most realistic phenomena. In this work, we present a new framework for introducing stochasticity into dynamical systems via intermittently switching between deterministic regimes. Extending the work by Belykh, Belykh, and Hasler, we provide analytical insight into how randomly switching network topologies behave with respect to their averaged, static counterparts (obtained by replacing the stochastic variables with their expectation) when switching is fast.

Beyond fast switching, we uncover a highly nontrivial phenomenon by which a network can switch between two asynchronous regimes and synchronize against all odds. Then, we establish rigorous theory for this framework in discrete-time systems for arbitrary switching periods (not limited to switching at each time step). Using stability and ergodic theories, we are able to provide analytical criteria for the stability of synchronization for two coupled maps and the ability of a single map to control an arbitrary network of maps. This work not only presents new phenomena in stochastically switching dynamical systems, but also provides the *first* rigorous analysis of switching dynamical systems with an arbitrary switching period.

INDEX WORDS: Stochastically Switching Dynamical Systems, Synchronization, Stability, Control, Complex Networks, Lyapunov Exponents, Stochasticity

THE STABILITY AND CONTROL OF STOCHASTICALLY SWITCHING DYNAMICAL SYSTEMS

by

RUSSELL CLARKE JETER

A Dissertation Submitted in Partial Fulfillment of the Requirements for the Degree of

Doctor of Philosophy

in the College of Arts and Sciences

Georgia State University

2018

THE STABILITY AND CONTROL OF STOCHASTICALLY SWITCHING DYNAMICAL SYSTEMS

by

RUSSELL JETER

Committee Chair: Igor Belykh

Committee: Vladimir Bondarenko

Yaroslav Molkov

Alexandra Smirnova

Electronic Version Approved:

Office of Graduate Studies

College of Arts and Sciences

Georgia State University

May 2018

DEDICATION

This dissertation is dedicated to Leeanna Jeter and the memory of Altha "Ann" Klepper, because even mathematicians need cheerleaders.

ACKNOWLEDGEMENTS

First, I would like to thank my advisor, Igor Belykh. You provided me the opportunity and direction to whatever research whims I had. You taught me what is required to be a well-rounded academic, and prepared me for professional success, regardless of what path I find myself on. You once assured me that I would never have to work at the car wash again, and I think I can finally say with confidence that you have made sure that promise will ring true.

Next, I would like to thank the two academics that were nearly co-advisors to me alongside Igor: Maurizio Porfiri and Draga Vidakovic. Maurizio, I admire your infectious drive and determination; they motivate me to constantly push forward. Draga, your kind and attentive ear was always welcome and refreshing when I needed professional direction.

Of course, I am severely indebted to the other professional contacts that helped me along this journey. My thesis committee: Vladimir Bondarenko, Yaroslav Molkov, and Alexandra Smirnova. Thank you all for your feedback, time, and effort during the final stages of my PhD. Thank you to administrative staff in the Mathematics Department at GSU: Sandra Ahuama-Jonas, Earnestine Collier-Jones, and Beth Conner. Thank you all for guiding me through the bureaucratic nonsense required to get anything done at a university. Thank you to the members of the Belykh lab: Douglas Carter Jr., Kevin Daley, Kelley Smith, Reimbay Reimbayev, and Barrett Brister. Thank you for providing a nurturing mathematical learning community that was never short on laughter.

While it's my name on the front page of this dissertation, literally none of this would have been possible without the love, support, patience, and understanding of my friends and family. You have all done so much for me, I could fill many pages rambling about all of you. I will try to control myself.

Kelvin Rozier, you saw potential in me that I did not even see myself. You took it upon yourself to push me to see that potential, and at the same time keep me humble. Brian Jeter, you always pull it together and follow through when I need you most. I am happy to not

only call you “brother,” but “friend.” Faith Chamberlain, you have been my spiritual guide. You have helped me grow into a more open, understanding, and loving person. Jonathan Spencer, you have nurtured my aggressive need to learn new things and push myself. You serve as a constant reminder of how unimpressive and insignificant I am. Aubrey Kemp, your positivity and optimism are infectious. Your encouragement and dependability have been invaluable. Darryl Chamberlain, you are too many things to me to concisely summarize in this small space. Your friendship speaks volumes to the profound transformative power of a single act of kindness. Brenda, Raven, and Rosie Calderon, you constantly remind me of the quiet power of gentleness, sincerity, kindness, and a dash of sass. You inspire and challenge me to be better in every facet of my life. Les quiero muchisimo.

Lastly, Leeanna Jeter, your unwavering support kept me going during the lowest points in my journey. You are my rock. You’ve given so much in your life to provide me with this opportunity. I hope that I turned it into something that you are proud of.

This work was supported by the National Science Foundation under Grant DMS-1009744US and the Army Research Office under Grant No. W911NF-15-1-0267.

IMPACT

The results contained in this thesis have been published in five journal articles: [79, 80, 14, 77, 61], one refereed conference proceedings: [78], and two articles under review: [121, 81]. Additionally, these doctoral studies resulted in the following journal articles that are not *directly* related to stochastically switching dynamical systems, but concentrate on switching dynamical models of human gait and pedestrian bridge interactions [20, 17] as well as synchronization in multilayer networks [15].

TABLE OF CONTENTS

LIST OF TABLES

LIST OF FIGURES

CHAPTER 1

INTRODUCTION

Anything that changes in time can be represented mathematically by a *Dynamical System*, from the population size of a bacterial culture [26], to the spread of HIV in the bloodstream [111], to even romantic feelings in a relationship [133]. Attempting to model the change of something (and the phenomena underlying that change) not only satisfies the basic human desire to describe the world around us, but also carries a significant amount of scientific worth. Mathematical models informed by scientific understanding can, in turn, give insight back to the scientists, because models provide a quick, cheap test bed for performing initial experiments. For example in [137] and [138], the authors present a mathematical model for accurately describing the mouse ventricular myocyte (heart cell), which they are able to use to ascertain the biochemical and electrophysical effects of various drugs. Because of this interplay between mathematicians and traditional lab scientists, it is critical to develop tools for creating and understanding dynamical systems in general. In this work, we present a new framework for dynamical systems that switch randomly in time, then prove and describe phenomena that are natural consequences of this new framework.

1.1 Dynamical Systems

Readers familiar with dynamical systems theory can skip ahead to Section 1.2 or even 1.3. Dynamical systems are divided into two categories, discrete- and continuous-time dynamical systems, based on how they treat time. Discrete-time dynamical systems, called *maps*, are characterized by countable, iterated steps. For example, if you were to use a map to describe how a rabbit population changes in time, you might only consider the change across generations, and not how the population changes at every physical instance of time.

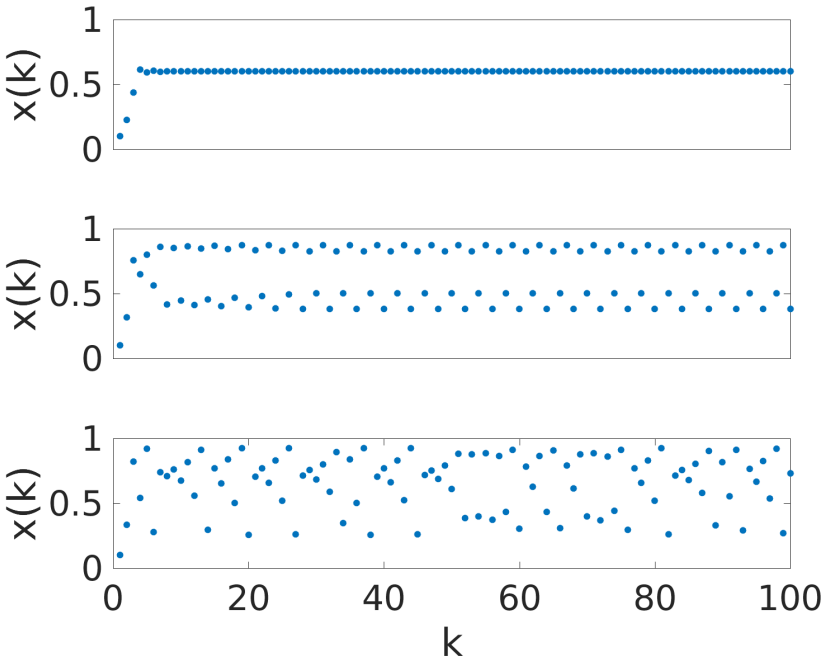

Figure 1.1 The behavior of the Logistic map for different values of the growth rate r. The dynamics are: constant ($r = 2.5$, top plot), periodic ($r = 3.5$, middle plot), and chaotic ($r = 3.7$, bottom plot).

Mathematically, a map is typically described by a recurrence relationship of the form:

$$x(k+1) = f(x(k)), \tag{1.1}$$

where k is the current time step (or iteration, or generation), $x(k)$ is the current state of the system, and f is a function that describes how the state changes from generation to generation. In words, (1.1) says that the state, x, at the next instance of time, $k+1$, is given by some function, f, of the current state, $x(k)$.

A common map, that exhibits the basic types of behavior for discrete-time dynamical systems is the Logistic map, which is given by

$$x(k+1) = rx(k)\left(1 - x(k)\right), \tag{1.2}$$

where r is the growth rate of a population. The Logistic map is a rudimentary model for

describing the growth of a population that reaches some carrying capacity, and then remains constant. However, depending on the value of growth rate r, the map can behave drastically differently. There are many types of behavior that maps can yield. These dynamics can be unconstrained growth (where $x(k) \to \infty$), fixed points (where $x(k+1) = x(k) = x^*$ after some amount of time), periodic orbits (where the trajectory repeats with some period m, for example $x(1) = x(4) = x(7) = \cdots$), and chaotic orbits (where $x(k)$ never repeats and its long-term state can not be predicted). These dynamics are summarized with respect to the Logistic map in Fig. 1.1.

Whereas, continuous-time dynamical systems, called *flows* (which are expressed as Ordinary Differential Equations, shortened ODEs), are characterized by a fluid, instantaneous time variable. For example, if you were to describe a rabbit population using a flow, you would be concerned with how the population changes at *every* instance of time. With how rabbit life cycles are, this may be a more appropriate method for modeling their population dynamics. Mathematically, a flow can be described by

$$\frac{dx}{dt} = F(x(t)), \tag{1.3}$$

where $x(t)$ is the state of the system at time t[a], $\frac{dx}{dt}$[b] is the *rate of change* of $x(t)$ with respect to time, and F is a function describing that rate of change. In words, (1.3) describes how some quantity *changes in time*, based on its state at a given instant of time.

The same types of behavior we have seen in discrete-time dynamical systems naturally extend to continuous-time systems. Possible dynamics for flows include: constant fixed points ($x(t) = c$ after some initial time), periodic limit cycles ($x(t) = x(t+T) = x(t+2T) = \cdots$ for some period T), chaotic orbits (where $x(t)$ never repeats and behavior is unpredictable beyond nearby instances of time), and many more. Some of the possible dynamical regimes are summarized in Fig. 1.2. With this preliminary understanding of dynamical systems

[a] In general, dynamical systems are described with respect to *some* independent variable, which is not limited to being time. However, this is the most natural way to describe them.

[b] Depending on the context, $\frac{dx}{dt}$ is often stylized as $\dot{x}$ where the overset dot indicates differentiation with respect to time.

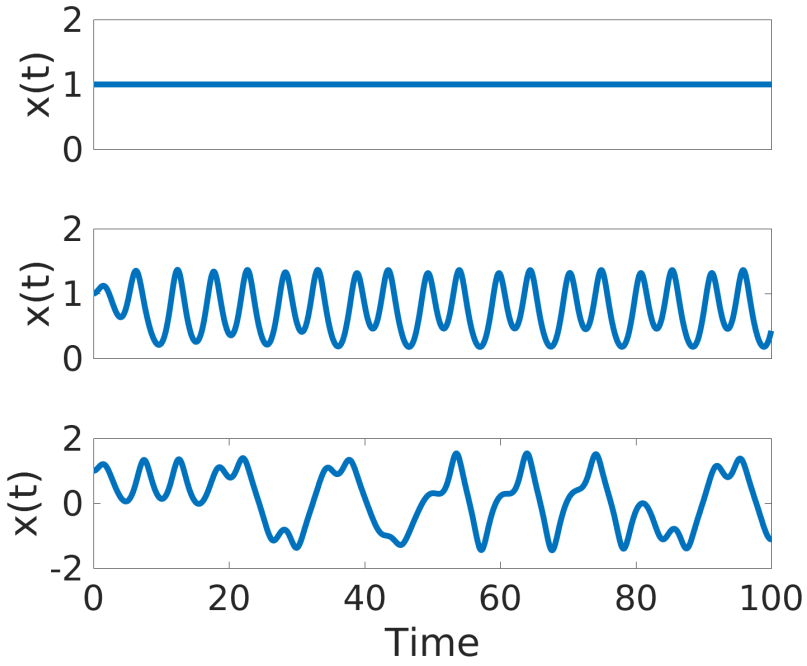

Figure 1.2 Illustration of different types of dynamical behavior in flows using the forced Duffing equation [83]. Flow dynamics include fixed points (top), limit cycles (middle), and chaotic orbits (bottom).

in place, we briefly focus our attention to a subclass of dynamical systems called *Complex Networks*. For a more detailed treatment of dynamical systems, see [148] or [106].

1.2 The Paradigm of Complex Networks

While some chapters of this work focus on general dynamical systems, to understand the original motivations in the literature, a basic understanding of complex networks is necessary.

Much like anything that changes in time can be described as a dynamical system, anything that has some inherent, underlying network structure can be described as a complex network. Networks are pervasive in science and engineering: from neuronal networks to power grids; from social networks to schools of fish; from the telephone network to artificial neural networks. Complex networks do not always have this immediately obvious network structure. Even a footbridge can be viewed as a network consisting of a girder node attached to pedestrian nodes by means of their impact on the motion of each other (for example, see

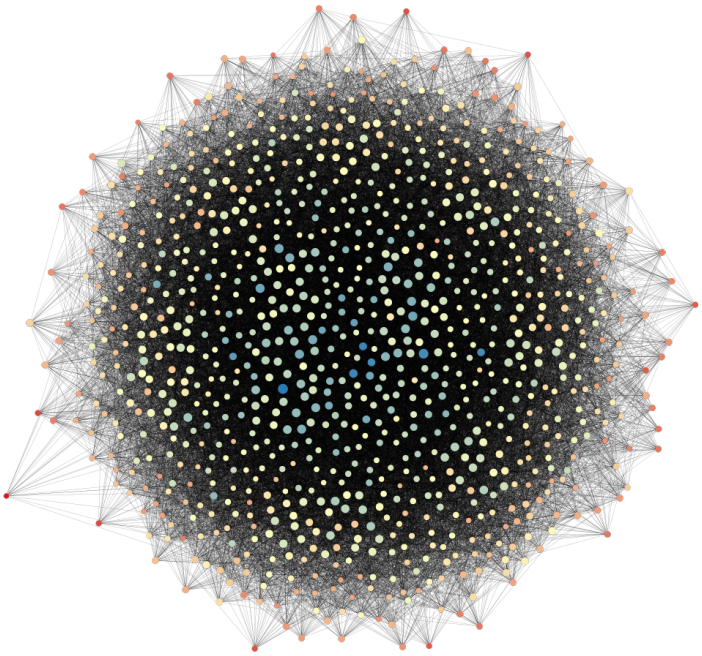

Figure 1.3 Typical visualization of a complex network. In this network, there are $N = 200$ nodes, and the probability of there being an edge between two nodes is $p = 0.05$.

[20] and [17]). More formally, a complex network network is defined as a graph $\mathcal{G} = (\mathcal{V}, \mathcal{E})$ which consists of a set of vertices (nodes), $\mathcal{V}$, and edges, $\mathcal{E}$, connecting those vertices. Figure 1.3 provides a visual representation of an arbitrary complex network.

1.2.1 Network Structure and Node Dynamics

A graph $\mathcal{G}$ can be described in many different ways mathematically, such as the tuple $(\mathcal{V}, \mathcal{E})$, an adjacency list, or a Laplacian or connectivity matrix. The two network descriptions that are particularly useful are the Laplacian matrix, and the adjacency list. An adjacency list is a list with three columns that indicate the source of an edge, the target of an edge, and the edge weight. Often this is simplified to two columns, ignoring the edge weight if the edges all have uniform weight. The adjacency list for the network in Fig. 1.4 is given in Table 1.1. Adjacency lists are a convenient way to describe networks, because they describe the network completely with as little information as possible. The other way we will describe

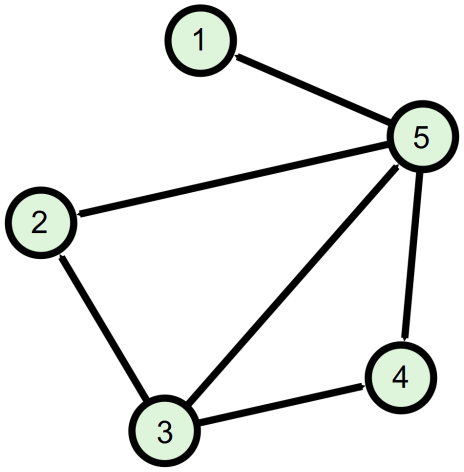

Figure 1.4 Simple network for describing different types of network representation.

is called a Laplacian matrix, which is an $N \times N$ matrix (where N is the number of vertices in the network) where the diagonal gives the out-degree (the number of edges for which this edge is the source), and the ij-th entry of the matrix is 1 if there is an edge from vertex i to j, and 0 otherwise. The Laplacian matrix, L^{c} for the network in Fig 1.4 is

$$L = \begin{bmatrix} -1 & 0 & 0 & 0 & 1 \\ 0 & -2 & 1 & 0 & 1 \\ 0 & 1 & -3 & 1 & 1 \\ 0 & 0 & 1 & -2 & 1 \\ 1 & 1 & 1 & 1 & -4 \end{bmatrix} \tag{1.4}$$

Beyond this graph $\mathcal{G}$ that describes the structure (topology) of the network, there are also dynamics that take place on each of the nodes. This means that each node describes some quantity (or quantities) that changes (change) in time (such as the human population in a specific area), and independent of influence from other nodes in the network (if the city is completely isolated) the dynamics change according to some rule, as in (1.1) or (1.3).

[c]For undirected networks (which are described a little later in the text), the Laplacian matrix is a real, symmetric matrix. This means that its eigenvalues are necessarily real, and it is diagonalizable.

Source	Target
1	5
2	3
2	5
3	4
3	5
4	5

Table 1.1 Adjacency list for the network in Fig. 1.4. Because the network is undirected, the sources and targets are interchangable.

With this understanding of the dynamics of the isolated node, now we must incorporate node-to-node interactions in the dynamical system. There are numerous ways to represent this "coupling" between nodes dynamically, including diffusive coupling, mean-field coupling, adaptive coupling, etc. In this work, we focus on diffusive coupling, which is simply adding the difference between the state of node i and node j (that is, $x_i - x_j$) multiplied by some "coupling strength," ε. More formally, a network can be described by the equation

$$\dot{x}_i = F(x_i(t)) + \varepsilon \sum_{j=1}^{N} l_{ij}(x_j - x_i), \quad \text{for } i = 1, 2, \ldots, N, \tag{1.5}$$

where $x_i(t)$ gives the state of node i at time t, $F(x_i(t))$ governs the evolution of node i when it is isolated from the network, and l_{ij} is the ij-th entry of the Laplacian matrix that describes the network topology. While (1.5) describes a network in which each node only has one state variable (an oversimplification in most cases), this equation can easily be extended to M state variables for each node (resulting in a $M \cdot N$-dimensional dynamical system). It is important to notice that the node dynamics as well as the edge interaction can be described by discrete- or continuous-time dynamical systems, and the impact of the difference between continuous and discrete model representations will be discussed at length in this work.

1.2.2 Network Properties and Types of Networks

While individual node dynamics can be complex themselves, there are also numerous ways that the underlying graph topology can affect the behavior of the network dynamically,

so it is worth studying important properties of the structure that describe the network. In this section, we review network properties (in terms of the structure, specifically).

As noted before, a network can be described by a graph, $\mathcal{G}$ that consists of a set of vertices (nodes), $\mathcal{V}$, and a set of edges, $\mathcal{E}$ that connect those vertices. Edges are represented by a tuple $e = (\text{Source}, \text{Target}, \text{Weight})$. Consider a network describing a social network that information flows through. The *source* is the node sending a signal to a specific *target*, and the edge *weight* is the strength of this signal. Edges (and subsequently networks) can be directed or undirected, meaning that information flows either unidirectionally from source to target, or bidirectionally from source to target and target to source. While there are networks with *self-loops*, in which a single node is both the source and the target, we limit our attention to networks without self-loops unless it is specifically stated otherwise.

The *degree* of a node is the number of incoming edges that either target that node (called the *in-degree*, d_{in}), or the number of edges for which that node is the source (called the *out-degree*, d_{out}). If the network is undirected, the in-degree and out-degree are equivalent, and usually referred to as the node degree d. The *average degree*, d_{avg}, of a network can be computed by averaging all of the d_{in} and d_{out} for a directed network, or simply dividing the number of edges by the number of nodes in an undirected network. The *density*, ρ of a network is a measure of how connected the graph is, computed by comparing the number of edges (denoted by $|\mathcal{E}|$) to the total possible number of edges in the network, $\binom{N}{2} = \frac{N(N-1)}{2}$. More compactly,

$$\rho = \frac{2|\mathcal{E}|}{N\,(N-1)}.$$

If $\rho \to 0$, the network is said to be *sparse* and if $\rho \to 1$, the network is *dense*.

A *path* is a route from one vertex in the graph to another. For example, in Fig. 1.4, $1 \to 5 \to 4 \to 3$ represents a path from vertex 1 to vertex 3 of *length* 3[d]. The *diameter* of a graph is the greatest distance between two nodes in the graph. If there is not a path from one node in the network to another node in the network, the graph consists of more than one

[d]That is, the path traverses three edges.

component, or self-contained subgraph, from which there are no paths between components of the graph.

1.2.3 Collective Behavior

How do these different network properties affect how the nodes *behave dynamically*? This question is actually the central question of study when studying dynamical complex networks. There are a few types of collective behavior[e] that a network can exhibit: incoherence (when the nodes behave seemlingly without interacting at all), complete synchronization (when all of the nodes act in unison), cluster synchronization (when the network is partitioned into groups of nodes that act as a cohesive unit, while between groups there is incoherence), and "chimera states" (where there is one group that is competely synchronized, and one group that is incoherent). These types of collective behavior are hardly a mathematical artifact: AC power generators *must be* running at the same frequency (synchronized to) the grid to supply power [25]. Groups of fireflies can synchronize their pulse frequency to an external driver (like a handheld flashlight), collectively blinking along with the driver ("pacemaker") [99]. These are just two examples of a ubiquitous tendency in nature for systems to synchronize.

Because of how prevalent synchronization is, it has been the subject of numerous studies in the literature, especially in regard to finding necessary and sufficient conditions for a network to synchronize. Two seminal works on network synchronization are [109] and [22], in which the authors reduce studying synchronization of a network of N nodes to studying synchronization in a network of two nodes. In [109], Pecora and Carroll show the relationship between the local stability of the synchronization solution[f], the eigenvalues of the Laplacian matrix, and the function describing the individual node dynamics. Whereas, in [22], Belykh, Belykh, and Hasler are able to place sufficient conditions on the coupling strength that ensure

[e]Collective behavior describes how all of the nodes in the network behave in reference to the other nodes in the network, not their individual dynamical behavior in time.

[f]That is, whether or not the network converges to synchronization when starting from an *almost* synchronous state.

the *global stability* of the synchronization solution. These conditions explicitly depend on the individual node dynamics as well as the collection of paths between nodes in the network. The conditions in [22] are particularly significant, because they even apply to networks that evolve in time (Evolving Dynamical Networks), which are discussed later in this chapter and are a topic of study in this work.

1.3 Network Control

As collective behaviors like synchronization are so wide-spread and important, it is reasonable to understand why there has been a significant amount of attention devoted to *network control*. Network Control is the process of influencing a subset of the network to drive it towards a desired state. For example, consider a robotically controlled fish that seeks to form a school with a group of real fish (complete synchronization of the shoal of fish), and in turn, lead those fish away from harm. Naturally, this desire to control dynamical systems has been the subject of a significant volume of literature.

One of the most significant works on control in recent memory was [107], in which the authors proposed a method in which one can strategically vary the system parameters to drive a chaotic orbit to a nearby periodic orbit embedded in the chaotic attractor. This work presented the first method for which one could consistently tame a chaotic trajectory, and subsequently spawned a significant number of experimental and theoretical studies, see for example [136, 48, 126]. While significant (and useful) in its own right, the glaring limitation of this type of control is that it is limited to a single dynamical system, and is not meant to specifically handle driving a network towards some dynamical regime, or towards network synchronization.

Network control was first studied in discrete-time dynamical systems with regular structures. In [59], Gang and Zhilin introduce the notion of "pinning control," which involves targeting a subset of the nodes in a network (pinning sites) with a feedback mechanism. Using this feedback mechanism on a few nodes, they were able to steer a network of chaotic maps towards both constant and periodic dynamics. This problem was later extended to

require fewer pinning sites and was then treated more rigorously in [65].

The next (and probably most significant in our context) major advancement in control was by Sorrentino, et. al. in [143], in which the authors consider the problem of driving a network of N nodes that are pinned at n sites towards some desired trajectory $s(t)$. This amounts to synchronizing the network to some predetermined dynamical regime, be it a chaotic attractor, periodic orbit, or fixed point. This method extends the Master Stability Function [109] approach, which gives conditions on the stability of synchronization in a network without control, to the controlled system by accounting for the pinned sites in the network Laplacian and increasing the dimensionality of the linearized system. Their approach largely reduces the understanding of pinning control to computing the eigenratio of the smallest (most negative) eigenvalue, μ_{N+1} (in their case), and the largest non-zero eigenvalue, μ_2. This work sparked a significant amount of literature directed toward finding even more optimal (often dynamic) control strategies (for example [151]), or used this work to explore the role of a driver in directed networks (for example [95]). For a more in-depth overview of the control literature, see the review paper [152] and the references therein.

Now that we have established the significance of understanding how to control dynamical systems, and its utility in practice, we are ready to motivate the class of dynamical systems that this body of work focuses on: stochastically switching dynamical systems. Before explicitly discussing stochastically switching dynamical systems, we will give some background on what caused their re-emergence in the literature (switching discrete-time systems, called "jump linear systems" have received attention *intermittently* for decades).

1.4 Evolving Dynamical Networks

While there are some examples of networks that are fixed, static things (such as mechanical structures), often networks are dynamic and evolve in time. Examples of this type are much more numerous, for example face-to-face human interactions or neuronal networks

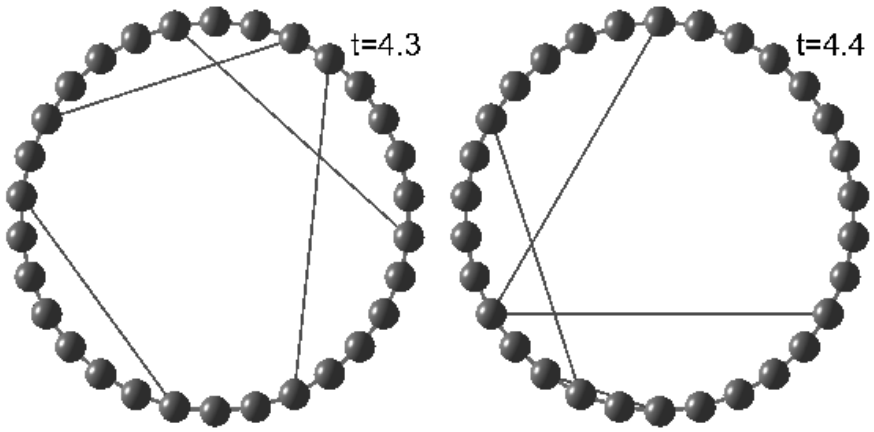

Figure 1.5 Schematic of the "Blinking" Network Model from [19] at two different time instances.

which are well-documented to change and adapt[g] in response to brain function [127] or even chronic pain [57]. Indeed, it is likely easier to think of examples of networks that inherently evolve randomly or according to some fixed rule than static networks. Technological and social networks are in a constant state of reinvention and adaptation. Within the complex networks framework that we have introduced, evolving networks were first introduced as intermittent or adaptive controllers[h], whose goal was to control the network like in the previous section, but only periodically driving the network [146, 86], or changing pinning sites [151]. While they had appeared in the literature for most of a decade by the time it was published, the definition of an Evolving Dynamical Network (EDN) was first formalized in [62] by Gorochowski, et. al in 2012. Much like a network is defined, an evolving dynamical network consists of a vertex set, $\mathcal{V}$, a possible edge set, $\mathcal{E} = \mathcal{V} \times \mathcal{V}$, and state spaces $\mathbf{V}$ and $\mathbf{E}$ where the dynamical states of the nodes and edges exist. In addition to these components of a dynamic graph, there is also a set I of inputs from the environment, and a set of evolu-

[g]Neuronal networks change through many means: the addition or removal of neurons and synapses, and even altering the weights along specific synapses.

[h]This is not entirely true. Both [142] and [46] utilize "Fluid Neural Networks" (FNNs) to represent a time-varying topology. Fluid neural networks describe mobile automatons on a grid, that activate based on their proximity to other automatons. Typically, fluid neural networks do not have complex dynamics on the nodes, though the networks can exhibit complex behavior. Their activation is similar to that of "neurons" in Artificial Neural Networks (ANNs), hence the name fluid neural network.

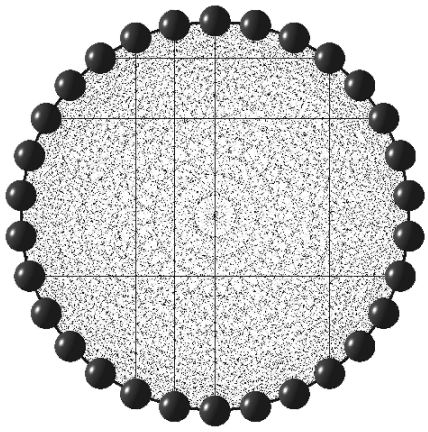

Figure 1.6 Schematic of the average of the "Blinking" Network Model from [19].

tionary plans τ that dictate the evolution of the network in time[i]. This formal mathematical framework certainly includes all of the networks we have mentioned, and will mention in this work, but is overly technical for understanding this material. More concisely, an evolving dynamical network is a complex network whose topology changes in time deterministically or according to a stochastic (random) rule.

Stepping back about a decade, the first examples of networks with evolving topologies[j] were developed concurrently, yet independently in [19] and [140]. In [19], Belykh, et al., present a $2K$-Nearest Neighbor Network[k] that has shortcuts across the network that turn on and off randomly at a fixed period τ[l]. They called this model a "Blinking Network Model," and an example is shown in Fig. 1.5. Each time the shortcuts reconfigure, the network describes a different *small-world* network[m] (described in [154] and [102]). The authors use their recently developed connection graph stability method [22] and averaging theory to

[i]This evolution can be through either a deterministic or stochastic rule or set of rules, depending on the context.

[j]These works were presented outside of the control framework, and the evolving topologies were not a control strategy, but a more realistic paradigm for approaching modeling real phenomena.

[k]A $2K$-Nearest Neighbor network is a network that is laid out on a circle, and each node is connected to its K neighbors on its left and K neighbors on its right.

[l]This τ is not to be confused with the set of evolutionary plans that describe a general Evolving Dynamical Network

[m]A small-world network is a regular graph (like a $2K$-Nearest Neighbor graph) with additional long-range connections that link distant nodes.

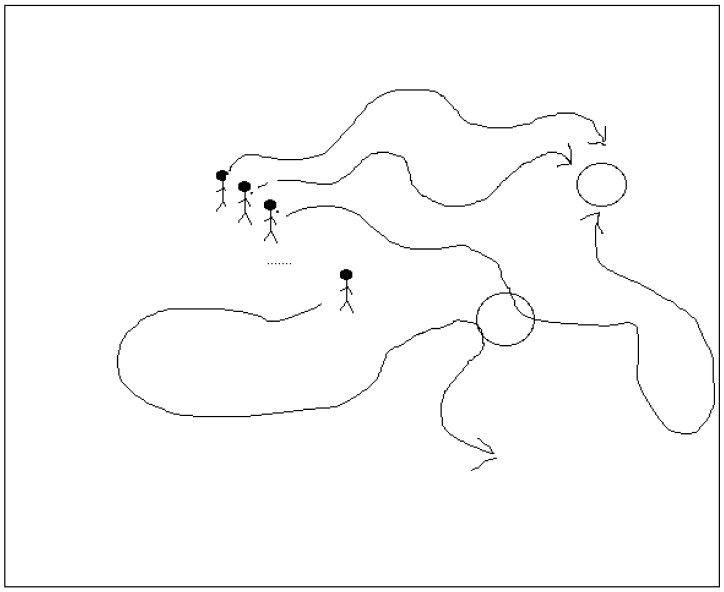

Figure 1.7 Moving neighborhood network from [140]. People can only spread diseases when within a radius r (depicted by the circles) of one another.

prove that the addition of these random shortcuts dramatically decreases synchronization thresholds (the coupling strength required for synchronization) compared to a $2K$-Nearest Neighbor graph without these random shortcuts. In fact, they find that if switching is fast relative to the timescale of the node dynamics, that the synchronization thresholds match those of a complete graph (see Fig. 1.6) with edge weights given by the expectation of the randomly switching coupling variables. This work is especially important, because it is the first work in continuous-time that describes stochastically switching dynamical systems as an "on-off" blinking process. Additionally, these are the type of dynamical systems we study in this work.

The other work that helped establish evolving dynamical networks that we will discuss is [140], which had a similar evolving network. Motivated by the idea of modeling the spread of infectious diseases by means of social interactions, the authors of [140] present what they call a "Moving Neighborhood Network" (MN), which is conceptually shown in Fig. 1.7. Their moving neighborhood network has both dynamics on the nodes, and 2D dynamics for the position of the nodes in space. If two nodes are within some distance r of each other, there

is an edge connecting them in the network topography. Using a network in which each node moves according to an identical chaotic Duffing oscillator with different initial conditions, the authors are able to prove the local stablity of synchronization using the Master Stability Function approach from [109]. Their results rely heavily on the fact that chaotic Duffing oscillators are ergodic (fill the state space), and therefore, the positions can be averaged over space, and not over time. This allows the connections in the network to be treated as weak, averaged connections, instead of as random, intermittent connections.

Both of these works reach a similar result, but through different means. They both find a way to replace the evolving dynamical network with a static, averaged network, that can be analyzed using traditional methods for proving the local and global stability of diffusively coupled complex networks. That is not to say these works were not significant. They represent a change in paradigm from the complex networks community, and since then, evolving dynamical networks have been subject of a substantial volume of work (see, for example, [63, 45, 146, 76, 19, 68, 140, 96, 97, 100, 38, 158, 125, 124, 122, 118, 115, 114, 63, 45, 157, 44, 42, 144, 141, 69, 70, 14, 49, 62, 1, 58, 43]).

1.5 Stochastically Switching Dynamical Systems

While evolving dynamical networks come in many forms, such as networks whose topologies evolve according to some fixed or dynamic predetermined rule, we will focus on networks that either randomly reconfigure themselves and/or the dynamics on the node randomly switch between states. While the original “blinking" model [19] was limited to switching edges in a network, and inspired the work presented here, we will define our stochastically switching system more generally.

1.5.1 Statement of the General Problem

Specifically, the general form for a stochastically switching continuous-time dynamical system (flow) is:

$$\frac{d\mathbf{x}}{dt} = \mathbf{F}(\mathbf{x}(t), \mathbf{s}(t)), \tag{1.6}$$

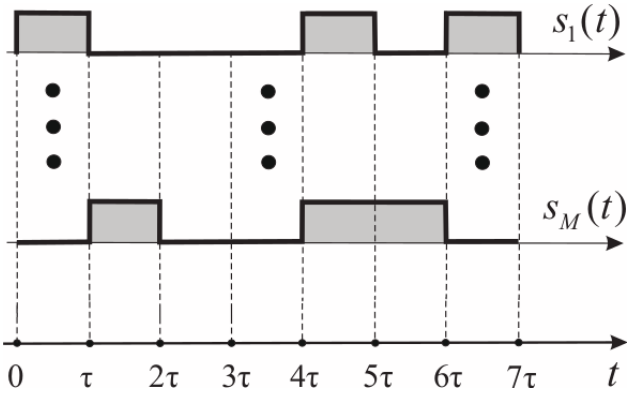

Figure 1.8 Illustration of the stochastic switching process. The time axis is divided into intervals of length τ. For each interval, $s_k(t) = 1$ with probability p_k and $s_k(t) = 0$ with probability $1 - p_k$.

where $\mathbf{x}(t) \in \mathbb{R}^N$ is the state of the system at time t, $\mathbf{F}$ gives the rate at which the state vector $\mathbf{x}(t)$ changes (dependent on the current state and the switching process), and $\mathbf{s}(t) \in \{0,1\}^M$ is a constant binary vector $\mathbf{s}^k = [s_1^k, s_2^k, \ldots, s_M^k]$ for the time interval $t \in [(k-1)\tau, k\tau)$. Put simply, we discretize the time axis into intervals of length τ time units. For the interval $[(k-1)\tau, k\tau)$ the i-th entry in the binary vector $\mathbf{s}^k$ is 1 with probability p_i, and 0 with probability $1 - p_i$. That is, after every τ time, we flip a weighted coin; if the coin is heads (with probability p), $s_i(t) = 1$, otherwise $s_i(t) = 0$, and remains constant until the next switching time. The switching vector $\mathbf{s}^k$ can be thought of as a random sequence generated by the switching process, and the events in $\mathbf{s}_i$ are independent and identically distributed (i.i.d). The switching process is illustrated in Fig. 1.8. This means that each successive event does not depend on preceeding events (a 0 in the i-th entry has no effect on the value of the $(i+1)$-th entry). When time is instead iterated in discrete units, the general form of the switching system (map) is given by:

$$\mathbf{x}(k+1) = \mathbf{F}(\mathbf{x}(k), \mathbf{s}(k)), \tag{1.7}$$

where $\mathbf{x}(k) \in \mathbb{R}^N$ gives the state of the system at iteration k, $\mathbf{F}$ updates the state vector based on its value at the current iteration, $\mathbf{x}(k)$ and the switching process, and $\mathbf{s}(k) \in \{0,1\}^M$ is again a binary vector. However, in this setting, the stochastic variables are re-switched

after m iterations, such that $\mathbf{s}((m-1)k) = \mathbf{s}((m-1)k+1) = \cdots = \mathbf{s}(mk-2) = \mathbf{s}(mk-1)$. Again, $s_i(k)$ (that is, the i-th entry of vector $\mathbf{s}(k)$ at time step k) is 1 with probability p_i, and 0 with probability $1-p_i$ and the switching process is i.i.d.

The nature of the switching process, while analogous in both of our settings, is quite different from other implementations of stochasticity in dynamical systems in the literature. Our blinking systems switch between a finite set of deterministic regimes, and are effectively deterministic at each time step, but randomly switch to a different regime after some predetermined length of time. This is markedly different from examples that have stochastic variables chosen from a distribution and continuous switching times. For example, the most common way to add randomness to a system is to introduce a stochastic variable $\xi(t)$ which follows either a uniform distribution with $\xi \in [0,1]$ or normal distribution with $\xi \sim N(0,1)$. Typically, this method of incorporating stochasticity is called "noise." Driving noise and is capable of inducing various dynamical phenomena, including stochastic synchronization [2, 6, 5] and stochastic resonance [155, 8, 7], and is so common that there is an entire class of differential equations (Stochastic Differential Equations) named for them[n]. Another, different, type of switching process was detailed in [91] in which the switching is a Markov process with a finite number of states, and switching rate is not fixed. In the discrete-time setting, typically stochasticity is implemented by switching at each time-step between random matrices pulled from a finite (or infinite) set of state matrices. Traditionally, the literature has focused on linear maps, and the term "Linear Jump Systems" has been coined for this setting [41].

Systems (1.6) and (1.7) provide the general mathematical description for switching dynamical systems. Although dynamical network models are covered by these general equations, it will improve readability to describe the general form for continuous- and discrete-time switching networks (as they appear throughout this dissertation). Mathematically, a

[n]See [104] and the references therein for a thorough introduction to Stochastic Differential Equations.

blinking network of ODEs is given by:

$$\frac{d\mathbf{x}}{dt} = \mathbf{F}(\mathbf{x}(t), \mathbf{s}(t)) + \mathbf{H}(\mathbf{x}, t) \tag{1.8}$$

which is the general form (1.6) with an additional term, $\mathbf{H}(\mathbf{x}, t)$ that is an arbitrary, potentially "blinking," vector-valued function that represents the manner in which the network topology affects each node. Typically, this $\mathbf{H}(\mathbf{x}, t)$ is simply diffusive coupling, and the equation for the dynamics reduce to:

$$\frac{d\mathbf{x}}{dt} = \mathbf{F}(\mathbf{x}(t), \mathbf{s}(t)) + \mathbf{L}(t) \otimes \mathbf{H}(\mathbf{x}), \tag{1.9}$$

where $\otimes$ is Kronocker matrix multiplication and $L(t)$ is the Laplacian matrix at time t. Unpacking this a little further, we assume that the network is composed of N nodes, and each node has n state equations. Vector $\mathbf{x}$ is organized $\mathbf{x} = [\mathbf{x}^1\mathbf{x}^2 \cdots \mathbf{x}^N]^T$ such that the state variables for node i are stacked on the state variables for node $i + 1$. $\mathbf{L}(t)$ gives the time-varying Laplacian matrix, and $\mathbf{H}(\mathbf{x})$ projects the coupling onto the appropriate state equations. For example, to describe a network of x-coupled Lorenz oscillators with a switching topology the equations for the i-th node would be:

$$\begin{aligned}
\dot{x}_i &= \sigma(y_i - x_i) + \sum_{j=1}^{N} l_{ij}(t)(x_j - x_i), \\
\dot{y}_i &= x_i(\rho - z_i) - y_i, \\
\dot{z}_i &= x_i y_i - \beta z_i.
\end{aligned}$$

The general form for a discrete-time blinking network is:

$$\mathbf{x}_i(k+1) = \mathbf{F}(\mathbf{x}_i(k), \mathbf{s}(k)) + \sum_{j=1}^{N} L(k)\mathbf{H}(\mathbf{x}_j(k)), \tag{1.10}$$

where $i = 1, 2, \ldots, N$, L is the Laplacian matrix for the network at time step k, and $\mathbf{H}$ is an arbitrary vector-valued function that defines the coupling between nodes.

While it may seem unnecessary to introduce these two general systems separately, the treatment of the time variable in either case is crucial to the analysis of the respective system. Mathematical tools for flows and maps are not the same, and even when they overlap, the implementation is not identical. For this reason, they must be treated as separate, though not entirely independent, cases.

With this in mind, we now review existing methods in blinking continuous- and discrete-time dynamical systems.

1.5.2 Existing Methods for Continuous-Time Dynamical Systems

In this section, we discuss the literature concerning the switching system in continuous time as defined in (1.6), and examine the existing methods for this type of switching system. The existing methods rely heavily on comparing the dynamics of the blinking system to that of the "averaged" system which is obtained by replacing the stochastic variables with their expectation. The averaged system for the general blinking model (1.6) is:

$$\frac{d\mathbf{x}}{dt} = \mathbf{\Phi}(\mathbf{x}(t)), \tag{1.11}$$

where $\mathbf{\Phi}(\mathbf{x}) = \mathbf{F}(\mathbf{x}(t), \mathrm{E}[\mathbf{s}(t)])$, and $\mathrm{E}[\mathbf{s}(t)]$ is the expectation (mean) of the stochastic vector $\mathbf{s}(t)$. In (1.11), the stochasticity has been removed, and replaced with a fixed, deterministic process. In a blinking network model, this means that the blinking network topology has been replaced with a static topology with weaker connections. In the seminal works on blinking dynamical systems [69] and [70] the authors sought to determine how and under what conditions the dynamics of the blinking systems relate to the dynamics of the averaged system. The authors extend and generalize the setting that they established in [19] to create a new class of continuous-time, stochastically switching dynamical systems (instead of the limited switching network that they originally presented). In general, they found that as $\tau \to 0$ (that is, the switching rate is infinitely fast), the dynamics of the blinking system follow those of the averaged system. However, their findings are more nuanced than that.

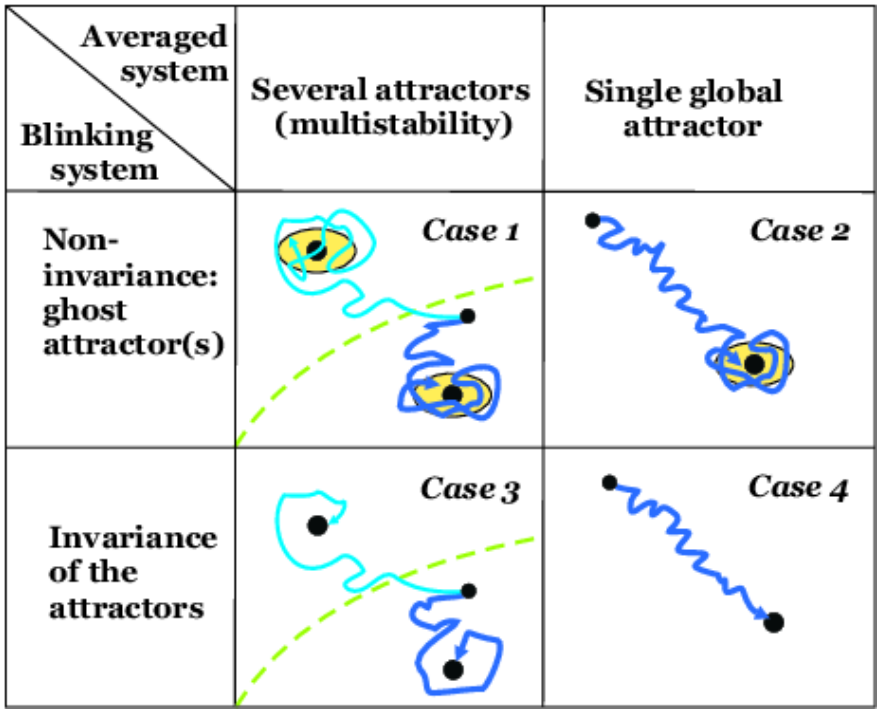

Figure 1.9 Four cases distinguishing the possible asymptotic behavior of a blinking system as shown in [70].

The work is divided into two parts: one focused on finite time properties [69] (what the authors could prove about switching dynamical systems near the initial time point) and one focused on the asymptotic properties [70] (what the authors could prove about the *eventual* behavior of switching dynamical systems). In finite time, they are able to place bounds on the switching period, τ, for which the stochastic system stays within some ε-neighborhood of the averaged system from some initial time ($t = 0$) to some final time ($t = T$). These bounds are obtained from Lipschitz constants, and are therefore conservative, but they depend explicitly on the parameters of the dynamical system. This means that it is clear *how* changes in the system parameters affect the requisite changes in the switching period (that is, how slow or fast the system needs to switch) for the stochastic system to stay near the averaged system.

When studying the asymptotic properties [70], the authors seek to understand the conditions under which the blinking system will converge to the attracting set of the averaged system (or near the attracting set if it does not exist in the blinking system). They isolate four distinct cases for switching dynamical systems, organized based on how restrictive the

class is. The cases are distinguished by the attracting sets in the different instances of the blinking system and the averaged system. There can be a single attractor (such as a globally stable fixed point) or multiple attractors (a stable fixed point and stable limit cycle separated by an unstable limit cycle), and this/these attractor/attractors can be invariant (present) in all of the instances of the switching system and averaged system or they can not be invariant. The cases are organized: Case I, multiple attractors in the averaged system that are not attractors in the blinking systems; Case II, a single global attractor in the averaged system that is not an attractor in the blinking systems; Case III , multiple attractors that are invariant between the switching and averaged systems; Case IV, a single global attractor that is invariant between the switching and averaged systems. These cases are summarized in Fig. 1.9. While each case poses different technical difficulties that lead to more or less conservative bounds, the overall message of the paper is that if switching is sufficiently fast, the long-term behavior of the blinking system is to converge to the same attractor as the averaged system (or to the neighborhood of the attractor of the averaged system if it is not invariant in the blinking systems).

1.5.3 Existing Methods for Discrete-Time Dynamical Systems

The study of switching discrete-time systems has primarily focused on two different approaches: switching linear systems ("Jump Linear Systems") and stochastically switching networks of maps (much like the switching networks in flows). We will review both of these approaches, as they both provide important pieces of foundation that we build on later in this work.

1.5.3.1 Jump Linear Systems Jump linear systems are both more specific and more general than our stochastically switching discrete time systems described by (1.7). In

[55], a jump linear system[o] is described by:

$$x(k+1) = A(\sigma(k))x(k), \tag{1.12}$$

where $\{\sigma_k\}$ is a finite-state Markov chain form process with transition matrix P, and the individual mode matrices $A(1), A(2), \ldots, A(N)$ are real, invertible $d \times d$ matrices (where d is the dimension of the state vector $x(k)$). This is more general than our setting, because the switching process is a Markov process, it is not assumed to be i.i.d. (though this i.i.d. assumption can be relaxed in our setting in a straightforward way). However, it is also more specific, because the system only switches between linear dynamical regimes, and switching occurs at every time step.

In [54] and [55] Fang and Loparo provide concise recipes for deducing the $\delta-$moment stability and sample path stability of jump linear systems, as well as the relationships between these types of stability. They study the stability of these systems using Lyapunov exponents. In general, a Lypaunov exponent gives a measure of the exponential convergence or divergence of nearby trajectories (that is, whether or not two initial conditions that are close by come together or separate with time). In discrete-time, this Lyapunov exponent is computed as

$$\lambda = \lim_{n\to\infty} \frac{1}{n} \sum_{i=0}^{n-1} \ln |f'(x(i))|. \tag{1.13}$$

For linear systems, like in (1.12), this reduces to

$$\lambda = \lim_{n\to\infty} \frac{1}{n} \sum_{i=0}^{n-1} \ln ||A(i)|| = \lim_{n\to\infty} \frac{1}{n} \ln || \prod_{i=0}^{n-1} A(i)||. \tag{1.14}$$

The authors concern themselves with two types of stability, *almost sure* stability, and δ-*moment* stability. We say that a stochastically evoloving discrete-time dynamical system is

[o]Indeed, jump linear systems have been extensively studied in the literature, and we can barely scratch the surface of this field. See [41] and the references therein for more on Jump Linear systems.

almost surely stable if

$$P(\lim_{k\to\infty} ||x(k)|| = 0) = 1, \tag{1.15}$$

where $||\cdot||$ is a suitible norm in $\mathbb{R}^N$ and P denotes a probability measure with respect to the σ-algebra induced by the switching process. In words, this means that for almost all initial conditions and stochastic sequences[p], the norm of the trajectory converges to 0. This is a convergence problem, hence almost sure stability can be reduced to computing the "top" or "sample path" Lyapunov exponent:

$$\lambda = \lim_{k\to\infty} \frac{1}{k} \ln ||A(\sigma(k-1)) \cdots A(\sigma(2))A(\sigma(1))||. \tag{1.16}$$

As (1.15) requires showing that almost every stochastic sequence converges, it is the most informative (and therefore least conservative) measure of stability, however it is also the hardest to prove, in general.

Because of the technical challenges in determining almost sure stability of a stochastic system, it is helpful to consider other, more conservative types of stability. One such type of stability, δ-moment stability, holds if

$$\lim_{k\to\infty} \mathrm{E}\left[||x(k)||^\delta\right] = 0, \tag{1.17}$$

where $\mathrm{E}[\cdot]$ denotes expectation with respect to the σ-algebra induced by the switching process. When $\delta = 2$ and (1.17) holds, we say that the switching system is asymptotically *mean-square* stable. Like almost sure stability, there is a δ-moment stability analogue to the sample path Lyapunov exponent. The top δ-moment Lyapunov exponent is computed as

$$g(\delta) = \lim_{k\to\infty} \frac{1}{k} \ln \mathrm{E}\left[||x(k)||^\delta\right], \tag{1.18}$$

[p]Almost all in the sense that the set of initial conditions and stochastic sequences for which this does not happen is of measure 0.

which for jump linear systems becomes

$$g(\delta) = \lim_{k\to\infty} \frac{1}{k} \ln \mathrm{E}\left[||A(\sigma(k-1)) \cdots A(\sigma(2))A(\sigma(1))||^{\delta}\right].$$

δ-moment stability is particularly useful in practice, because it reduces the study of a stochastic system to the study of a deterministic one (which significantly more tools have been developed for). The authors go on to show the relationships between these two types of stability and under what conditions they are equivalent. Further discussions of these types of stability can be found in Appendix D.

1.5.3.2 Stochastic Synchronization for Coupled Maps Much like [125] and [123] sought to establish a theory for switching networks of ODEs, [114, 115, 1] (to name a few) worked to establish a similar theory for switching networks of discrete-time dynamical systems. The significant seminal work is [114], which aims to present a master stability function for the synchronization of stochastically switching networks of maps (like [109] did for static, diffusively coupled networks of ODEs). It utilizes tools from probability theory, stability theory, and matrix analysis to present concise criteria that ensure the mean-square stability of a switching network of maps. Their setup is as follows:

$$\mathbf{x}_i(k+1) = \mathbf{F}(\mathbf{x}_i(k)) - \sum_{j=1}^{N} M_{ij}(k)\mathbf{H}(\mathbf{x}_j(k)) \quad \text{for } i = 1, 2, \ldots, N, \tag{1.19}$$

where $\mathbf{x}(k) \in \mathbb{R}^n$ is an n-dimensional vector composed of the states of one node, $\mathbf{F} : \mathbb{R}^n \to \mathbb{R}^n$ is the vector-valued function governing the individual dynamics of each node, $M(k)$ is the random (i.i.d.), time-varying connectivity matrix for the network, and $\mathbf{H} : \mathbb{R}^n \to \mathbb{R}^n$ is the vector-valued coupling function between the nodes.

The authors linearize the system about the synchronization solution to construct variational equations[q] in order to determine the local stability of that solution. Next, the authors construct the autocorrelation matrix $\Xi(k) = E\left[\xi(k)\xi(k)^T\right]$, which is a symmetric, positive

[q]The *variation* is denoted by $\xi_i = \mathbf{x}_i - \mathbf{s}$ where s is the common trajectory the nodes synchronize to.

semidefinite matrix with trace $E\left[||\xi(k)||^2\right]$. This trace (the sum of the eigenvalues) converging to zero (meaning all of the variation converge to zero, i.e the nodes converge to a common trajectory) means that the system is mean-square stable. The analysis of the autocorrelation matrix reduces the stochastic problem to the stability of a higher dimensional, static system that can be decomposed into the eigendirections transverse to the synchronous manifold, and studied using classical methods in dynamical systems.

1.6 Dissertation Outline

With these building blocks in place, we are prepared to discuss the novel additions to this framework of stochastically switching dynamical systems. This work is divided into two parts. In the first part[r] we explore the complex behaviors of stochastically switching dynamical systems in continuous-time, uncovering surprising phenomena beyond the fast-switching limit. Then, in the second part[s] (in an effort to uncover the mechanism for these phenomena in continuous-time) we rigorously analyze stochastically switching discrete-time systems when switching is either fast or has an arbitrary period.

In Chapter 2 we examine a simple dynamical example in polar coordinates to illustrate how stochastically switching flows work in practice. Using this example, we show how to use the theory from [69] and [70] to describe the asymptotic properties of a switching system in the fast-switching limit. While the behavior of the stochastic system in the fast-switching limit is straightforward, we show that beyond fast switching, stochastic systems can behave unpredictably. Next, in Chapter 3 we consider stochastically switching networks (in which all links are randomly chosen in time) and place bounds on the switching period for which a network of Lorenz oscillators will synchronize, even when the network is potentially disconnected at *every* time instant. Beyond fast switching, we present examples of networks that can synchronize, despite switching between two coupling regimes that discourage synchronization, with an averaged coupling that also discourages synchronization. That is, when

[r] This includes Chapters 2, 3, and 4.
[s] This includes Chapters 5 and 6.

switching is too fast or too slow the synchronization solution is not stable, however for intermediate switching periods, the network converges to synchrony remarkably consistently[t]. Then, in Chapter 4 using the lens of interconnected ecological systems, we provide a real-world example for which stochastically switching systems fill an obvious gap in traditional modeling of ecological systems. We show that stochasticity can play an important role in ecological systems, and insist that it be taken into account for future modeling efforts.

Turning to part two, in Chapter 5 we examine the simplest case for stochastically switching coupled maps: two stochastically coupled 1-D maps. We derive an analytical expression for the stochastic Lyapunov exponent for two coupled maps, and using the paradigm of coupled sigmoid maps[u] and the stochastic Lyapunov exponent, we discover a bounded window of intermediate switching periods for which synchronization is stable, even when it is not stable for fast or slow switching. Next, in Chapter 6 we add layers of complexity to the previous chapter by considering a broadcasting control problem. We study the stochastic synchronization of a network to a reference node that is randomly broadcasting a signal to an arbitrary network of nodes. We examine the role that the static network topology and the properties of the stochastic broadcasting signal have in the network's ability to synchronize to the reference node.

Lastly, we detail the appendices. Appendix A includes the details of the proof for the bounds on the switching period in Chapter 2. Appendix B includes the derivation of the bounds found in Chapter 4. Appendix C describes the Sigmoid map that is introduced in Chapter 5 and includes the proof of the closed-form expression for the stochastic Lyapunov exponent for two coupled sigmoid maps. Lastly, in Appendix D we compare δ-moment stability and almost sure stability in more detail than we did in this introduction.

ENJOY!

[t]We call this optimal range of switching periods for which synchronization is stable a "Window of Opportunity" for the system.

[u]The sigmoid map is a generalization of a class of maps that includes the logistic map and tent map. It is introduced and explored thoroughly in Chapter 5.

CHAPTER 2

MULTISTABLE RANDOMLY SWITCHING OSCILLATORS: THE ODDS OF MEETING A GHOST

In this chapter we familiarize the reader with the stochastically switching setup for continuous-time dynamical systems by considering simple example of oscillators whose parameters randomly switch between two values at equal time intervals. If random switching is fast compared to the oscillator's intrinsic time scale, one expects the switching system to follow the averaged system, obtained by replacing the random variables with their mean. In this example, the averaged system is multistable and one of its attractors is not shared by the switching system and acts as a ghost attractor for the switching system. Starting from the attraction basin of the averaged system's ghost attractor, the trajectory of the switching system can converge near the ghost attractor with high probability or may escape to another attractor with low probability. We apply the general results on convergent properties of randomly switching dynamical systems developed in [69] and [70] to derive explicit bounds that connect these probabilities, the switching frequency, and the chosen initial conditions.

2.1 Introduction

We consider a multistable switching oscillator as an example of a blinking system. The oscillator randomly and rapidly switches its damping coefficient between two values, yielding an averaged system with two attractors: a stable equilibrium and a stable limit cycle, being a ghost attractor for the switching oscillator[a]. We apply the general theory [69, 70] to derive bounds on the probability that the trajectory of the switching oscillator converges to a neighborhood of the ghost attractor and on the remainder of the time interval it may

[a]Ghost attractor in the sense that the attractor in the averaged system is not invariant in the switching systems.

stay in this neighborhood. We construct an appropriate Lyapunov function and show how to estimate its various bounds and decreasing rate to describe the probabilistic convergence to the ghost attractor. We also analyze the switching oscillator's system numerically within and beyond the fast switching limit.

The layout of this chapter is as follows. First, in Section 2.2, we describe the randomly switching oscillator and the corresponding averaged system. Then, in Section 2.3, we construct a Lyapunov function for the switching system and derive the preliminary results, necessary for formulating the main theorem. In Section 2.4, we derive the main analytical result of the chapter (see Theorem 2.1) and discuss its implications for the convergence properties of the switching oscillator. Finally, a brief discussion and summary of the obtained results is given in Section 2.5.

2.2 Multistable Switching Oscillator: The Model

We consider the following randomly switching (blinking) system[b]:

$$\begin{aligned} \dot{x} &= -y - \tfrac{\lambda}{2}\left[\rho^2 - 2(2 - s(t))\rho + (7 - 10s(t))\right] x \\ \dot{y} &= x - \tfrac{\lambda}{2}\left[\rho^2 - 2(2 - s(t))\rho + (7 - 10s(t))\right] y, \quad \text{where } \rho = (x^2 + y^2)/2, \end{aligned} \tag{2.1}$$

$\lambda > 0$ is a damping parameter, and $s : [0, \infty) \to \{0, 1\}$ is a binary switching function. To define $s(t)$, we divide the time axis into intervals of length τ and let $s(t)$ take the value 1 with probability $p = 1/2$ and the value 0 with probability $q = 1 - p = 1/2$ in the time interval $t \in [(k-1)\,\tau,\ k\tau)$. The binary switching function $s(t)$ can be viewed as a switch in system (2.1); the switch is closed when $s_k = 1$ and open when $s_k = 0$. The sequence of binary vectors s_k, $k = 1, 2, ...$ is called the switching sequence as each component s_k switches on ($s_k = 1$) or off ($s_k = 0$) during the k-th time interval. These switching random variables are independent for different time intervals and identically distributed. Put simply, our stochastic model is as follows. During each time interval of length τ, the switch is closed with probability $p = 0.5$,

[b]This simple example was designed to explicitly show the existence of a ghost attractor that is not invariant in the switching systems to demonstrate the power of the general theory for switching systems.

independently of whether or not it has been closed during the previous time interval.

System (2.1) can be rewritten in polar coordinates with $\rho = (x^2 + y^2)/2$ and $\Theta = \arctan(y/x)$ as follows

$$\dot{\rho} = F(\rho, s(t)) = -\lambda\rho\left[\rho^2 - 2(2 - s(t))\rho + (7 - 10s(t))\right]; \qquad \dot{\Theta} = 1. \tag{2.2}$$

When the switch is closed ($s = 1$), system (2.2) takes the form

$$\dot{\rho} = -\lambda\rho\left[\rho^2 - 2\rho - 3\right] = -\lambda\rho(\rho + 1)(\rho - 3); \qquad \dot{\Theta} = 1. \tag{2.3}$$

System (2.3) has a unique stable limit cycle at $\rho = 3$, encircling an unstable fixed point at the origin (see Fig. 2.1a).

When the switch is open ($s = 0$), system (2.2) transforms into the following equations

$$\dot{\rho} = -\lambda\rho\left[\rho^2 - 4\rho + 7\right]; \qquad \dot{\Theta} = 1. \tag{2.4}$$

System (2.4) has a unique globally stable fixed point at the origin (see Fig. 2.1b). Thus, the blinking system (2.1) randomly switches between system (2.3) with a stable limit cycle and system (2.4) with the globally stable origin.

If the switching period τ is small with respect to the characteristic times of systems (2.3) and (2.4), one can expect that the dynamics of the stochastically switching system (2.1) is close to that of the averaged system where the stochastic variable $s(t)$ is replaced by its mean value $p = 0.5$.

The averaged system associated with the switching system (2.1) reads as

$$\begin{aligned} \dot{\xi} &= -\eta - \tfrac{\lambda}{2}\left[r^2 - 3r + 2\right]\xi \\ \dot{\eta} &= \xi - \tfrac{\lambda}{2}\left[r^2 - 3r + 2\right]\eta, \quad \text{where } r = (\xi^2 + \eta^2)/2. \end{aligned} \tag{2.5}$$

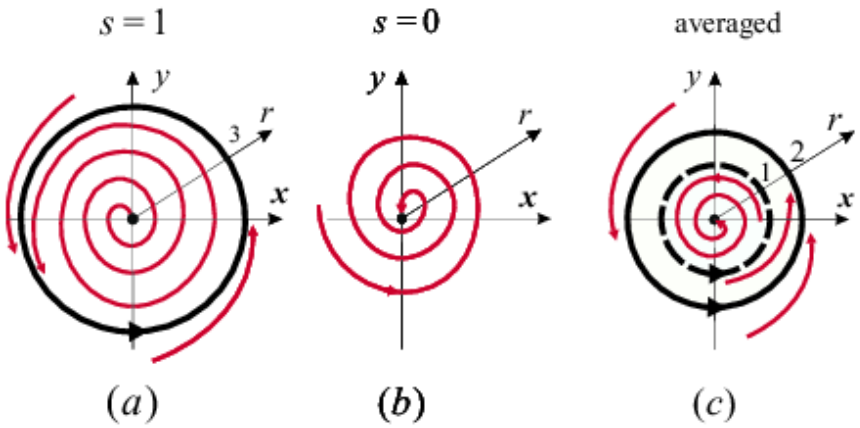

Figure 2.1 The oscillator randomly switches between two systems: the one with closed switch $s = 1$ (a) and the one with open switch $s = 0$ (b). Its averaged system is multistable and has a stable equilibrium at the origin and a stable limit cycle at $r = 2$, separated by an unstable limit cycle at $r = 1$ (c). Note that the stable limit cycle of the averaged system is not an invariant set of the two systems with $s = 1$ and $s = 0$.

Written in polar coordinates, it takes the form

$$\dot{r} = \Phi(r) \equiv E(F(\rho, s(t))) = -\lambda r(r-1)(r-2); \qquad \dot{\Theta} = 1, \tag{2.6}$$

where $E(F(\rho, s(t)))$ is the expected value of $F(\rho, s(t))$. The averaged system has a stable limit cycle at $r = 2$ and a stable fixed point at the origin; an unstable limit cycle at $r = 1$ separates their basins of attraction (see Fig. 2.1 (c)). It is worth noticing that while the trivial equilibrium at the origin is shared by both the switching and averaged systems, the stable limit cycle of the averaged system is not an invariant set of the switching system. Therefore, the trajectory of the switching system cannot converge to the stable limit cycle of the averaged system, it can only reach a neighborhood of the stable limit cycle and remain close most of the time with high probability when switching is fast (this statement will be made more precise later in Section 2.4). In this case, the stable limit cycle of the averaged system acts as a *ghost* attractor for the switching system (see Figs. 2.2 and 2.3).

The averaged system is *multistable*, therefore the main question in this study is whether

or not the trajectory of the switching system will converge near the same (ghost) attractor as the averaged system when starting from the same initial state. In the following, we will derive explicit bounds that relate the probability of convergence near the ghost limit cycle, the switching period, and the choice of initial conditions to each other. In other words, we will analyze the odds of converging to a neighborhood of the ghost attractor and link them to the switching period. Before formulating the main result regarding the switching system, we need to analyze the convergent properties of the averaged system.

2.3 Preliminary Analysis: The Lyapunov Function and Its Bounds

To apply the general theory developed in [69, 70], we need to introduce and estimate the following functions and constants. To facilitate cross-paper reading, we shall use the same notation as in [69, 70].

We first estimate the sizes of the compact absorbing (attracting) domain R for both the switching and averaged systems. Clearly, these domains are $0 \leq \rho \leq 3$ and $0 \leq r \leq 2$, respectively, such that the ultimate bound for both the systems is $R : 0 \leq \rho \leq 3$.

The averaged system (2.6) has a Lyapunov function that can be constructed as an integral of the system's (2.6) nonlinearity:

$$W_{\Phi}(r) = \int_0^r (q(q-1)(q-2))dq = r^2(r-2)^2/4. \tag{2.7}$$

The graph of Lyapunov function $W(r)$ is a fourth-order parabola with two minima, the r-intercepts, $W(0) = 0$ and $W(2) = 0$, corresponding to the stable origin and the stable limit cycle, respectively. Its local maximum is at $r = 1$, corresponding to the unstable limit cycle. The absolute maximum of $W(r)$ in the absorbing domain $R : 0 \leq r \leq 3$ is reached at the endpoint $r = 3$.

The derivative of $W_{\Phi}(r)$ along the trajectories of the averaged system (2.6) becomes

$$\dot{W}_{\Phi} = -\lambda r^2(r-1)^2(r-2)^2. \tag{2.8}$$

Following the notation used in [70], this derivative represents $D_\Phi W$ in [70] such that $\dot{W}_\Phi \equiv D_\Phi W$. In what follows, we will use $\dot{W}_\Phi$ to calculate various quantities in Theorem 2.1.

Similarly, we introduce a Lyapunov function for the switching system (2.1)-(2.2)

$$W_F(\rho) = \rho^2(\rho-2)^2/4. \tag{2.9}$$

Upper bounds for the first and second derivatives of Lyapunov functions W_Φ and W_F in the absorbing domain $R : 0 \le \rho \le 3$ can be estimated as follows (the detailed calculations are given in Appendix A):

$$\begin{aligned} B_{W\Phi} &= \max_{0\le r\le 3}\left|\dot{W}\right| = 36\lambda \\ LB_{W\Phi} &= \max_{0\le r\le 3}\left|\ddot{W}\right| = 792\lambda^2 \\ B_{WF} &= \max_{s\in\{0,1\}}\max_{0\le r\le 3}\left|\dot{W}_F\right| = 72\lambda \\ LB_{WF} &= \max_{s\in\{0,1\}}\max_{0\le r\le 3}\left|\ddot{W}_F\right| = 33264\lambda^2. \end{aligned} \tag{2.10}$$

2.4 The main result: the odds of converging near the ghost attractor

Let a trajectory of the averaged system (2.6) start from the initial condition $r(0) = 1+\delta$, where $0 < \delta < 1/2$ is a constant. This trajectory converges to the stable limit cycle of the averaged system at $r = 2$. Let $V_1 = (1-\varepsilon_1)/4$ be a level of the Lyapunov function, corresponding to $r(0) = 1+\delta$ (see Fig. 2.2). The constant ε_1 satisfies $W_\Phi(1+\delta) = (1-\varepsilon_1)/4$.

Let C_1 be a connected component of the level set $\{r \mid W_\Phi(r) \le V_1\}$. Note that C_1 is an annulus that contains the stable limit cycle of the averaged system and is bounded from below by $r = 1+\delta$ and from above by $r = 1+\sqrt{2}-\delta''$, where constant δ'' is chosen to satisfy $W_\Phi(1+\sqrt{2}-\delta'') = (1-\varepsilon_1)/4$.

Choose a neighborhood of the stable limit cycle of the averaged system $2-\delta < r < 2+\delta'$. Constants δ and δ' are chosen such that the two bounds $2-\delta$ and $2+\delta'$ satisfy the same level of Lyapunov function $V_0 = \varepsilon_0/4$, where ε_0 is a constant that depends on δ. This neighborhood $2-\delta < r < 2+\delta'$ will be related to a region around the ghost limit cycle in the switching

system. Its trajectory should reach this neighborhood and stay inside with high probability (see Theorem 2.1) .

Before formulating Theorem 2.1, we shall estimate the following minimal convergence speed of Lyapunov function W_Φ in C_1 :

$$\gamma = \min_{r\in C_1,\, V_0\le W_\Phi\le V_1} |\dot{W}_\Phi|. \tag{2.11}$$

Simple analysis shows that this minimum in the annulus C_1 is reached at $r = 1 + \delta$, the endpoint value closest to the unstable limit cycle at $r = 1$, separating the basins of attraction for the origin and the stable limit cycle. Therefore,

$$\gamma = |\dot{W}_\Phi(1 + \delta)| = \lambda\delta^2(1 - \delta^2)^2. \tag{2.12}$$

We introduce the following quantities to be used for deriving Theorem 2.1:

$$\begin{aligned} \Delta t &= \tfrac{\gamma}{2(LB_{WF}+LB_{W\Phi})} = \tfrac{\delta^2(1-\delta^2)^2}{68112\lambda} \\ \alpha &= B_{WF} + B_{W\Phi} = 108\lambda \\ c &= \tfrac{1}{64(LB_{WF}+LB_{W\Phi})B_{WF}^2} = \tfrac{1}{11298963456\lambda^4}, \end{aligned} \tag{2.13}$$

where constants $B_{W\Phi}$, $LB_{W\Phi}$, B_{WF}, LB_{WF}, and γ are given in (2.10) and (2.12), respectively.

The following theorem is obtained from Theorem 8.3 in [70] by substituting constants (2.12) and (2.13) into the conditions of Theorem 8.3 and therefore is given without the proof (the detailed proof of Theorem 8.3 can be found in [70]). Theorem 8.3 describes the behavior of a general blinking system in the most general case where the blinking system has multiple ghost attractors. The main merit of this study is in giving the first example of a randomly switching dynamical system with probabilities of converging to a neighborhood of a ghost attractor, explicitly calculated via the parameters of the switching system (the damping parameter λ and switching period τ) and the initial conditions, expressed via δ.

Theorem 2.1 *Choose the neighborhood V_0 of the ghost limit cycle in the averaged system such that*

$$V_1 - V_0 = \frac{1 - 6\delta^2 + 4\delta^3}{4} \geq \frac{3\delta^4(1-\delta^2)^4}{136224}. \tag{2.14}$$

Assume that the switching period τ is sufficiently small such that

$$2e \cdot \left(\frac{216\lambda}{\lambda\delta^2(1-\delta^2)^2} + 1 \right) \exp\left(-\frac{\delta^6(1-\delta^2)^6}{11298963456\lambda} \cdot \frac{1}{\tau} \right) \leq 1 - \sqrt{\frac{e}{3}}. \tag{2.15}$$

Consider the two open regions

$$\begin{aligned} U_0 &= \left\{ \rho \;\middle|\; W_F(\rho) < \tfrac{(2-\delta)^2\delta^2}{4} + \tfrac{\delta^4(1-\delta^2)^4}{68112} \right\}, \\ U_\infty &= \left\{ \rho \middle| W_F(\rho) > \tfrac{(1-\delta^2)^2}{4} + \tfrac{\delta^4(1-\delta^2)^4}{68112} \right\}. \end{aligned} \tag{2.16}$$

Then the following inequalities hold:

1. *The probability P_{escape}^{direct} that the solution $\rho(t)$ of the switching system (2.1)-(2.2) reaches U_∞ before reaching U_0 (see Fig. 2.2) is bounded by*

$$P_{escape}^{direct} \leq \frac{419904}{\delta^4(1-\delta^2)^4} \exp\left(-\frac{\delta^6(1-\delta^2)^6}{11298963456\lambda} \cdot \frac{1}{\tau} \right). \tag{2.17}$$

Conversely, the probability that the solution $\rho(t)$ of the switching system reaches U_0 before reaching U_∞ is at least

$$P_{attraction}^{direct} \geq 1 - \frac{839808}{\delta^4(1-\delta^2)^4} \exp\left(-\frac{\delta^6(1-\delta^2)^6}{11298963456\lambda} \cdot \frac{1}{\tau} \right). \tag{2.18}$$

2. *Let $T_{attraction}$ be the time for the solution of the switching system to enter U_0 through its boundary and T_{remain} be the time it stays close to the ghost attractor and remains in*

$$\bar{U}_{0+} = \left\{ \rho \;\middle|\; W_F(\rho) \leq \frac{(2-\delta)^2\delta^2}{4} + \left(\frac{3\delta^2(1-\delta^2)^2}{2} + 108 \right) \frac{\delta^2(1-\delta^2)^2}{68112} \right\} \tag{2.19}$$

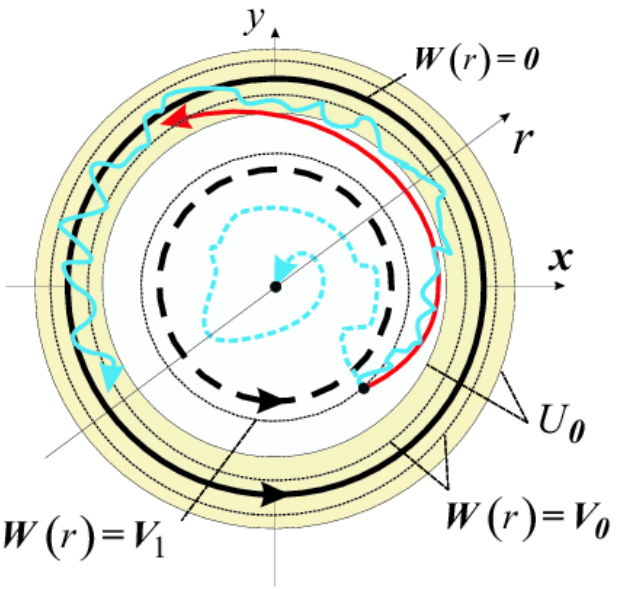

Figure 2.2 Illustration of Theorem 2.1. The trajectory of the averaged system (regular red line) starts from an initial condition, corresponding to a level $W_\Phi(r) = V_1$ and converges to the stable limit cycle at which $W_\Phi(r) = 0$. This limit cycle acts as a ghost attractor for the switching system whose trajectory (solid irregular blue line) reaches a small neighborhood U_0 of the ghost attractor in time $T_{attraction}$ with probability $P^{direct}_{attraction}$. The trajectory oscillates around the ghost attractor and may eventually, after some time T_{remain}, diverge from the ghost attractor; however, this probability can be made arbitrarily small by decreasing the switching period τ (cf. (2.21)). There also is a non-zero probability P^{direct}_{escape} that the trajectory of the switching system may also escape from the attraction basin C_1 right away and converge to the origin (dashed irregular blue line). Note that this probability decreases exponentially fast when $\tau \to 0$.

after reaching U_0. These times are random variables with the following properties

$$\begin{aligned} P\left(T_{attraction} \leq \frac{1-6\delta^2+4\delta^3}{2\lambda\delta^2(1-\delta^2)^2}\right) &> 1-\frac{68112(1-6\delta^2+4\delta^3)}{\delta^4(1-\delta^2)^4}\times \\ &\times \exp\left(-\frac{\delta^6(1-\delta^2)^6}{11298963456\lambda}\cdot\frac{1}{\tau}\right) \end{aligned} \tag{2.20}$$

and

$$P\left(T_{remain} > T\right) > 1 - T\frac{136224\lambda}{\delta^2(1-\delta^2)^2}\exp\left(-\frac{\delta^6(1-\delta^2)^6}{11298963456\lambda}\cdot\frac{1}{\tau}\right). \tag{2.21}$$

Remark 1 *The switching period τ appears only in the denominator of the exponent in conditions (2.15), (2.17), (2.18). Therefore, the probability P_{escape}^{direct} of escaping from the ghost attractor's basin of attraction before reaching the ghost attractor's neighborhood U_0 can be made arbitrarily small by decreasing the switching period τ. Note that if the trajectory of the switching system converges to the "wrong" attractor (the origin), it has to pass first through U_∞. Therefore, P_{escape}^{direct} is an upper bound on the probability that the trajectory escapes from the ghost attractor and converges to the origin.*

Remark 2 *The bounds for the probabilities of escaping from and converging to the ghost attractor's neighborhood, given in Theorem 2.1, explicitly depend on the choice of initial conditions $\rho(0) = 1 + \delta$. These bounds indicate that the smaller parameter δ (i.e., the closer the initial condition is to the unstable limit cycle that separates the attraction basins), the higher the probability of escaping to the origin.*

Remark 3 *Note that probability bounds P_{escape}^{direct} and $P_{attraction}^{direct}$ do not sum to* 1, *as one would expect. Therefore, the trajectories of the switching system that never reach U_0 or U_∞ and get trapped between the ghost attractor and the origin might have positive probability. However, this probability could not be larger than P_{escape}^{direct} and the case that this probability vanishes is compatible with the bounds [70].*

Figure 2.3 presents numerical simulations of the switching system (2.1)-(2.2) for different switching periods and initial conditions. When the initial state of the switching system is

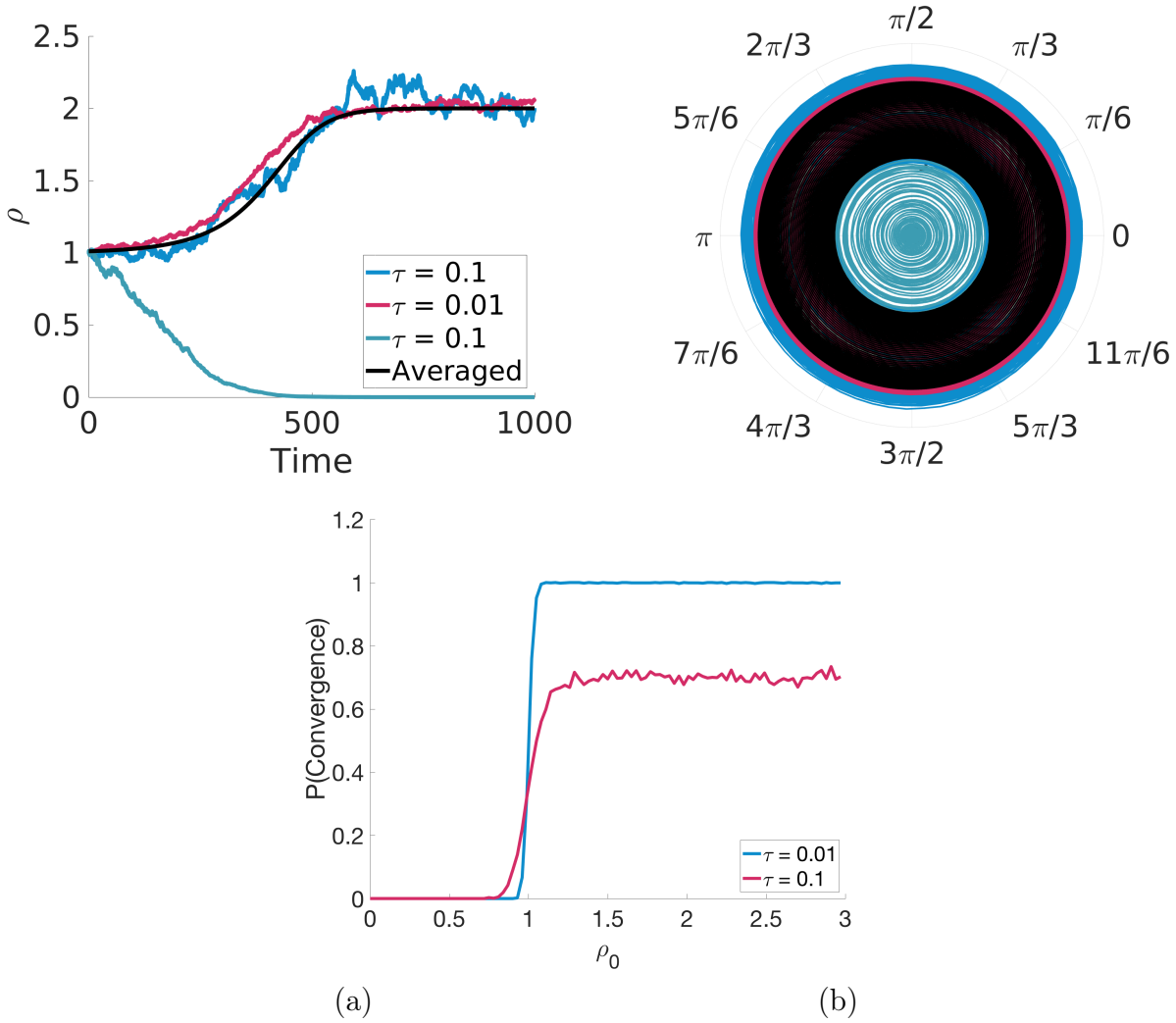

(a) (b)

Figure 2.3 (top left) Trajectories of the averaged system (black smooth curve) and stochastic system with switching times $\tau = 0.1$ (blue and teal) and $\tau = 0.01$ (pink). The trajectories start from the same initial condition $\rho = 1 + \delta$ with $\delta = 0.01$ in the attraction basin of the stable (ghost) limit cycle. For the given stochastic sequence the switching system follows the averaged system for $\tau = 0.01$ and oscillates about the ghost limit cycle. For slower switching with $\tau = 0.1$ (blue and teal), two different stochastic sequences cause the trajectory of the switching system to converge near the ghost limit cycle (blue) or to escape to the wrong attractor (teal). (top right) Plot of the trajectories in (top left), but in the polar phase space. (bottom) Probability of converging to a neighborhood of the ghost limit cycle $\rho = 2$, starting from initial conditions with radius ρ_0 for $\tau = 0.1$ (pink) and $\tau = 0.01$ (blue). Notice a sharp transition around $\rho = 1$, corresponding to the unstable limit cycle, separating the attraction basins of the ghost limit cycle and origin. As the analytical bounds (2.17), (2.18) suggest, decreasing τ significantly increases the odds of converging near the ghost. Probability calculations are based on 1000 trials. The damping parameter equals $\lambda = 0.01$.

close to the attraction basin boundary (see Fig. 2.3 top left), i.e., for small δ, there always is a small probability P_{escape}^{direct} of escaping to the wrong attractor. This can also be clearly viewed from the bound (2.17) and the expression for the speed of convergence γ (2.12), where δ is the distance from the attraction basin boundary, defined by the unstable limit cycle at $r = 1$. The smaller δ and the slower the switching, the bigger this probability is (see Fig. 2.3 bottom).

In Fig. 2.4, we examine probability outcomes for different switching periods across a range of different initial conditions ρ_0. We find that for larger switching periods τ the switching system can converge to the origin despite the initial conditions chosen in the attraction basin of the ghost attractor, far away from the attraction basin boundary. Though it is important to remember that Fig. 2.4 is only one realization (one trial from each initial condition) and not an average of numerous trials, it does show that there are certain "windows of opportunity" for which the optimal stochastic sequence/frequency can give the system enough kicks in the wrong direction at the appropriate time and to cause the system to rather consistently converge to the wrong attractor.

2.5 Chapter Summary

We have considered a multistable switching oscillator as an example of a stochastically blinking system. The switching oscillator has two attractors with the stable limit cycle being a "ghost". Switching is assumed to be a stochastic process (with identically distributed independent random switching variables), therefore the convergence properties of the switching oscillator have a probabilistic flavor. We applied the general theory [69, 70] to prove weak convergence (with probability $P_{attraction}^{direct}$ approaching 1 when the switching period $\tau \to 0$) to a neighborhood of the correct (ghost) attractor. Using the Lyapunov function method, we gave explicit bounds on the probabilities of converging to and escaping from the ghost attractor's neighborhood and switching time. More precisely, we have derived the following result. We choose an initial condition for the switching and averaged systems in the attraction basin of the ghost attractor. For this initial condition, we identify V_1, a level of a

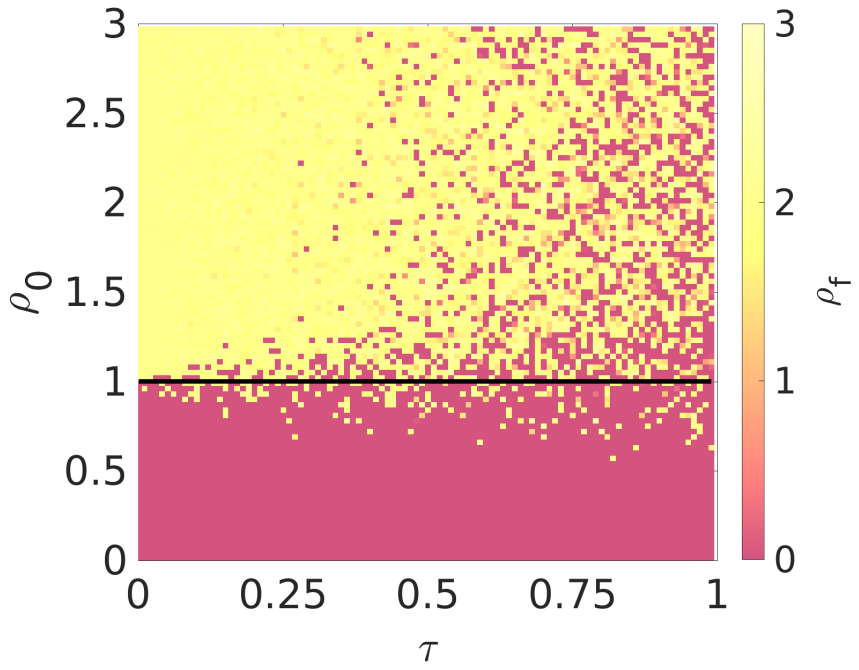

Figure 2.4 The role of different initial conditions and stochastic frequencies. For each fixed τ, we vary ρ_0 and observe where ρ_f ends, namely whether or not the switching system converges near the ghost or to the origin. Yellow corresponds to convergence near the ghost, while pink is convergence to the origin. The intermediate colors (dark yellow and orange) indicate that the system is still oscillating in between the attractors (with yellow closer to the ghost and green closer to the origin). This is only a single realization for each set of initial conditions, the system becomes more unpredictable as τ increases. For larger values of τ, the system can converge to the origin despite initial conditions near the ghost (note the pink "valleys" at $\rho_0 \approx 2$ and $\tau \approx 0.75$). The damping parameter equals $\lambda = 0.01$.

Lyapunov function for the averaged system. We also choose a neighborhood U_0 of the ghost attractor of the switching system. We then find a bound for the minimum convergence speed γ of the Lyapunov function in the subregion of the ghost's attraction basin, bounded by V_1 and U_0. Consequently, we prove that the probability that the trajectory of the switching system rapidly reaches U_0 can be made arbitrarily close to 1 by decreasing the switching period. We find the reciprocal of τ to be a critical quantity, effectively controlling the probability of convergence.

We also showed that if switching is not sufficiently fast, the switching system may have "windows of opportunity", in terms of optimal switching periods and sets of initial con-

ditions, within which the trajectory escapes to the wrong attractor against all the odds. Loosely speaking, the existence of the windows of opportunity in randomly switching multistable oscillators may be viewed somewhat similarly to stochastic resonance [155, 8, 7]. Although, the two phenomena have completely different dynamical origins; the coincidence of favorable initial conditions and stochastic sequences for the switching oscillator and a favorable condition to go over a threshold in a bistable system due to matching the time scales of a periodic driving force and driving noise for stochastic resonance.

In the next chapter, we will add a layer of complexity to these switching systems by considering the synchronization of a network of chaotic oscillators that can be completely disconnected at any given time instant.

CHAPTER 3

SYNCHRONIZATION IN ON-OFF STOCHASTIC NETWORKS: WINDOWS OF OPPORTUNITY

With this simple example to give an idea of how stochastically switching dynamical systems work, as well as a teaser of some of the complex behavior that can emerge beyond fast switching, we approach a more challenging problem. Namely, in this chapter, we study dynamical networks whose topology and intrinsic parameters stochastically change, on a time scale that ranges from fast to slow. This is an especially interesting problem, because at any given moment in time, the network can be disconnected (which does not allow for synchronization, in general). When switching is fast, the stochastic network synchronizes as long as synchronization in the averaged network, obtained by replacing the random variables by their mean, becomes stable. We apply a recently developed general theory of blinking systems to prove global stability of synchronization in the fast switching limit. We use a network of Lorenz systems to derive explicit probabilistic bounds on the switching frequency sufficient for the network to synchronize almost surely and globally. Going beyond fast switching, we consider networks of Rössler and Duffing oscillators and reveal unexpected windows of intermediate switching frequencies in which synchronization in the switching network becomes stable even though it is unstable in the averaged/fast-switching network.

The purpose of this chapter is two-fold. First, we show how the established theory on fast-switching can be applied to synchronization in dynamical networks of concrete periodic or chaotic oscillators (Sections 3.1 and 3.2). In particular, we consider a network of chaotic Lorenz systems with both stochastically switching connections *and* intrinsic parameters and derive bounds on the switching frequency and the time sufficient to converge globally and surely to approximate synchronization (Section 3.2). Remarkably, these bounds are explicit in the parameters of the blinking network. We also demonstrate how the probability of stable

synchronization scales with the switching frequency beyond the conservative bounds. Second, we focus on synchronization of networks with non-fast switching connections (Section 3.3). We show the advantages of slower switching over fast switching by means of prototypical examples such as networks of (i) chaotic Rössler systems; (ii) non-autonomous Duffing oscillators in which slow switching provides opportunities for network synchronization while fast switching does not. More specifically, the network switches between topologies where synchronization is unstable, with its averaged network also being unstable for synchronization. Yet, there is a "window of opportunity" in which an intermediate, not-fast switching frequency causes synchronization in the unstable network to stabilize. We also reveal this unexpected behavior in periodically switched dynamical networks with additional windows of opportunity.

3.1 The Stochastic Network Model

Introduced in [19], the blinking network consists N oscillators interconnected pairwise via a stochastic communication network:

$$\frac{d\mathbf{x}_i}{dt} = \mathbf{F}_i(\mathbf{x}_i, \hat{s}_i(t)) + \varepsilon \sum_{j=1}^{N} s_{ij}(t) P \left(\mathbf{x}_j - \mathbf{x}_i\right), \tag{3.1}$$

where $\mathbf{x}_i(t) \in \mathbb{R}^d$ is the state of oscillator i, $\mathbf{F}_i : \mathbb{R}^d \to \mathbb{R}^d$ describes the oscillators' individual dynamics, $\varepsilon > 0$ is the coupling strength. The $d \times d$ matrix P determines which variables couple the oscillators, $s_{ij}(t)$ are the elements of the time-varying connectivity (Laplacian) matrix $G(t)$. The existence of an edge from vertex i to vertex j is determined randomly and independently of other edges with probability $p_{ij} \in [0, 1]$. Expressed in words, every switch in the network is operated independently, according to a similar probability law, and each switch opens and closes in different time intervals independently. All possible edges $s_{ij} = s_{ji}$ are allowed to switch on and off so that the communication network $G(t)$ is constant during each time interval $[k\tau, (k + 1)\tau)$ and represents an Erdös-Rényi graph of N vertices. Figure 3.1 gives an example of a "blinking" graph. The generalization of all the

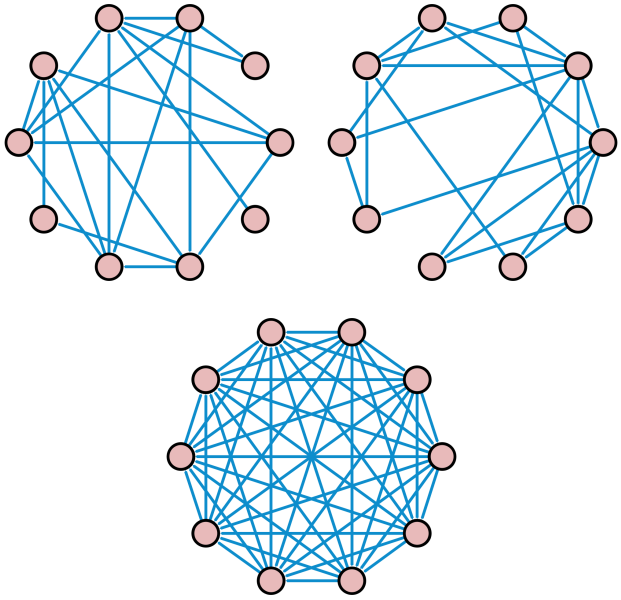

Figure 3.1 (top) Two subsequent instances of the switching network. Probability of an edge is $p = 0.5$. (bottom): The corresponding averaged network where the switching connections of strength ε are replaced with static all-to-all connections of strength $p\varepsilon$, representing their mean value.

results of chapter to more complex switching topologies [147, 3] and directed graphs [124] is straightforward. In the model (3.1), we have also introduced stochasticity into one of the intrinsic system parameters, such that it switches between two values according to the same stochastic rule $\hat{s}_i(t)$ (though with an independent switching frequency and sequence). This stochastic intrinsic parameter accounts for internal fluctuations in the circuit. As a result, the randomly switching oscillators are non-identical and complete synchronization between the oscillators is impossible. Thus, we have chosen to tackle a more difficult problem of proving the stability of approximate synchronization in this switching network with stochastic intrinsic parameters, rather than considering identical oscillators. However, all the results of this chapter are directly applicable to networks with identical oscillators. This can be done by setting the mismatch parameter $a = 0$ in the network of Lorenz oscillators (3.2) (Section 3.2) and applying more restrictive Theorem 11.1 from [70], which yields tighter bounds on the switching period.

The switching network (3.1) is a relevant model for stochastically changing networks

such as information processing cellular neural networks [68] or epidemiological networks [125, 58]. For example, independent and identically distributed (i.i.d.) stochastic switching of packet networks communicating through the Internet comes from the fact that network links have to share the available communication time slots with many other packets belonging to other communication processes and the congestion of the links by the other packets can also occur independently. As far as network synchronization is concerned, local computer clocks, that are required to be synchronized throughout the network, are a representative example. Clock synchronization is achieved by sending information about each computer's time as packets through the communication network [19]. The local clocks are typically implemented by an uncompensated quartz oscillator. As a result, the clocks can be unstable/inaccurate and need to receive synchronizing signals, that aim to reduce the timing errors. These signals must be sufficiently frequent to guarantee sufficient precision of synchronization between the clocks. At the same time, the communication network must not be overloaded by the administrative signals. This is a compromise between the precision of synchronization and the traffic load on the network. Remarkably, this blinking network administration can provide precise functioning of a network composing of imprecise elements. It also indicates the importance of optimal switching frequencies that ensure this compromise.

In the following, we will explore the dependence of network synchronization on different stochastic switching rates.

3.2 Fast Switching: Lorenz Oscillators

If switching is fast compared to the oscillator's intrinsic time scale, it is natural to expect the switching system (3.1) to follow the averaged system, which is obtained from taking the expectation of all of the stochastic variables $s_{ij}(t)$ and $\hat{s}_i(t)$. This amounts to replacing the non-zero entries of G ($i \neq j$) and the intrinsic parameter $\hat{s}_i(t)$ with the switching probability p. We denote this averaged system Φ, as in the previous chapter. Conceptually, for the coupling, this equates to connections between nodes that are always present, but that are weaker than 'on' connections (as a connection in Φ has coupling $p\varepsilon$ and an 'on' connection

in **F** has coupling ε) (see Fig. 3.1).

3.2.1 Rigorous Bounds

In this section, we apply this rigorous theory to network synchronization and demonstrate what bounds on the dynamics of the switching network must be satisfied to guarantee the convergence to stable synchrony. We use the Lorenz oscillator as an individual unit, comprising the network (3.1). The network (3.1) of x-coupled Lorenz oscillators with stochastic coupling and a stochastic intrinsic parameter is given as follows:

$$\begin{aligned} \dot{x}_i &= \sigma(y_i - x_i) + \varepsilon \sum_{j=1}^{N} s_{ij}(t)\,(x_j - x_i) \\ \dot{y}_i &= x_i\,([1 + a\hat{s}_i(t)]\,r - z_i) - y_i \\ \dot{z}_i &= x_i y_i - b z_i, \end{aligned} \tag{3.2}$$

where $i = 1, 2, \ldots, N$ and a is an additional positive parameter, forcing the main parameter r to switch between two values r and $(1 + a)r$. The corresponding averaged system Φ reads:

$$\begin{aligned} \dot{x}_i &= \sigma(y_i - x_i) + \varepsilon p \sum_{j=1}^{N} (x_j - x_i) \\ \dot{y}_i &= x_i\,(r^* - z_i) - y_i \\ \dot{z}_i &= x_i y_i - b z_i, \end{aligned} \tag{3.3}$$

where $r^* = (1 + pa)r$. Synchronization in the averaged network (3.3) with all-to-all connections of strength $p\varepsilon$ is defined by the invariant manifold $M = \{x_1 = x_2 = ... = x_N,\ y_1 = y_2 = ... = y_N,\ z_1 = z_2 = ... = z_N\}$. It is important to emphasize that this synchronization solution *does not* exist in the stochastically switching network (3.2) due to the presence of the intrinsic parameter a, bringing stochastically changing parameter mismatch into the system. Therefore, the trajectory of the switching network cannot converge to the completely synchronized solution, and it can approach and reside in its δ-neighborhood, corresponding to approximate δ-synchronization. The faster the switching, the smaller the synchronization mismatch (error) δ is. Our goal is to prove the global stability of δ-synchronization and

demonstrate that the set of on-off switching sequences that fail to trigger δ-synchronization is of measure zero as long as synchronization in the averaged network is globally stable and switching is fast enough. We also aim at deriving the probabilistic bounds on the switching frequency and δ that can be calculated explicitly via the parameters of the switching network (3.2).

The proof involves two steps. In the first step, we construct a Lyapunov function for the difference (transverse) oscillators' variables in the averaged network (3.3) and proves that it decreases to zero. Therefore, we prove that complete synchronization is globally stable in the averaged network. In the second step, we use that same Lyapunov function for the convergence to the δ-neighborhood of the ghost synchronized solution in the switching network (3.2). Due to the stochastic nature of the switching, this Lyapunov function may increase at a given time step, but the general tendency is to decrease. Switching is a stochastic process, therefore, the convergence properties also have a probabilistic flavor. This can be expressed by showing that after a certain time the Lyapunov function decreases with high probability as long as the switching frequency is sufficiently fast.

We define the Lyapunov function as:

$$W = \frac{1}{2} \sum_{i=1}^{N-1} \left\{ X_{i,i+1}^2 + Y_{i,i+1}^2 + Z_{i,i+1}^2 \right\}, \tag{3.4}$$

where $X_{i,i+1} = x_i - x_{i+1}$, $Y_{i,i+1} = y_i - y_{i+1}$, $Z_{i,i+1} = z_i - z_{i+1}$ are the $N-1$ difference variables. We notice that both the averaged system (3.3) and the stochastic system (3.2) are assumed to have the same Lyapunov function, so we will differentiate between the two of them using W_Φ and W_F for the averaged and stochastic systems, respectively. Before we can begin to understand the behavior of the stochastic network, it is important to understand the dynamics of the static, averaged network. Global stability of complete synchronization in networks of x-coupled Lorenz systems has been extensively studied, for example, in [22]. Based on the previous analysis [22], we can formulate the following statement.

Proposition 3.1: *Synchronization in the averaged all-to-all x-coupled Lorenz network (3.3)*

with coupling strength $p\varepsilon$ and the averaged intrinsic parameter $r^* = (1+pa)r$ is globally stable if

$$p\varepsilon > p\varepsilon^* = \left(\frac{1}{N}\right)\left(\frac{b\,(b+1)\,(r^*+\sigma)^2}{16\,(b-1)} - \sigma\right). \tag{3.5}$$

Proof *The direct application of the bound on the coupling strength sufficient for global synchronization in the x-coupled network of Lorenz oscillators with arbitrary topologies (see Appendix A in [22]) to the averaged network (3.3) yields the condition (3.5).* □

This bound can be generalized to more complex averaged network topologies, corresponding to networks with given switching connections that are not all-to-all. For example, the bound for a $2K$-nearest neighbor network of x-coupled Lorenz oscillators can be obtained by replacing the $\frac{1}{N}$ in (3.5) with $\left(\frac{1}{N}\right)\left(\frac{N}{2K}\right)^3\left(1+\frac{65K}{4N}\right)$, using the Connection Graph method [22]. In the case of directed networks, one can use the Generalized Connection graph [13].

The theory for the behavior of stochastic on-off systems [69] and [70] involves placing upper bounds on the first and second time derivatives of the Lyapunov function W, calculated along solutions of the averaged and switching systems:

$$\begin{aligned} B_{W\Phi} &= \max_{\mathbf{x}\in\mathbb{R}} |D_\Phi W(\mathbf{x})| \\ LB_{W\Phi} &= \max_{\mathbf{x}\in\mathbb{R}} |D^2_\Phi W(\mathbf{x})| \\ B_{WF} &= \max_{\mathbf{s}} \max_{\mathbf{x}\in\mathbb{R}} |D_F W(\mathbf{x},\mathbf{s})| \\ LB_{WF} &= \max_{\mathbf{s},\bar{\mathbf{s}}} \max_{\mathbf{x}\in\mathbb{R}} |D^2_F W(\mathbf{x},\bar{\mathbf{s}},\mathbf{s})|, \end{aligned} \tag{3.6}$$

where $\mathbf{x}$ is the vector composed of $\mathbf{x}_i = \{x_i, y_i, z_i\}$, $i = 1, ..., N$, $\mathbb{R}$ represents the systems' absorbing domain, vector $\mathbf{s}$ indicates a set of stochastic sequences corresponding to $\binom{N}{2}$ stochastic connections and N intrinsic parameter switching sequences; similarly, $\bar{\mathbf{s}}$ corresponds to a set of another realizations of the stochastic switching sequences.

Before giving all of the explicit bounds (3.6) for the N-node networks (3.2) and (3.3), we will walk the reader through the process of obtaining B_{WF} and LB_{WF} for the two-node network (3.2) with $\hat{s}_1 = \hat{s}_2 = s(t)$. We shall use the notation $X = x_1 - x_2$ and $Y = y_1 - y_2$, and $Z = z_1 - z_2$. We start with the first time derivative of the Lyapunov function (3.4) along

the solutions of the stochastic two-node system (3.2):

$$D_F W(\mathbf{x}, \mathbf{s}) = X\dot{X} + Y\dot{Y} + Z\dot{Z}, \tag{3.7}$$

where the derivatives of the difference variables are governed by the following equations, obtained from the system (3.2) with $N = 2$ [22, 12]:

$$\begin{aligned} \dot{X} &= \sigma(Y - X) - 2s_{12}(t)\varepsilon X \\ \dot{Y} &= \left[(1 + as(t))r - U^{(z)}\right] X - Y - U^{(x)} Z \\ \dot{Z} &= U^{(y)} X + U^{(x)} Y - bZ, \;\; i, j = 1, ..., N, \end{aligned} \tag{3.8}$$

where $U^{(\xi)} = (\xi_1 + \xi_2)/2$ for $\xi = x, y, z$ are the corresponding sum variables. For simplicity, we assume that the coupling and intrinsic stochastic parameters are governed by the same stochastic sequence $s_{12}(t) = s(t)$. The generalization to different sequences is straightforward. We can rewrite the equation (3.7) as a quadratic form

$$D_F W(\mathbf{x}, \mathbf{s}) = -\left[(2s(t)\varepsilon + \sigma)X^2 + \left[U^{(z)} - (1 + as(t))r + \sigma\right] XY + Y^2 - U^{(y)} XZ + bZ^2\right]. \tag{3.9}$$

To bound the absolute value of this derivative by its maximum and obtain B_{WF}, we will maximize each term in the quadratic form (3.9). It is well-known that the individual Lorenz system has bounds that guarantee its trajectories will remain in the absorbing domain. These bounds can be found, for example, in [22] and are $|x, y| < |\varphi|$ and $|z| < |\varphi| + r + \sigma$, where $\varphi = \frac{b(r+\sigma)}{2\sqrt{b-1}}$. Therefore, for example, $X = x_1 - x_2 = \varphi - (-\varphi) = 2\varphi$ is the upper bound for the difference X. As we are maximizing the quadratic form term by term, we can guarantee that it is maximized if $s(t) = 1$. While in practice, this will lead us to a more conservative result, it is much more analytically tractable. We show this term by term maximization

$$\begin{aligned} \max_{\mathbf{x} \in \mathbb{R}} |D_F W(\mathbf{x}, \mathbf{s})| &= |4(2\varepsilon + \sigma)\varphi^2 + [\varphi + r + \sigma + ((1 + a)r - \sigma)]\varphi^2 + 4\varphi^2 + 4\varphi^3 + 4b\varphi^2| \\ &= |4(2\varepsilon + \sigma) + 5\varphi + (2 + a)r + 4(b + 1)|\varphi^2 = B_{WF}. \end{aligned} \tag{3.10}$$

To get LB_{WF}, we follow a similar procedure, but using the second derivative of the Lyapunov function:

$$\begin{aligned} D_F^2 W(\mathbf{x},\mathbf{s}) = \quad & \dot{X}\left[\sigma(Y-X) - 2s(t)\varepsilon X\right] + X\left[\sigma(\dot{Y}-\dot{X}) - 2s(t)\varepsilon\dot{X}\right] + \\ & \dot{Y}\left[\left([1+as(t)]r - U^{(z)}\right)X - Y - U^{(x)}Z\right] + \\ & Y\left[((1+as(t))r - U^{(z)})\dot{X} - X\dot{U}^{(z)} - \dot{Y} - U^{(x)}\dot{Z} - Z\dot{U}^{(x)}\right] + \\ & \dot{Z}\left[U^{(y)}X + U^{(x)}Y - bZ\right] + Z\left[U^{(y)}\dot{X} + X\dot{U}^{(y)} + U^{(x)}\dot{Y} + Y\dot{U}^{(x)} - b\dot{Z}\right]. \end{aligned} \tag{3.11}$$

Of course, the stochastic sequences in these new derivatives are different from the stochastic sequences in the previous derivatives. To make this clear, we denote these new stochastic variables $\bar{\mathbf{s}}$, which means $D^2W(\mathbf{x},\mathbf{s},\bar{\mathbf{s}})$ is a function of the state variables and two different stochastic sequences. We place the bound on LB_{WF} in much the same way that we placed the bound on $B_{W\Phi}$. When finding the maximum value of the function $D^2W(\mathbf{x},\mathbf{s},\bar{\mathbf{s}})$, we must consider not only the optimal values of the state variables and the stochastic variables from the first derivative D_FW (i.e whether the function is maximized for $s=0$ or $s=1$), but we must also find the optimal values including the stochastic variables introduced by the second derivative D_F^2W. These calculations are somewhat tedious, so we omit them here. However, the reader should be able to reproduce the results, following these steps. Using the ideas above (term-by-term maximization of the derivatives and conservative (optimal) choices for the stochastic variables (0 vs 1)), we get the following bounds for the original

N-node networks (3.2) and (3.3):

$$\begin{aligned}
B_{W\Phi} = \quad & (N-1)\,\varphi^2|4(Np\varepsilon+\sigma)+5\varphi+(2+ap)r+4(b+1)|,\\
LB_{W\Phi} = \quad & (N-1)4\varphi\big[11\varphi^2+2\varphi\big(6r+3apr+8\sigma+3b+3p\varepsilon(N-1)+7\big)+2+2b^2+\\
& (2p\varepsilon(N-1))^2+r(6+3ap+4r+4apr+a^2p^2r+b+5ap\sigma+10\sigma)+4\sigma+\\
& 10\sigma^2+\sigma b+p\varepsilon(N-1)((2+ap)r+12\sigma)\big]\\
B_{WF} = \quad & (N-1)\,\varphi^2|4(N\varepsilon+\sigma)+5\varphi+(2+a)r+4(b+1)|\\
LB_{WF} = \quad & (N-1)4\varphi\big[11\varphi^2+2\varphi\big(6r+3ar+8\sigma+3b+3\varepsilon(N-1)+7\big)+2+2b^2+\\
& (2\varepsilon(N-1))^2+r(6+3a+4r+4ar+a^2r+b+5a\sigma+10\sigma)+4\sigma+10\sigma^2+\\
& \sigma b+\varepsilon(N-1)((2+)r+12\sigma)\big].
\end{aligned} \tag{3.12}$$

This completes the first step towards formulating the stability criterion.

The second step is to define the size of the δ-neighborhood of the ghost synchronization solution of the stochastic system (3.2). This is done by choosing a level curve of the Lyapunov function W_Φ for the averaged system (3.3):

$$V_0: \quad W_\Phi = \frac{1}{2}\sum_{i=1}^{N-1}\left\{\delta^2_{X_{i,i+1}}+\delta^2_{Y_{i,i+1}}+\delta^2_{Z_{i,i+1}}\right\}. \tag{3.13}$$

We let $\delta = \max\{\delta_{X_{12}},\ldots,\delta_{Z_{N-1,N}}\}$, which gives us the level $V_0 : W_\Phi \le \frac{3}{2}(N-1)\delta^2$. We define another level, V_1 as absorbing domain of the Lyapunov function, which we obtain by replacing each difference variable with its maximum value, subject to the constraints on $\mathbf{x}$. We obtain

$$V_1 : W_\Phi \le \frac{1}{2}(N-1)\left(8\varphi^2+4\left(\varphi+r+\sigma\right)^2\right). \tag{3.14}$$

These level curves let us define the following quantity:

$$\gamma = \min_{\mathbf{x}\in\mathbb{R},V_0\le W_\Phi\le V_1}|DW_\Phi(\mathbf{x})|.$$

Notice that the derivative of the Lyapunov function DW_Φ for the averaged system is similar to the quadratic form (3.9) where the stochastic variables $s(t)$ are replaced with probability

p. Under the condition that the coupling strength ε exceeds the threshold (3.5), we can bound γ by:

$$\gamma = (N-1)\left|Np\varepsilon + \sigma - 2\varphi - apr + 1 + b\right|\delta^2, \tag{3.15}$$

where the level V_0, corresponding to δ-synchronization yields the minimum value γ on the interval $V_0 \leq W_\Phi \leq V_1$. To derive the bound (3.15), we have used term-by-term mimimization/maximization and replaced the difference variables with δ and set $U^{(z)} = -(\varphi + r + \sigma)$ and $U^{(y)} = \varphi$.

We also define the following constants [69, 70] that use the bounds from (3.6), which help make the statement of the following theorem more manageable and explicit:

$$\begin{aligned} c &= \tfrac{1}{64(LB_{WF}+LB_{W\Phi})B_{WF}^2} \\ D &= 8(LB_{WF} + LB_{W\Phi}) \\ U_0 &= \left\{\mathbf{x} | W_\Phi(\mathbf{x}) < V_0 + \tfrac{4\gamma^2}{D}\right\}, \end{aligned} \tag{3.16}$$

where U_0 is a neighborhood of the synchronization solution of the averaged system (3.3) and is slightly larger that the level curve V_0, corresponding to δ-synchronization.

Theorem 3.1. *Assume that the coupling strength ε is strong enough, i.e greater than the bound given in (3.5), such that synchronization in the averaged network (3.3) is globally stable. Then, the following properties hold:*

- *If the switching time τ is small enough to satisfy*

$$\tau < \frac{c\gamma^3}{\ln\left[D\frac{(V_1-V_0)}{\gamma^2}\right]}, \tag{3.17}$$

  then the trajectory of the switching system (3.2) almost surely reaches the U_0-neighborhood of the ghost-synchronization solution, in finite time. Therefore, the switching network (3.2) converges to approximate synchronization globally and almost surely.

- *Assume that (3.17) holds and that $W(x(0)) \leq V_1$ (i.e the initial condition is chosen in*

the attracting domain). Let $P_1(n)$, $\forall n \in \mathbb{N}$, be the probability that it takes time $2n\frac{V_1-V_0}{\gamma}$ to reach U_0. Then

$$P_1(n) \leq \exp\left(-n\left(\frac{c\gamma^3}{\tau} - \ln\left[D\frac{V_1 - V_0}{\gamma^2}\right]\right)\right). \tag{3.18}$$

Proof *This theorem is a shortened version of the general theorem, Theorem 9.1, given in [70] and applied to the Lyapunov function (3.4) and its bounds (3.12)-(3.16) for the global stability of approximate synchronization in the stochastic network (3.2). The complete statement and proof of Theorem 9.1 can be found in [70].* □

Remark 1. *The difference between the δ- and U_0-neighborhoods is a technicality, coming from the proof of Theorem 9.1. The desired precision of the approximate synchronization in the switching network is defined by U_0 and can be explicitly calculated through δ. As δ is typically chosen arbitrarily, we generally view U_0-synchronization as δ-synchronization.*

Remark 2. *The probability bound (3.18) depends on the number of discrete steps n as this is the probability that the system will take at least time $2n\frac{V_1-V_0}{\gamma}$ to converge to the U_0-neighborhood. Notice that this time depends on how far from the neighborhood of the ghost synchronization solution lies from the border of the attracting domain, expressed via V_1.*

In order to make the theorem more explicit, we shall consider what this looks like when the attractor is in a typical chaotic regime, i.e let $r = 30$, $a = 2/30$, $b = \frac{8}{3}$, and $\sigma = 10$. Also, let $\delta = 0.1$. Doing this, we get

$$\begin{aligned} c = \; & 2187\Big[274877906944000(N-1)^2 \cdot \big(175 + 80\sqrt{15} + 6N\varepsilon\big)^2 \big(242021 + 52704\sqrt{15} + \\ & 9\big(173 + 34\sqrt{15}\big)p + 18p^2 + 18\varepsilon^2(N-1)^2(1+p^2) + 9\varepsilon(N-1)\big(91 + 32\sqrt{15} + \\ & (90 + 32\sqrt{15})p + p^2\big)\big)\Big]^{-1}, \end{aligned}$$

$$
\begin{aligned}
D = \quad & \tfrac{40960}{27} \cdot \Big(242021 + 52704\sqrt{15} + 9\big(173 + 64\sqrt{15}\big)p + 18p^2 + 18\varepsilon^2(N-1)^2(1+p^2) + \\
& 9\varepsilon(N-1)\big(91 + 32\sqrt{15} + (90 + 32\sqrt{15})p + p^2\big)\Big), \\
\gamma = \quad & |3.33 \times 10^{-3}(N-1)(-2.0687 \times 10^3 + (-6 + 3\varepsilon N)p|.
\end{aligned}
$$

To give the reader an idea of the magnitude of these numbers, we set $N = 2$, $\varepsilon = 1$ and $p = 0.5$, which gives us:

$$c \approx 7.14722 \times 10^{-23}, \;\; D \approx 6.84128 \times 10^{8}, \;\; \gamma \approx 6.895 \times 10^{-1}.$$

These values determine the size of the neighborhood $U_0 = \{\mathbf{x} | W(\mathbf{x}) < 0.05\}$. Turning our attention back to (3.17), we use the values that we have computed to get the explicit bound on τ for the two node stochastic network (3.2). Thus, if:

$$\tau < 7.5615 \times 10^{-25}, \tag{3.19}$$

then the probability (3.18) is bounded by:

$$P_1(n) \leq \exp\left(\frac{n\left(-2.34354 \times 10^{-23} + 30.993\tau\right)}{\tau}\right).$$

Of course, given the bound that we have on τ, it is evident that the probability (3.18) converges to 0 very quickly if τ is this small. This probability guarantees a few things that are not immediately clear. It shows that if the switching rate is fast enough, the stochastic system will not just asymptotically converge to the U_0-neighborhood, but converge in a finite amount of time, with the faster switching is, the shorter the time guaranteeing convergence is. This leads to an additional implication of this probability bound: it ensures that there is a window for values of τ in which the stochastic system will converge within some given finite time, i.e for $0 < \tau \leq \tau^*$. As we emphasized, the explicit bound given in (3.19) is very conservative; however, it rigorously proves that synchronization can be stably achieved in the switching network (3.2) even if the probability of switching p is small and *the network is disconnected most of the time*. It also suggests that the probability of not converging to

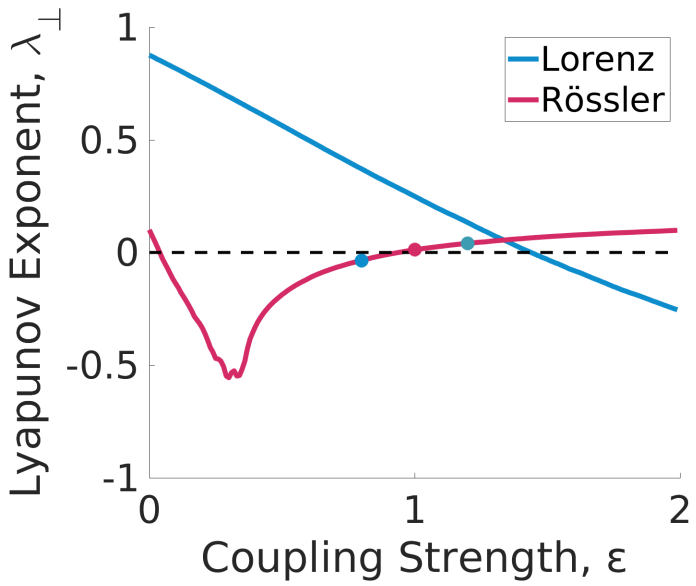

Figure 3.2 Transversal stability of synchronization in the averaged ten-node, x-coupled Lorenz network (blue) and the averaged ten-node, x-coupled Rössler system (pink), expressed via the Lyapunov exponent. For the Lorenz network, when $\varepsilon > \varepsilon^* \approx 1.5$, the system tends to synchrony, whereas for the Rössler system, there is a synchronization window for $\varepsilon^- < \varepsilon < \varepsilon^+$ the system exhibits synchronous behavior. The values of ε used in Fig. 3.5 are marked with dot in blue, pink, and green on the pink curve.

δ-synchronization within the finite time (see (3.18)) decreases at least exponentially fast as τ decreases.

In the following subsection, we present numerically calculated bounds in order to isolate a more realistic range of switching periods τ, corresponding to δ-synchronization.

3.2.2 Numerical Results

As an example, we consider a ten-node network of coupled Lorenz oscillators (3.2). Hereafter, the intrinsic parameters and the switching probability are chosen and fixed as follows: $r = 30$, $a = 2/30$, $b = \frac{8}{3}$, $\sigma = 10$, and $p = 1/2$. The coupling strength $\varepsilon = 3$ is chosen such that synchronization in the averaged system with $p\varepsilon = 1.5$ is stable (see Fig. 3.2.

Considering small values of τ, Fig. 3.3 shows that for $\frac{\varepsilon}{2} \approx \varepsilon^*$, the system synchronizes with probability 1 for $\tau = 0.0001$, but the probability decays rapidly for bigger values of τ, until $\tau \approx 0.01$, where there is no longer synchrony (also see Fig. 3.4). The window for

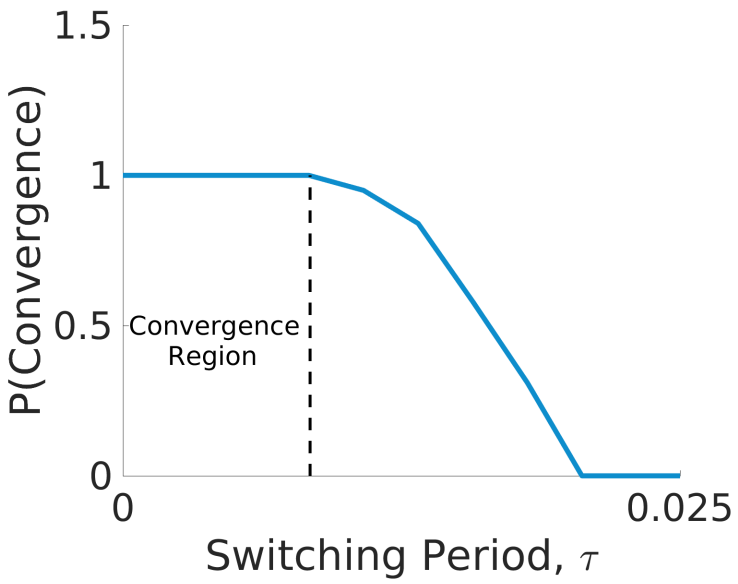

Figure 3.3 Probability of δ-synchronization in the stochastic ten-node Lorenz network (3.2) for small values of τ. For $\tau = 0.001$, and $\varepsilon = 3$, there is convergence with probability 1, which rapidly decays as τ increases. Nearly identical convergence probabilities for different choices of the integration steps.

convergence, $0 < \tau \leq \tau^*$ is guaranteed by the probability bound given by (3.18), and while this window is expected, the extent of it shown in Fig. 3.3 is not. There are circumstances for which not converging to the averaged system is favorable, and the present theory is not able to make definitive claims about the behavior of the stochastic system *beyond fast switching*. This leads us to explore the effects of non-fast-switching (where τ is not necessarily small) on the dynamics of the switching network.

3.3 Beyond Fast Switching: Windows of Opportunity

We consider switching networks (3.1) of Rössler and Duffing oscillators. These networks are known to exhibit synchronization properties distinct from those of the Lorenz network considered in Section 3.1. While the Lorenz network belongs to Class I, x-coupled Rössler networks and networks of coupled Duffing-type oscillators [145] are in Class II [28]. Class I networks synchronize when the coupling exceeds a threshold value, and synchronization remains stable for infinitely strong coupling (see Fig. 3.2 for the unbounded stability window

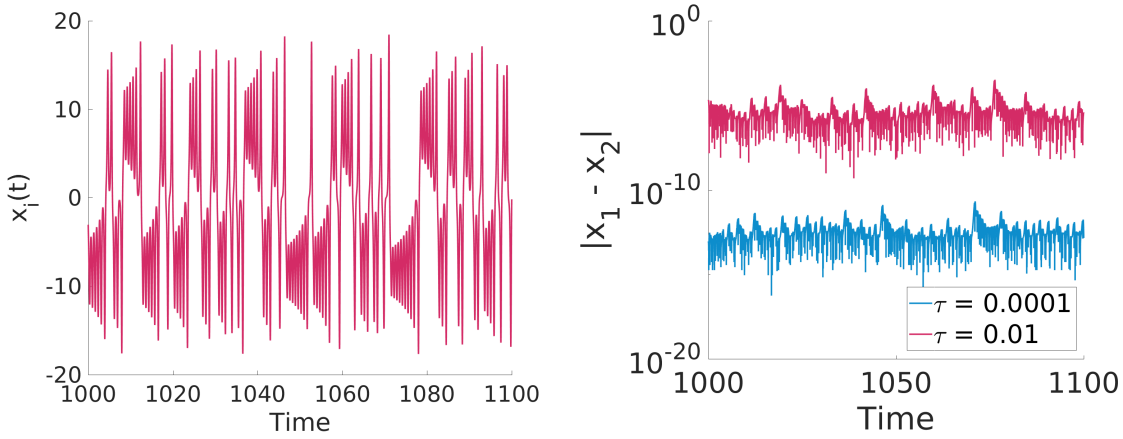

Figure 3.4 (left) Traces for x_1 (blue) and x_2 (pink) in the stochastic Lorenz network for $\tau = 0.0001$. The two traces practically coincide, showing δ-synchronization. (right): The synchronization error corresponding to two switching frequencies, $\tau = 0.01$ (pink) and $\tau = 0.0001$ (blue). The blue curve oscillates about a small value, close to 10^{-13}, because the stochasticity in the parameter r prevents the stochastic network from converging to complete synchronization. This mimics the expected behavior from Fig. 3.3.

.

for synchronization in the Lorenz networks, to the right from the threshold coupling value). Class II networks have a bounded range of coupling where synchronization remains stable (see a well in the stability diagrams of the Rössler and Duffing networks in Fig. 3.2 where synchronization loses its stability when the coupling increases). These differences between Class I and Class II networks generate distinct windows of switching frequencies, yielding stable synchrony in the corresponding switching networks.

It is important to emphasize that Class II networks such as x-coupled Rössler networks can only exhibit local synchronization within the stability well and global synchronization cannot be achieved/proved for any coupling. This is due to so-called shortwave length bifurcations [108] and the persistent presence of saddle fixed points, lying outside of the synchronization manifold in the phase space of the x-coupled Rössler system [21]. Hence, there are trajectories that escape to infinity, and the existence of the global absorbing domain cannot be proved. As a result, the above rigorous theory of global convergence to synchronization in fast switching networks cannot be applied to the Class II networks considered below.

3.3.1 x-Coupled Rössler Oscillators

We begin with a switching network of ten x-coupled Rössler oscillators:

$$\begin{aligned} \dot{x}_i &= -(y_i + z_i) + \sum_{j=1}^{N} \varepsilon_{ij} s_{ij} (x_j - x_i) \\ \dot{y}_i &= x_i + a y_i \\ \dot{z}_i &= b + z_i (x_i - c). \end{aligned} \tag{3.20}$$

Hereafter, the intrinsic parameters are chosen and fixed as follows: $a = 0.2$, $b = 0.2$, $c = 7$. To simplify multi-trial simulations, we did not include a stochastic intrinsic parameter into this system; however, all the reported windows of switching are robustly seen when it is present [78]. The averaged network is an all-to-all network, similar to that of the Lorenz network. As discussed above, synchronization in a network of x-coupled Rössler systems is known [109] to destabilize after a critical coupling strength ε^*, which depends on the eigenvalues of the connectivity matrix G. We choose the coupling strengths in the stochastic network such that the coupling in the averaged network is defined by one of the three values, marked in Fig. 3.2. In particular, for $\varepsilon = 1$, synchronization in the averaged network is unstable. As a result, synchronization in the fast-switching network is also unstable. Surprisingly, there is a window of intermediate switching frequencies for which synchronization becomes stable (see Fig. 3.5). In fact, the stochastic network switches between topologies whose large proportion does not support synchronization or is simply disconnected.

To better isolate the above effect and gain insight into what happens when switching between a connected network in which the synchronous solution is unstable, and a completely disconnected network in which the nodes' trajectories behave independently of one another, we consider a two-node Rössler network (3.20). Figures 3.6 and 3.7 demonstrate the emergence of synchrony windows for various intermediate values of τ for which the fast-switching network does not support synchronization. In essence, the system is switching between two unstable systems, and yet when the switching period τ is in a favorable range, the system stabilizes. Figure 3.7 also indicates the role of switching probability p and shows that the

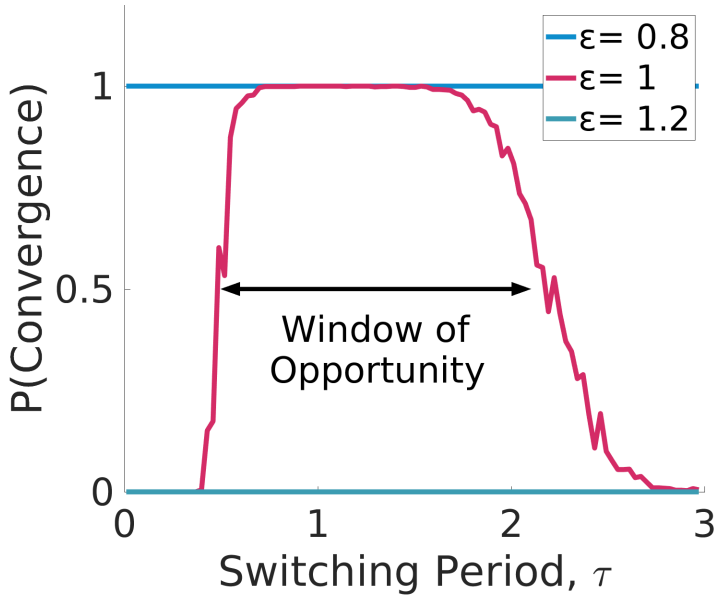

Figure 3.5 Probability of synchrony in the ten-node stochastic Rössler network with differing coupling strengths, showing the effects of varying τ. These are coupling strengths for which synchronization in the averaged system is stable (blue), weakly unstable (pink), and strongly unstable (teal), respectively (cf. Fig. 3.2 for the values marked with appropriately colored dots). The bell-shaped curve corresponds to an optimal range of non-fast switching $0.6 < \tau < 2.2$ (the "window of opportunity"), where synchronization in the stochastic network becomes stable with high probability, whereas synchronization in the corresponding averaged system is unstable ($\varepsilon = 1$). Switching probability $p = 0.5$. Probability calculations are based on 1000 trials.

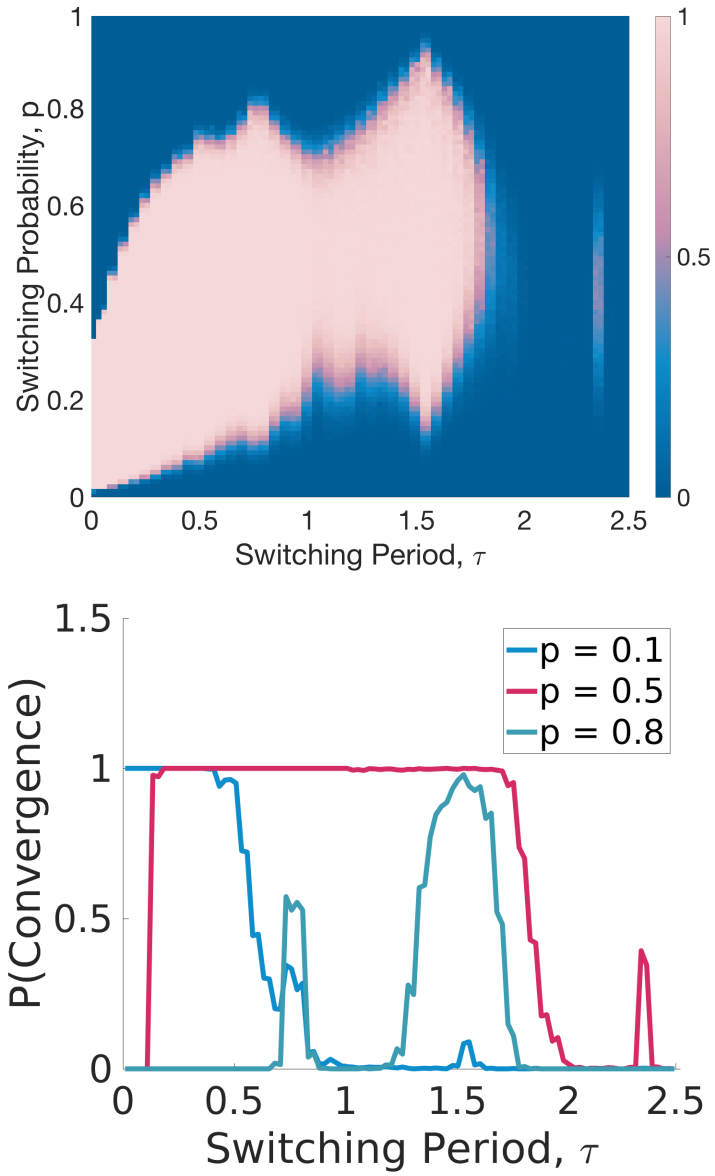

Figure 3.6 (top) Probability of synchrony in the two-node Rössler network (3.20) as a function of the switching probability p and switching period τ. Pink (lighter) colors correspond to higher probability of convergence (with light pink at probability 1) and blue (darker) colors correspond to lower probabilities (dark blue at probability 0). The coupling strength of the connection is fixed at $\varepsilon = 7$. As p increases, $p\varepsilon$, the effective coupling in the averaged/fast-switching network progresses through the window of synchrony indicated in Fig. 3.2. For the two-node network this interval is $p\varepsilon \in [0.08\ 2.2]$, yielding the stability range $p \in [0.011\ 0.31]$ (the pink interval on the y-axis) for $\epsilon = 7$ and small τ. (bottom) Slices from the top Figure for different p. Notice the emergence of "windows of opportunity" for not-fast switching periods at which synchrony in the fast-switching network is unstable. Switching probability around $p = 0.5$ yields the largest stability window. Probability calculations are based on 1000 trials.

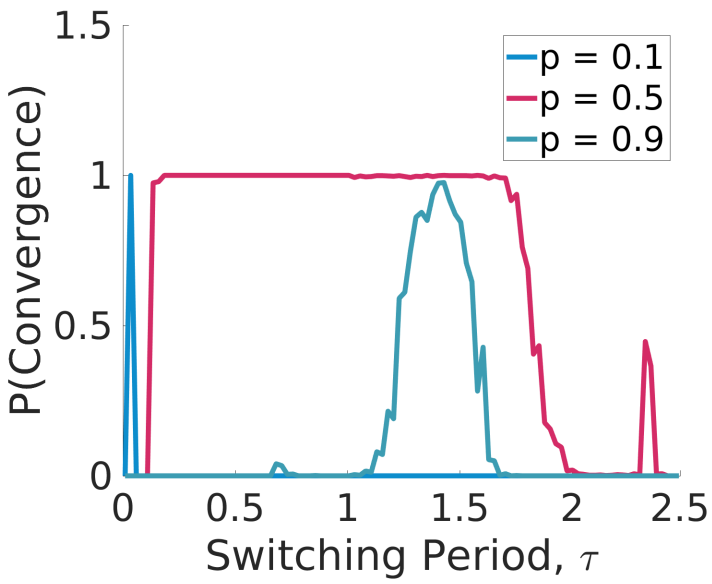

Figure 3.7 Role of switching probability p in the two-node Rössler network. $p\varepsilon = 3.5$ is chosen in the instability window in the fast switching network and kept constant when changing p. There is a window of opportunity for each chosen value of p ($p = 0.1$ (blue), $p = 0.5$ (pink), $p = 0.9$ (teal). Notice the largest window for $p = 0.5$, indicating a positive role of more probable re-switching between the unstable systems.

largest synchrony window is achieved at probability $p = 0.5$. This probability corresponds to the most probable (frequent) re-switching for a fixed switching period τ and indicates a stabilizing effect of re-switching. In an attempt to better understand the underlying phenomenon, we consider what happens in this connected/disconnected network when the switching is periodic instead of stochastic. We find that for periodic switching (the pink curve in Fig. 3.8) there is a window of similar length to when switching is stochastic, and for similar values of τ. Furthermore, when switching is periodic, we have an additional, though smaller, window for $\tau \in [4.5, 5]$.

The appearance of additional windows of opportunity in the periodically switching network and the overall better stability of synchronization, compared to the stochastic network can be explained by an analogy to the dynamics of Kapitza's pendulum. Kapitza's pendulum is a rigid pendulum in which the pivot point vibrates in a vertical direction, up and down [84]. The unusual property of Kapitza's pendulum is that the vibrating suspension can stabi-

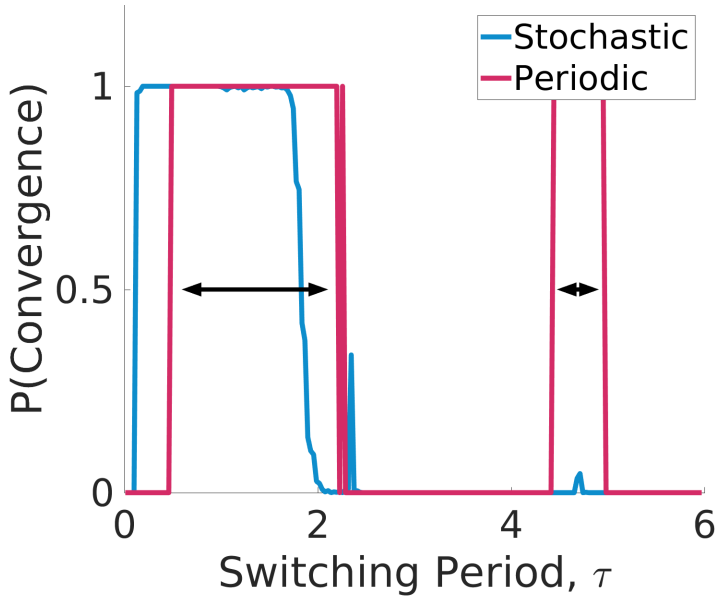

Figure 3.8 Comparison of the probability of synchrony in the two-node Rössler network in which switching is stochastic (blue) and periodic (pink) when switching is slow. The networks switch between two couplings strengths: $\varepsilon = 0$ and $\varepsilon = 7$, both corresponding to unstable synchrony. The averaged network with $\varepsilon = 3.5$ is also unstable for synchronization. There is substantial overlap between the two switching frequency windows that induce synchrony. Notice the second stability window for periodic switching (around $\tau = 4.5$) where stochastic switching fails to stabilize synchronization. Probability calculations are based on 1000 trials.

lize the pendulum in an upright vertical position which corresponds to an otherwise unstable equilibrium in the absence of suspension vibrations. This effect is also known as dynamic stabilization. Loosely speaking, the switching network of Rössler oscillators performs a similar function as it switches between two unstable networks, yet it dynamically stabilizes the synchronous state. In this context, the stabilizing oscillations around the unstable equilibrium in Kapitza's pendulum may be viewed as switchings in our network. While both periodic and stochastic vibrations of the suspension can stabilize Kapitza's pendulum, the periodic forcing clearly has an advantage over the stochastic perturbation as the latter can generate a sequence of "unfortunate" pushes in one direction, letting the pendulum pass the point of no return and fall down. The same is likely to happen in our network of Rössler systems where periodic switching provides better dynamic stabilization of the unstable synchronous state and has wider ranges of favorable switching frequencies.

3.3.2 Duffing Network

To demonstrate that the emergence of windows of opportunity is a general phenomenon in Class II networks, we consider a network of driven Duffing oscillators:

$$\begin{aligned} \dot{x}_i &= y_i \\ \dot{y}_i &= -x_i^3 - h y_i + q \sin(\eta t) + \varepsilon (x_j - x_i) \end{aligned} \tag{3.21}$$

for $i, j = 1, 2$, $i \neq j$. This network has a multiple window diagram for stability of synchronization (see Fig. 3.2 (bottom)) and belongs to Class II networks. The intrinsic parameters are chosen and fixed as follows: $\eta = 1$, $h = 0.1$, and $q = 5.6$ [145]. Figure 3.9 demonstrates the emergence of windows of opportunity for stable synchronization in an intermediate range of switching periods.

3.4 Chapter Summary

We have studied the stability of synchronization in dynamical networks with both stochastically switching connections and intrinsic parameters. In particular, we have proven

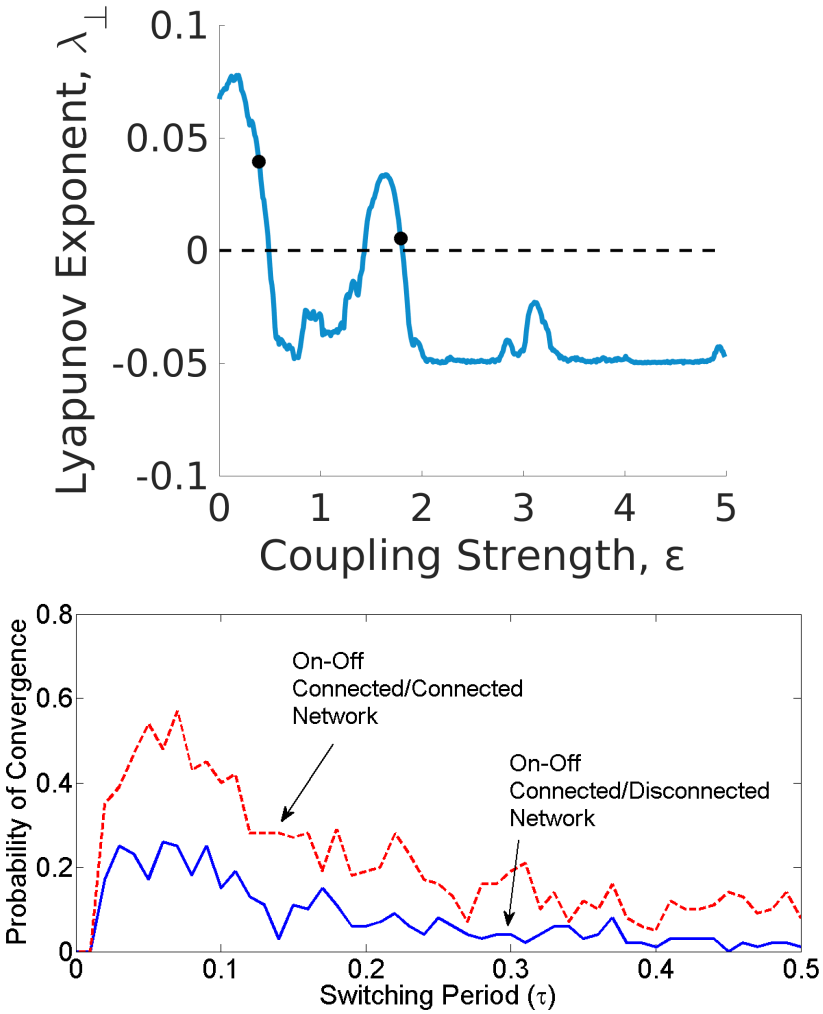

Figure 3.9 (top) Transversal stability of synchronization in the two-node, Duffing network (3.21). There are two synchronization windows, for $\varepsilon_1 < \varepsilon < \varepsilon_2$ and $\varepsilon_3 < \varepsilon$. (bottom) Probability of synchrony in the Duffing network. Switching probability: $p = 1/2$, number of trials: 100. (Blue solid line) On-off connected/disconnected network, switching between $\varepsilon = 0$ and $\varepsilon = 1.75$ (right black dot in (top)). (Red dashed line) On-off connected/connected network, switching between $\varepsilon = 0.45$ and $\varepsilon = 1.75$, (black dots in (top)) corresponding to two instability zones (top). In either case, the network switches between two configurations that do not support stable synchronization. Synchrony in the fast switching/averaged network is unstable, yet there are windows of opportunity, yielding stable synchrony for intermediate τ.

that approximate synchronization in the fast-switching network of Lorenz oscillators can be achieved globally and almost surely, provided that the corresponding averaged network synchronizes globally. For the first time, we have given the *explicit* bounds on the switching frequency sufficient for global synchronization and the probability that synchronization is achieved within some given finite time.

In this chapter, we have used examples to show that connections, that are only present with some probability p in a complex network, can stabilize synchronization even in a normally unstable regime. We have explored the possibilities when the time scale for the stochastic process does not approach zero, and showed that not-fast switching can be favorable, compared to fast switching, when one does not want to follow the dynamics of the averaged system. We have also shown that switching cannot be too slow, as this can make the system even more unpredictable. This gives the impression that there is some window for each system for which we have a sense of "controlled unpredictability." Moreover, this phenomenon also seemed to appear in [14] when we were analyzing an entirely different system whose parameters blink stochastically (i.e, not a network with stochastic connections). We named this controlled unpredictability, "windows of opportunity," to further emphasize that there seem to consistently be favorable conditions in which the stochastic and deterministic parameters match up appropriately, and allow the system to behave favorably, against all odds.

The numerical results for the non-fast switching networks reveal unexpected windows of opportunity and give plenty of insight as to the effects of stochastic coupling in dynamical networks (and how stochastic connections can actually be favorable to static ones). The effect of non-fast switching between stable two-dimensional nonlinear [10] and linear [91] systems has previously been analytically explored. An interesting observation is that switching at *exponential times* between two stable linear degenerate nodes can cause the trajectory to escape to infinity when the switching is not fast [91]. The highly nonlinear dynamical effects in multidimensional stochastic networks with non-fast switching reported in this chapter call for analytical approaches and techniques and represent a subject of future study.

CHAPTER 4

SYNCHRONY IN METAPOPULATIONS WITH SPORADIC DISPERSAL

In this chapter, we present a realistic example for which our framework of stochastically switching dynamical systems can be used. We study synchronization in ecological networks under the realistic assumption that the coupling among the patches is sporadic/stochastic and due to rare and short-term meteorological conditions. Each patch is described by a tritrophic food chain model, representing the producer, consumer, and predator. If all three species can migrate, we rigorously prove that the network can synchronize as long as the migration occurs frequently, i.e, fast compared to the period of the ecological cycle, even though the network is disconnected most of the time. In the case where only the top trophic level (i.e., the predator) can migrate, we reveal an unexpected range of intermediate switching frequencies where synchronization becomes stable in a network which switches between two non-synchronous dynamics. As spatial synchrony increases the danger of extinction, this counterintuitive effect of synchrony emerging from slower switching dispersal can be destructive for overall metapopulation persistence, presumably expected from switching between two dynamics which are unfavorable to extinction.

4.1 Introduction

Synchronization of the growth cycles in ecological networks of multi-species populations, called metapopulations, across a geographic region has been widely documented and studied (see, for example, [129, 50, 40] and the references therein). Multiple examples of population synchronization include moths and butterflies [67, 82], crabs [74], fish [129], birds [35], hares [129], lynx [51] and sheep [64].

The first example of population synchrony was given in the study of fur returns of Canadian lynx to the Hudson Bay Company [52]. The cause for spatial synchrony is believed

to be a combination of correlated atmospheric conditions (the Moran effect) [128, 36, 40, 73] and the presence of migration between population patches. Synchronization of Canadian lynx was initially attributed to the Moran effect; however, several studies have indicated that sufficiently strong dispersal in networks of tritrophic food chain models, related to the Canadian boreal forest, can induce synchrony without common atmospheric conditions (see for example, [27, 18]). These studies, supported by DNA analysis [139] revealing high dispersal of Canadian lynx over large distance between the East and West Coasts, suggest that dispersal plays a key role in spatial synchronization of the Canadian lynx. Moreover, there are numerous factors which can influence both the frequency and rate at which species migrate, and subsequently inhibit or promote spatial synchrony. It is generally accepted that the Moran effect is typically responsible for synchrony on the continental scale, whereas migration facilitates local, metapopulation synchrony.

In most theoretical studies, the migration is assumed to be a continuous process with net migration flow proportional (through a constant dispersal coefficient) to the unbalance of population densities. Under this assumption, the metapopulation model is an N-patch network of linearly coupled food-chain models with a static graph. The static interaction is typically assumed to be of diffusive nature (on an arbitrary coupling graph) and defined by a zero-row sum connection matrix (see, for example, [18]). There has also been a fair amount of work focused on density dependent migration models (for example, a model where predator migration is dependent on the prey density in a given patch [75]). However, a more realistic assumption could be that the dispersal among the patches is not constant, but of intermittent nature. More precisely, migration episodes are due to rare and short-term particular meteorological conditions such as high winds or strong water currents, but occur relatively frequently during the period of the ecological cycle. The prominent example of an ecological network with random, "blinking" interactions is a chain of lakes connected via narrow, shallow channels where the migration of algae and zooplankton is due to weak, random water currents. These sporadic algae-zooplankton interactions among the lakes have been shown to trigger synchronous algae outbreaks and crashes, resulting in synchronous

clear water episodes in Lake Lugano, Switzerland [130, 131]. Synchronization of insect-pest outbreaks in forests, connected by high, but sporadic winds has also been largely debated (see [132] and the references therein).

When considering migration within a metapopulation, it is natural to think of the metapopulation as a network of patches that is sporadically connected through migration routes by which species can travel from a patch to a nearby patch, such as, e.g., insects dispersing using favorable wind conditions. This means that to model the inherent stochasticity in the migration, we can turn the links between nodes in the network "on" and "off" randomly. This requires that both the time scale of the metapopulation and the stochastic process be considered in modeling (see [92, 37, 33] for the discussion on the problem of pattern and scale in Ecology). While stochastic dispersal and its role in population persistence have received a great deal of attention (see [156]), the patches are typically assumed to have simple dynamics and often described by simple discrete-time models.

In this chapter, we aim at the hardest case where individual patches can have chaotic dynamics which are described by the tritrophic Rosenzweig-MacArthur model [135]; in addition, one of the intrinsic parameters and the on-off dispersal between the patches are stochastic, with their own time-scales, ranging from fast to slow. We put the general blinking network model [19] with fast on-off stochastic connections into the ecological context and use the rigorous theory [69, 70, 14] on probabilistic convergence to derive upper bounds on the switching frequency of on-off dispersal to achieve approximate synchronization in the stochastic metapopulation network in the fast switching limit. More precisely, we show that if the migration of all three species is allowed, the stochastic ecological network converges to approximate synchrony globally and almost surely as long as the switching is fast and the dispersal strength is sufficiently strong to guarantee synchronization in the averaged network, obtained by replacing the stochastic variables with their means. Going beyond fast switching, we report a counterintuitive effect when non-fast switching makes synchronization stable even though it is unstable in the averaged/fast-switching network. In this case, the network, switching between two non-synchronous states, each of which supports population

persistence, can promote spatial synchrony and therefore increase the risk of extinction. We show that the effect is maximized when the probability of switching p is close to 0.5, suggesting a stabilizing effect of the most probable re-switching.

The layout of this chapter is as follows. First, in Section 4.2, we introduce the stochastic model and discuss its synchronization properties. Then, in Section 4.3, we consider the case when switching is fast. We formally state the main theorem, in which we derive explicit analytical upper bounds for the switching frequency for migration that guarantees synchrony. While we would ideally like to lead the reader through all of the ins and outs of the proof, we recognize some of the details are too technical (and spatially cumbersome) to include in the main text. For this reason, the majority of the proof can be found in Appendix B. In Section 4.4, we consider the case in which the switching is not fast (relative to the time scale of the ecological system), but not too slow. We find somewhat striking results for this intermediate switching, for which a rigorous theory has not yet been established. Finally, in Section 4.5, a brief discussion of the obtained results is given.

4.2 The Model and Problem Statement

4.2.1 Individual Patch Model

We use the tritrophic extension of the Rosenzweig-MacArthur prey-predator model [135] as the individual patch in the metapopulation stochastic network. The individual model reads

$$\begin{aligned} \dot{x} &= rx\left(1-\tfrac{x}{K}\right) - \tfrac{a_1xy}{1+a_1b_1x} \\ \dot{y} &= \tfrac{a_1xy}{1+a_1b_1x} - m_1y - \tfrac{a_2yz}{1+a_2b_2y} \\ \dot{z} &= \tfrac{a_2yz}{1+a_2b_2y} - m_2z, \end{aligned} \tag{4.1}$$

where x, y, and z are the producer, consumer, and predator population densities, respectively, r and K are the growth rate and carrying capacity of the producer, while a_1 and a_2 are conversion rates (a_1 from producer to consumer and a_2 from consumer to predator), with their respective saturation constants b_1 and b_2. Lastly, m_1 and m_2 are the mortality rates

of the consumer and predator, respectively[a]. The model (4.1) can exhibit periodic and chaotic behavior, including Shilnikov-type chaos [47, 90]. Hereafter, the mortality rate of the predator population m_2 is assumed to be lower than that of the consumer m_1 as predators typically have a longer life span than consumers (e.g., fish v.s. zooplankton in the algae-zooplankton-fish food chain). This assumption together with a high carrying capacity of the producer, K, typically leads to chaotic dynamics in the patch. Unless specified otherwise, the values of parameters $r = 1.15$, $K = 1.07$, $a_1 = 5$, $b_1 = 0.6$, $m_1 = 0.4$, $a_2 = 0.1$, $b_2 = 20$, $m_2 = 0.0037$ are chosen and fixed to place the individual model in a chaotic regime (see Fig. 4.1).

4.2.2 The Stochastic Network

Introduced in [19], the general "blinking" network [69, 70] fits well with the peculiar nature of random, sporadic interaction between metapopulations and can be used as the main tool in the study of synchronization in ecological models with realistic sporadic interactions. We consider a network composed of N tritrophic Rosenzweig-MacArthur prey-predator models (4.1), interconnected pairwise via stochastic dispersal:

$$\begin{aligned}
\dot{x}_i &= rx_i\left(1-\tfrac{x_i}{K}\right) - \tfrac{[a_1+\Delta a\xi_i(t)]x_iy_i}{1+a_1b_1x_i} + \varepsilon_x\sum_{j=1}^{N} s_{ij}(t)\,(x_j - x_i) \\
\dot{y}_i &= \tfrac{[a_1+\Delta a\xi_i(t)]x_iy_i}{1+a_1b_1x_i} - m_1y_i - \tfrac{a_2y_iz_i}{1+a_2b_2y_i} + \varepsilon_y\sum_{j=1}^{N} s_{ij}(t)\,(y_j - y_i) \qquad (4.2)\\
\dot{z}_i &= \tfrac{a_2y_iz_i}{1+a_2b_2y_i} - m_2z_i + \varepsilon_z\sum_{j=1}^{N} s_{ij}(t)\,(z_j - z_i)\,, \quad i = 1, ..., N,
\end{aligned}$$

where ε_x, ε_y, and ε_z are the coupling strengths (strengths of dispersal of the producer, consumer, and predator populations, respectively). Stochastic variables $s_{ij}(t)$ form the time-varying connectivity (Laplacian) matrix $C(t)$. We define the stochastic variables s_{ij} as we did in the previous chapter. Every migration link in the metapopulation network turns on and off, according to a similar probability law, and the migration between any two patches opens and closes in different time intervals independently. All possible migration links $s_{ij} = s_{ji}$ are

[a]The mortality rate for the producer is inherently included in the growth rate, r.

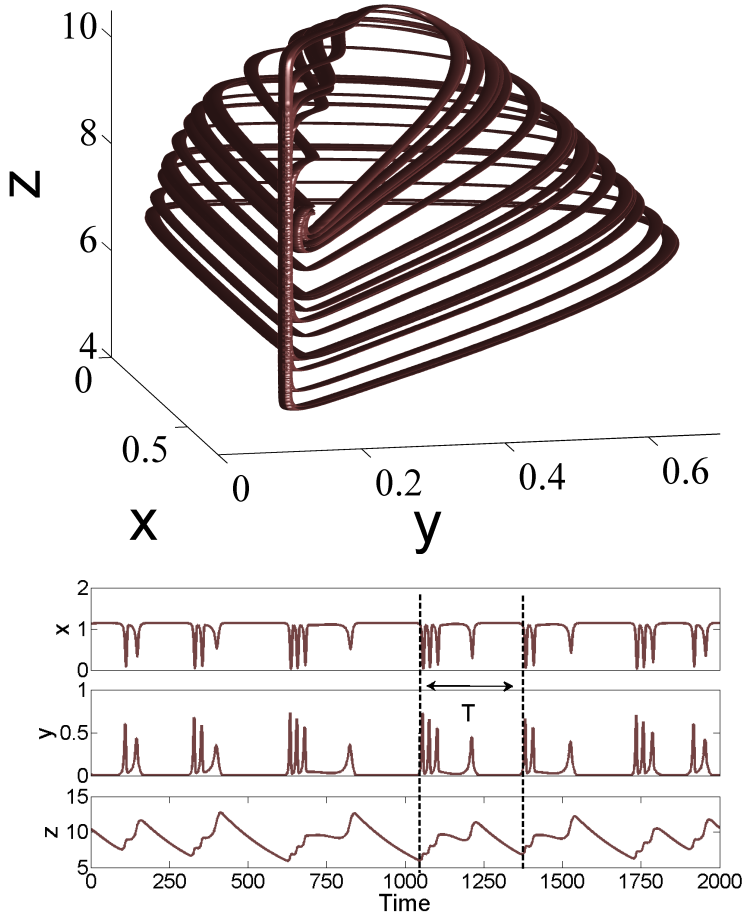

Figure 4.1 (Top): The chaotic attractor of the uncoupled patch model (4.1). The attractor resembles an upside down tea cup shape. (Bottom): The corresponding time series. The top, middle, and bottom graphs depict the time series for x, y, and z, respectively. The population size is given in a dimensionless unit. The dashed lines indicate the beginning and end of a population cycle, the characteristic period (T) of the metapopulation, which is approximately $T = 200$ units of time.

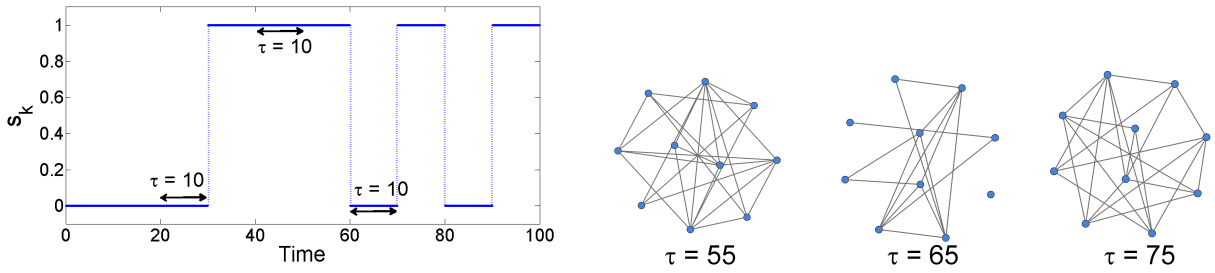

Figure 4.2 (Left): Example of the stochastic process with $p = 0.5$ and $\tau = 10$. The time axis is divided into intervals of length τ; for each interval, $s_k = 1$ with probability p and $s_k = 0$ with probability $1 - p$. (Right): Three different instances of the same stochastically switching network. Note the disconnected node in the network at $t = 65$, making network synchronization impossible during this lapse of time.

allowed to turn on and off so that the metapopulation network $C(t)$ remains constant during each time interval $[k\tau, (k + 1)\tau)$ between the re-switching and represents an Erdös-Rényi graph of N vertices (see Fig. 4.2).

The stochastically blinking sporadic interactions $s_{ij}(t)$ in the network (4.2) describe the stochastic opening of migration corridors when conditions are favorable (for example, heavy rains allowing fish to migrate to another lake through streams that are normally too shallow to traverse). It is also reasonable to assume that the intrinsic parameters of the individual patch model (4.1) can also be stochastic functions, similar to $s_{ij}(t)$. For example, when producer-consumer interaction rate a_1 switches between two different values based on some stochastic process; for instance, when the weather is especially fierce, a rabbit may not leave his burrow to eat grass. To account for this intrinsic stochasticity in patch i, we have replaced the traditional parameter a_1 (cf. (4.1)) with $[a_1+\Delta a\xi_i(t)]$, where $\xi_i(t)$ is a stochastic variable. For simplicity, we assume that $\xi_i(t)$ is governed by the same stochastic process (but by a different stochastic sequence) and can switch on and off at the same times as $s_{ij}(t)$. For example, strong winds, allowing the migration of insects between nearby patches, can also prevent the insects, already present in the patches, from food searching, thereby affecting parameter a_1.

This intrinsic stochasticity parameter makes the patches, comprising the network (4.2), non-identical such that complete synchronization between the patches is no longer possible.

However, approximate synchronization with fluctuating synchronization errors can be observed in this metapopulation network with stochastic connections and intrinsic parameters. Thus, we have knowingly decided to handle approximate synchronization in the mismatched network that better represents realistic ecological systems with no perfect symmetries. In the next section we will derive sufficient stability conditions of approximate synchronization in the stochastic network. The generalization of all the results of this chapter to networks of identical patches is straightforward.

4.3 Fast Switching

4.3.1 Comparing the Switching and Averaged Networks

If dispersal switching is fast compared to the ecological cycle of the individual patch, one can expect the behavior of the stochastic network (4.2) to be close to that of the averaged network, obtained by replacing the stochastic variables $s_{ij}(t)$ and $\xi_i(t)$ by their expected value, the switching probability p. Hence, the averaged network is an all-to-all coupled static network with weaker connections:

$$\begin{aligned}
\dot{x}_i &= r x_i \left(1 - \tfrac{x_i}{K}\right) - \tfrac{[a_1 + \Delta a \cdot p] x_i y_i}{1 + a_1 b_1 x_i} + \varepsilon_x p \sum_{j=1}^{N} (x_j - x_i) \\
\dot{y}_i &= \tfrac{[a_1 + \Delta a \cdot p] x_i y_i}{1 + a_1 b_1 x_i} - m_1 y_i - \tfrac{a_2 y_i z_i}{1 + a_2 b_2 y_i} + \varepsilon_y p \sum_{j=1}^{N} (y_j - y_i) \qquad (4.3) \\
\dot{z}_i &= \tfrac{a_2 y_i z_i}{1 + a_2 b_2 y_i} - m_2 z_i + \varepsilon_z p \sum_{j=1}^{N} (z_j - z_i) \,.
\end{aligned}$$

The fact that the fast switching network has the same dynamics as the averaged network seems apparent; however, there are exceptions and a rigorous proof is needed to show what parameters are responsible for the occurrence of the exceptions.

In the following, we apply this theory to synchronization in the ecological network (4.2) and derive bounds on the switching frequency that guarantees stable synchronization. Note that synchronization in the static averaged network (4.3) of identical patches is defined by the invariant hyperplane $M = \{x_1 = x_2 = ... = x_N,\ y_1 = y_2 = ... = y_N,\ z_1 = z_2 =$

$... = z_N\}$. At the same time this hyperplane is no longer invariant under the dynamics of the switching network (4.2) with stochastically mismatched parameters $[1+\Delta a\xi_i(t)]a_1$. Therefore, only approximate synchronization, when trajectories of the switching network approach and stay in a δ-neighborhood of the "ghost" synchronization solution is possible. We show that under the condition that the averaged network exhibits globally stable synchronization, the switching network reaches approximate synchronization, provided that the switching period is sufficiently small. While expected, this effect is not obvious as the switching network is disconnected most of the time, yet is able to synchronize.

4.3.2 Synchronization in the Averaged Network

Before proceeding with the study of the stochastic network, we should first understand synchronization properties of the averaged network. Following [18], we explore several scenarios of possible migration schemes between ecological patches when all three trophic levels (x, y, z-coupling) or only one trophic level can migrate. Figure 4.3 presents the Master Stability function [109] for synchronization in the averaged network. As Fig. 4.3 suggests the x, y, z-coupling when three species can migrate is the most effective mechanism for promoting spatial synchrony. Notice that the x, y, z-coupling has the lowest synchronization threshold $\varepsilon_x = \varepsilon_y = \varepsilon_z = \varepsilon = \varepsilon^*_{xyz}$ among the four migration schemes; and the largest stability zone, expanding to the right from $\varepsilon^*_{xyz} = 0.002$ up to infinite coupling strengths. If only one species can migrate, the dispersal of the consumer (i.e., the intermediate trophic level) is the most effective in establishing spatial synchrony. Notice that the dispersal of only producer (x-coupling) never induces synchrony, whereas the dispersal of predator (z-coupling) yields a bounded stability well such that increasing the dispersal strength ε_z eventually destabilizes the synchronization solution. The latter property of the z-coupled migration scheme will be used later in the chapter to discuss synchronization when exploring the effects of non-fast switching.

We choose the most effective migration scheme of x, y, z-coupling with $\varepsilon_x = \varepsilon_y = \varepsilon_z = \varepsilon$ to study synchronization in the averaged network (4.3) and approximate synchronization in

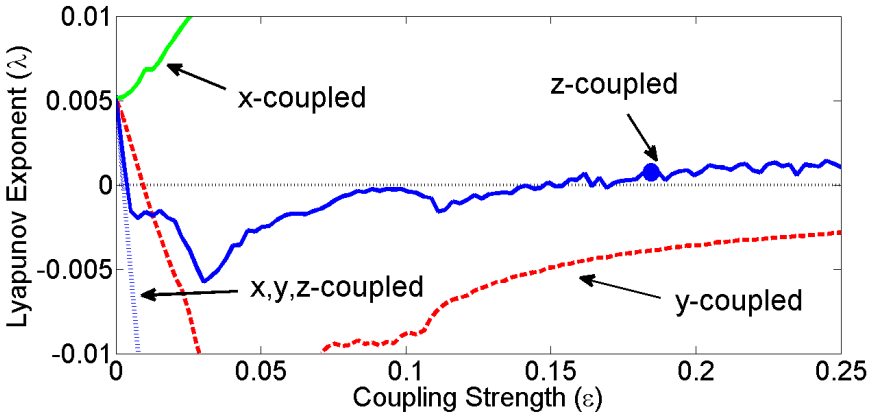

Figure 4.3 The largest transversal Lyapunov exponent (λ) vs. coupling strength ε for the two-patch x-coupled (green curve), y-coupled (red, dashed curve) z-coupled (blue curve) and x,y,z-coupled (blue, dotted curve) averaged network (4.3). $\lambda < 0$ corresponds to stable synchronization. While the x,y,z-coupled system is stable for all $\varepsilon > \varepsilon^*_{xyz} = 0.002$ (not shown), the z-coupled system has a window of stability, outside of which the patches exhibit asynchronous behavior. The solid circle ($\bullet$) indicates the value of $\varepsilon = 0.175$ used in the calculations for the non-fast switching case of Fig. 4.5.

the stochastic network (4.2). We first formulate conditions on the coupling strength sufficient for global stability of the synchronization hyperplane M.

Theorem 4.1: *Synchronization in the averaged x, y, z-coupled network (4.3) of n patches with coupling strength $p\varepsilon_x = p\varepsilon_y = p\varepsilon_z = p\varepsilon$ and the averaged intrinsic parameter $a_1^* = [1 + \Delta a \cdot p]a_1$ is globally asymptotically stable if coupling ε exceeds the critical value*

$$
\begin{aligned}
&\varepsilon^* = \tfrac{1}{p}\max\{\varepsilon_1, \varepsilon_2, \varepsilon_3, \varepsilon_4, \varepsilon_5\}, \ \text{ such that} \\
&p\varepsilon_1 > \tfrac{r}{N}; \ \ p\varepsilon_2 > \tfrac{1}{N}[\tfrac{1}{b_1} - m_1]; \ \ p\varepsilon_3 > \tfrac{1}{N}[\tfrac{1}{b_2} - m_2] \\
&(N\varepsilon_4 - r)(N\varepsilon_4 + m_1 - 1/b_1) > \tfrac{1}{2b_1^2}; \\
&(N\varepsilon_5 + m_1 - 1/b_1)(N\varepsilon_5 + m_2 - 1/b_2) > \tfrac{1}{2b_2^2}.
\end{aligned}
\tag{4.4}
$$

Proof. *The proof directly follows from the one given in [18] for the two-patch static network (4.3) (see the Appendix in [18]) where the coupling ε is replaced with $p\varepsilon$ and the network is extended to the all-to-all configuration with N patches.* □

4.3.3 Absorbing Domain

To obtain the lower bound for trajectories of the averaged network (4.3) with $\varepsilon_x = \varepsilon_y = \varepsilon_z = \varepsilon$, we notice upon examining (4.3) that the trajectories may not leave the region $A^+ = \{x_i > 0, y_i > 0, z_i > 0\}$ for initial conditions x_i,y_i,$z_i \geq 0$ such that the system is restricted to the positive orthant of $\mathbb{R}^{3N}$. Next, we must show that the system (4.3) is bounded in that orthant as well. To do this, we will introduce the following function:

$$V = \sum_{i=1}^{N} (x_i + y_i + z_i - \varphi), \tag{4.5}$$

where φ is a constant to be determined. We need to find the constant φ that makes V a Lyapunov-type function such the vector field of (4.3) on levels of V is oriented towards the origin.

We take the derivative of V with respect to system (4.3) and get

$$\dot{V} = \sum_{i=1}^{N} (\dot{x}_i + \dot{y}_i + \dot{z}_i) = \sum_{i=1}^{N} \left(r x_i (1 - \frac{x_i}{K}) - m_1 y_i - m_2 z_i \right), \tag{4.6}$$

where the terms $\pm \frac{[a_1 + \Delta ap] x_i y_i}{1 + a_1 b_1 x_i}$ and $\pm \frac{a_2 y_i z_i}{1 + a_2 b_2 y_i}$ and the coupling terms have canceled out.

Using the assumption that $m_1 > m_2$ (which is a natural assumption in ecological models), we can bound the RHS of (4.6) by replacing the term $m_1 y_i$ with $m_2 y_i$. This yields

$$\dot{V} < \sum_{i=1}^{N} \left(r x_i (1 - \frac{x_i}{K}) - m_2 (y_i + z_i) \right) < \sum_{i=1}^{N} \left(r x_i - \frac{r x_i^2}{K} - m_2 (\varphi - x_i) \right)_{V=0}, \tag{4.7}$$

where we have replaced the term $m_2(y_i + z_i)$ with its minimum value $m_2(\varphi - x_i)$, reached at $V = \sum_{i=1}^{N} (x_i + y_i + z_i - \varphi) = 0$ and, hence, $y_i + z_i = \varphi - x_i$. Therefore,

$$\dot{V} < \sum_{i=1}^{N} \left(r x_i (1 - \frac{x_i}{K}) - m_2 (\varphi - x_i) \right) \tag{4.8}$$

which implies that $\dot{V} < 0$ if $\varphi > \psi$, where

$$\psi = \frac{K}{4rm_2} \left(r + m_2\right)^2 . \tag{4.9}$$

This means that the region of the positive orthant bounded by V_ψ is an absorbing domain such that $0 \leq x_i, y_i, z_i \leq \psi$.

4.3.4 Stochastic Network: Rigorous Bounds

As in Chapter 3, to obtain the rigorous bounds for the switching system, we introduce the Lyapunov function

$$W = \sum_{i=1}^{N} \sum_{j>i}^{N} \frac{1}{2} \left(X_{ij}^2 + Y_{ij}^2 + Z_{ij}^2\right), \tag{4.10}$$

where $X_{ij} = x_j - x_i$, $Y_{ij} = y_j - y_i$, $Z_{ij} = z_j - z_i$ are the difference variables between the population densities in patches i and j. The averaged x, y, z-coupled network (4.3) and the corresponding stochastic network (4.2) have the same Lyapunov function, so we will differentiate between the two of them using W_Φ and W_F for the averaged and stochastic networks, respectively. Clearly, the zero of the Lyapunov function W_Φ corresponds to complete synchronization in the averaged network. At the same time, the trajectories of the stochastic network can only reach the neighborhood of the ghost synchronization solution in the stochastic network, therefore the Lyapunov function W_F cannot converge to zero, yet can become small. Governed by the stochastic switching, this Lyapunov function may increase temporarily, but the general tendency is to decrease. Therefore, the bounds of the sufficiently fast switching will have a probabilistic flavor.

The calculations of the probabilistic bounds are spatially cumbersome, therefore for clarity, we present a bound for the two-cell stochastic network (4.2) and its averaged analog (4.3) with the Lyapunov function (4.10) and $N = 2$. The two-cell stochastic network helps isolate the robust effect of synchronization as a result of stochastic switching as the network becomes and stays completely uncoupled for a large fraction of time when the probability of switching p is small. At the same time, the larger N-patch network can remain connected

or have at least most of the patches connected during a switching event (see Fig. 4.2). The extension of the rigorous bound to the n-patch network (4.2) is straightforward and can be performed.

Theorem 4.2. *Assume that the coupling strength $\varepsilon = \varepsilon_x = \varepsilon_y = \varepsilon_z$ is sufficiently strong, i.e greater than the bound given in (4.4), such that synchronization in the two-patch averaged x, y, z-coupled network (4.3) is globally stable. Assume that the switching period τ is small enough to satisfy*

$$\tau < \tau^*, \tag{4.11}$$

where the bound τ^* is given in (B.18) (see Appendix B). Then, the trajectory of the two-patch stochastic x, y, z- coupled network (4.2) almost surely reaches the U_0-neighborhood of the ghost synchronization solution, in finite time. Therefore, the stochastic x, y, z-coupled network converges to approximate synchronization globally and almost surely. The size of the U_0-neighborhood is defined by the level of the Lyapunov function W_Φ (4.10) ($N = 2$) such that $U_0 = V_0 + C_1$, where $V_0 = \frac{3}{2}\delta^2$ is the level of W_Φ with uniform synchronization mismatch $X_{12} = Y_{12} = Z_{12} = \delta$ and constant C_1 is given in (B.16). The constant δ in (B.17) controls the size of the U_0-neighborhood (i.e. the desired synchronization mismatch) and can be chosen arbitrarily small.

Proof. *This theorem directly follows from the conditions of the general theorem, Theorem 9.1, given in [70] and applied to the Lyapunov functions W_Φ and W_F (4.10) with $N = 2$ and their bounds on the first and second time derivatives, calculated along solutions of the averaged (4.3) and stochastic (4.2) networks. The details of their calculations are given in Appendix B.* □

Remark 1. *The bound (4.11)-(B.18) is conservative as it comes from the application of Lyapunov functions and large deviation bounds [70]. However, it explicitly relates the sufficient switching period τ with the probability p and strength of switching connections ε, the precision of synchronization δ, the size of the absorbing domain ψ, and the intrinsic parameters on the individual patch model. In particular, it suggests that the carrying capacity K and growth rate r of the producer, being the leading terms in (B.18), are destabilizing*

factors for promoting synchrony in the switching network as their increase lowers the bound τ^* and requires faster switching to maintain spatial synchronization.

Remark 2. *The bound (4.11)-(B.18) guarantees a few things that are not immediately clear. It shows that if the switching rate is fast enough, the stochastic system will not just asymptotically converge to the U_0-neighborhood, but converge in a finite amount of time. It also guarantees globally stable synchronization in the switching x, y, z-coupled network (4.2) even if the probability of switching p is very small and the network is decoupled most of the time.*

4.3.5 Numerics

We present numerically calculated bounds on τ to isolate the real window of switching periods τ, corresponding to approximate synchronization. As an example, we consider the two-patch xyz-coupled network (4.2) switching on and off with probability $p = 0.5$. The intrinsic parameter $a_1 = 4.99$ and $\Delta a = 0.04$ are such that the individual patch system switches between $a_1 = 4.99$ and $a_1 + p\Delta a = 5.01$, both corresponding to chaotic dynamics. The averaged individual system is the model (4.1) with $a_1 = 5$, being the mean value of the two parameter values. The other switching parameters, s_{ij}, turn on and off stochastically, according to the process that we laid out in Section 2. Note that s_{ij} and a_1 switch with separate identically and independently distributed stochastic processes both with the probability of an 'on' connection given by $p = 0.5$. To test how the theory holds up, we pick a coupling strength such that the average coupling is slightly stronger that the synchronization threshold, representing a challenging case for the onset of synchronization in the stochastic network. If switching is fast enough, we expect that the network synchronizes, whereas is switching is not fast enough, we expect to see asynchrony. In Fig. 4.4, we observe exactly what we expect to see from the theory. As switching is fast ($\tau = 0.0001$), the system tends to synchrony (this is shown by the red, dashed curve). Slower switching at $\tau = 0.01$ and $\tau = 1$ does not provide the desired synchronization accuracy. We also notice that as switching becomes less fast, our intuition about the behavior of the network is less and less

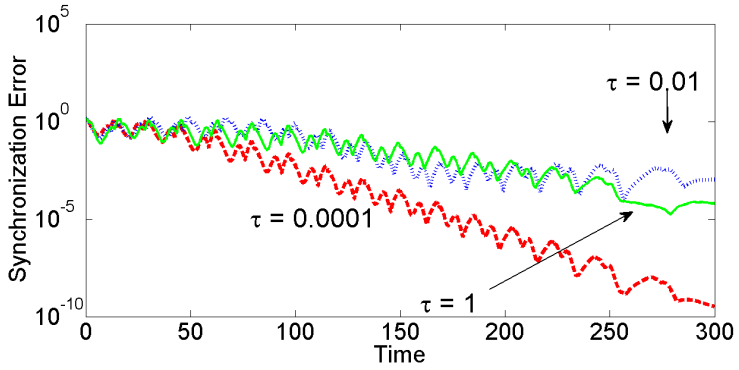

Figure 4.4 The effect of the switching period τ on synchronization in the two-patch (x, y, z)-coupled stochastic network. The synchronization error corresponding to three switching periods, $\tau = 0.0001$ (red, dashed curve), $\tau = 0.01$ (blue, dotted curve), and $\tau = 1$ (solid, green curve). Non-zero size oscillations in the neighborhood of the ghost synchronization solution are due to stochastic parameter mismatch. The coupling strength $\varepsilon = 0.005$.

reliable, because slower switching periods can tend to synchrony more quickly than faster switching periods when switching is not fast (compare the green ($\tau = 1$) and blue ($\tau = 0.01$) curves where the slower switching with $\tau = 1$ provides smaller synchronization errors for these particular switching sequences).

4.4 Non-Fast Switching

While in the previous section we considered x, y, z-coupled network desynchronizes when the switching is not sufficiently fast, z-coupled stochastic networks (4.2) yield a highly non-trivial synchronizing effect. This migration coupling scheme where only predators are allowed to migrate (coupling through the z-variable only) has synchronization properties distinct from those of x-, y- and x, y, z-coupled networks. This is the only migration scheme which has a *bounded* range of coupling ε, where synchronization remains stable (see a well in its stability diagrams in Fig. 4.3). As a result, a stronger coupling, pushing the network out of the stability well, destabilizes synchronization. It is important to notice that the z-coupled networks of Rosenzweig-MacArthur prey-predator models demonstrate only locally stable synchronization within the stability well and global synchronization cannot be achieved for any coupling. Therefore, the rigorous theory of global convergence to synchronization in fast

switching networks cannot be used for this network.

We choose the coupling strength $\varepsilon_z = \varepsilon = 0.35$ in the two-node z-coupled network, switching on and off with probability $p = 0.5$. When turned on, this excessively strong coupling corresponds to an asynchronous state of the network. When the coupling is turned off, the network is decoupled and cannot be synchronized. It is worth noticing that synchronization in the averaged network is also unstable as the mean coupling value $p\varepsilon = 0.175$, marked by a solid circle in Fig. 4.3, is outside its stability well. Thus, the network switches between two asynchronous regimes; when the switching is fast and its dynamics becomes close to those of the averaged network, synchronization in the network is unstable, as expected. However, we find a window of intermediate switching periods ($5 < \tau < 20$) in which approximate synchronization becomes stable with high probability, against all odds (see Fig. 4.5). To give the reader a sense of how these switching periods relate to the characteristic period of the individual patch's ecological cycle $T \approx 200$, we present the window of their ratio: $\frac{1}{40} < \frac{\tau}{T} < \frac{1}{10}$, suggesting that the coupling between the patches must be activated at least as many as 10 and as few as 40 times during the ecological cycle for stable approximate synchronization to emerge from switching between two non-synchronous dynamics. Figure 4.5 also shows that the probability $p = 0.5$ yields the largest window of synchronization and suggests the importance of the most probable re-switching between the non-synchronous dynamics to maximize the stabilization effect.

4.5 Chapter Summary

We have proposed a switching "blinking" network of tritrophic food-chain models as a realistic description of ecological networks where migration episodes are due to short-term meteorological conditions; however, the migration occurs relatively frequently during the characteristic period of the ecological cycle. Following [18], we showed that the dispersal of all the species is much more effective that those of one trophic level in promoting synchronized dynamics. We used this three-species dispersal case to derive explicit probabilistic bounds on the switching frequency sufficient for the switching stochastic network to synchronize almost

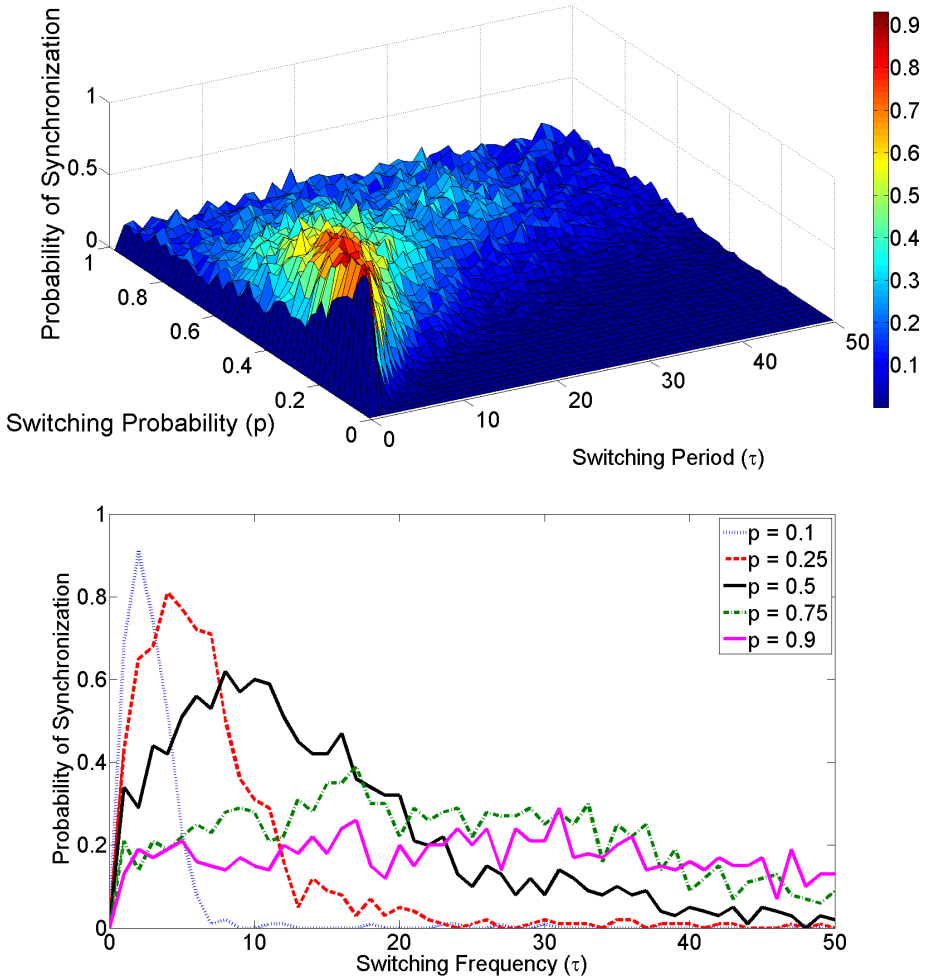

Figure 4.5 (Top) Probability of approximate synchronization in the two-patch z-coupled network as a function of the switching probability p and the switching period τ. The colors mirror the values on the z-axis, with red (lighter colors) corresponding to higher probability of convergence (with dark red at probability 1) and blue (darker colors) corresponding to lower probabilities (dark blue at probability 0). The coupling in the averaged network is fixed at $p\varepsilon = 0.175$, marked by • in Fig. 4.3, to be outside the stability well. As the probability p changes, the coupling strength ε in the stochastic network is adjusted to keep $p\varepsilon = 0.175$ unchanged. When switching is fast and the switching period τ is close to zero, the probability of synchronization is zero as the switching network behaves similarly to the unstable averaged network. Notice the large bump on the irregular surface indicating the emergence of approximate synchronization in a window of non-fast switching periods. (Bottom) Various cross-sections from the surface above. When p is small, such as for $p = 0.1$ (blue, dotted curve) and $p = 0.25$ (red, dashed curve), there are narrow windows for intermediate switching for which approximate synchronization is stable with high probability. For $p = 0.5$ (black curve), there is a trade-off between high probability of approximate synchronization and the length of the window for τ. Switching probability around $p = 1/2$ yields the largest stability window. When p is large, such as for $p = 0.75$ (green dotted curve), and $p = 0.9$ (magenta curve), the network does not converge to approximate synchronization consistently for any value of τ. Probability calculations are based on 100 trials.

surely and globally.

Going beyond fast switching, we considered a switching network where only the predator population can migrate and discovered a large window of intermediate switching periods in which synchronization in the switching network becomes stable even though it is unstable in the averaged/fast-switching network. In this case, the network switches between two asynchronous regimes; one corresponds to the uncoupled network, whereas the other is determined by a network topology with overly strong, desynchronizing dispersal. Yet, the network can synchronize in this "resonant" window of intermediate switching periods with high probability. In this context, the sporadic stochastic switching plays a constructive role in stabilizing metapopulation synchrony and indicates the importance of re-switching between the unstable states. At the same time, metapopulation synchrony increases the probability of extinction as all patches synchronously follow the same ecological cycle with typical outbreaks and crashes such that one patch in an endangered state cannot be saved by the migration from another equally endangered patch. In this respect, the role of stochasticity in the switching ecological network can be viewed as destructive as it decreases overall metapopulation persistence. Remarkably, the opposite examples of stochastic dispersal are available [156] where switching between two sets of dynamics, each of which leads to extinction, can promote persistence of marine organisms' metapopulations. However, the models and type of stochastic dispersal used in this study [156] are quite different from ours.

We have chosen identically distributed independent random variables as the driving stochastic process for the migration in the ecological network. As a result, migration episodes occur independently from each other. As the migration episodes are often governed by meteorological conditions that could be driven by a Markov process, the extension of this study to ecological networks where the probability of a migration episode depends on the present migration connections is an important research topic.

CHAPTER 5

WINDOWS OF OPPORTUNITY FOR SYNCHRONIZATION IN STOCHASTICALLY COUPLED MAPS

Several complex systems across science and engineering display on-off intermittent coupling among their units. Most of the current understanding of synchronization in switching networks relies on the fast switching hypothesis, where the network dynamics evolves at a much faster time scale than the individual units. We have presented numerical evidence demonstrating the existence of windows of opportunity, where synchronization may be induced through non-fast switching. Here, we study synchronization of coupled maps whose coupling gains stochastically switch with an arbitrary switching period. In this chapter, we determine the role of the switching period on the synchronization through a detailed analytical treatment of the Lyapunov exponent of the stochastic dynamics. Through closed-form and numerical findings, we demonstrate the emergence of windows of opportunity and elucidate their nontrivial relationship with the stability of synchronization under static coupling. Our results are expected to provide a rigorous basis for understanding the dynamic mechanisms underlying the emergence of windows of opportunity and leverage non-fast switching in the design of evolving networks.

5.1 Introduction

We focus on a *discrete-time* setting, where the coupling between the maps is held fixed for a finite number of time steps (switching period) and then it stochastically switches, independent of the time history. In this case, non-fast switching can be contemplated by rescaling the time variable and consequently modifying the individual dynamics of the coupled maps. This enables the formulation of a rigorous mathematical framework for the analysis of the stochastic stability of synchronization as a function of the switching period. We restrict

our analysis to two coupled maps with the two-fold aim of: i) providing a clear demonstration for the origin of this phenomenon, which may be hidden by topological factors in large networks and ii) establishing a toolbox of closed-form results for the emergence of windows of opportunity.

We study the stability of synchronization by analyzing the linear stability of an augmented system, associated with the linear mean square transverse dynamics. We perform a detailed analysis of the Lyapunov exponent of the transverse dynamics, based on the knowledge of the probability density function for the synchronized trajectory. We establish a necessary condition for stochastic synchronization in terms of the synchronizability of the coupled maps with a static coupling. The necessary condition can be used to demonstrate that switching between configurations which do not individually support synchronization will not stabilize stochastic synchronization for any switching frequencies. This is in contrast with networks of continuous-time oscillators where windows of opportunity for stable synchronization may appear as a result of switching between *unstable states* [78, 79, 80].

To illustrate our approach, we use the paradigm of two linearly coupled one-dimensional "sigmoid" maps, which encompasses the traditional logistic and tent maps. Statically coupled tent maps are known to have two symmetric ranges of positive and negative coupling for which synchronization is locally stable [71], and a similar behavior is observed for their smooth versions in the form of sigmoid maps. In our setting, we let the coupling stochastically switch between values within and outside these stability regions to explore the emergence of windows of opportunity. We demonstrate that while fast switching, occurring at each time step may not synchronize the maps, there can be a range of lower frequencies that yields stable synchronization. We argue that this is possible for coupled maps where the probability of switching between stable and unstable configurations is uneven, inducing a non-trivial balance between the dynamics of the coupled maps and the switching periods.

The layout of this chapter is as follows. First, in Section 5.2, we present the stochastic model of coupled maps and introduce the mean square stability of the transverse dynamics. In Section 5.3, we establish a mathematically-tractable form for the Lyapunov exponent of

the stochastic dynamics, which unveils its relationship with the stability of synchronization when the maps are statically coupled. We discuss two distinct cases where the individual map has a fixed point or exhibits chaotic dynamics. We derive a necessary condition for stochastic synchronization, implicitly involving the switching period required for stable synchronization. In Section 5.4, we study in detail the case of coupled sigmoid maps through both analysis and numerics. In Section 5.5, a brief discussion of the obtained results is given. Appendix C.1 contains the description of the sigmoid map along with its probability density function. Finally, Appendix C.2 presents the derivation of the closed-form expression of the Lyapunov exponent of stochastically coupled tent maps used to reveal windows of opportunity.

5.2 Linear Stability of Synchronization Under Stochastic Switching

5.2.1 Problem Statement

We study the stochastic synchronization of two maps characterized by the state variables $x_i \in \mathbb{R}$, $i \in \{1, 2\}$. We assume that the individual dynamics of each node evolves according to $x_i(k+1) = F(x_i(k))$, where $k \in \mathbb{Z}^+$ is the time step and $F\colon \mathbb{R} \to \mathbb{R}$ is a smooth nonlinear scalar function. The maps are linearly coupled through the stochastic gains $\varepsilon_1(k), \varepsilon_2(k) \in \mathbb{R}$, such that

$$\begin{bmatrix} x_1(k+1) \\ x_2(k+1) \end{bmatrix} = \begin{bmatrix} F(x_1(k)) + \varepsilon_1(k)(x_2(k) - x_1(k)) \\ F(x_2(k)) + \varepsilon_2(k)(x_1(k) - x_2(k)) \end{bmatrix}. \tag{5.1}$$

Each of the sequences of coupling gains, $\varepsilon_1(0), \varepsilon_1(1), \varepsilon_1(2), \ldots$ and $\varepsilon_2(0), \varepsilon_2(1), \varepsilon_2(2), \ldots$, is assumed to be switching stochastically at the same period $m \in \mathbb{Z}^+ \setminus \{0\}$. Every m time steps, the coupling gains simultaneously switch, such that $\varepsilon_1(mk) = \varepsilon_1(mk+1) = \ldots = \varepsilon_1(mk+m-1) = \tilde{\varepsilon}_1(k)$ and $\varepsilon_2(mk) = \varepsilon_2(mk+1) = \ldots = \varepsilon_2(mk+m-1) = \tilde{\varepsilon}_2(k)$ for every time step k, where $\tilde{\varepsilon}_1(0), \tilde{\varepsilon}_1(1), \ldots$ and $\tilde{\varepsilon}_2(0), \tilde{\varepsilon}_2(1), \ldots$ are two sequences of independent and identically distributed random variables.

The evolution of the coupled maps in equation (5.1) is determined by the random

variables $\tilde{\varepsilon}_1$ and $\tilde{\varepsilon}_2$, from which the coupling gains are drawn. In general, these random variables may be related to each other and may not share the same distribution. For example, in the case of uni-directional stochastic coupling, one of the random variables is zero; on the other hand, for bi-directional interactions, the two random variables coincide.

The current state of knowledge on stochastic synchronization of coupled discrete maps is largely limited to the case $m = 1$, for which the coupling gains switch at every time step [16]. In this case, the random variables $\varepsilon_i(0), \varepsilon_i(1), \varepsilon_i(2), \ldots$, for $i \in \{1, 2\}$, are mutually independent. For each value of k, $x_1(k+1)$ and $x_2(k+1)$ are functions only of the previous values $x_1(k)$ and $x_2(k)$, and equation (5.1) reduces to a first order Markov chain with explicit dependence on time through the individual dynamics. In the case of $m > 1$, the random variables $\varepsilon_i(0), \varepsilon_i(1), \varepsilon_i(2), \ldots$, for $i \in \{1, 2\}$, are no longer independent, which poses further technical challenges for the analysis of the system, while opening the door for rich behavior to emerge from the stochastically driven coupling.

The oscillators synchronize at time step k if their states are identical, that is, $x_1(k) = x_2(k)$. From equation (5.1), once the oscillators are synchronized at some time step, they will stay synchronized for each subsequent time step. The common synchronized trajectory $s(k)$ is a solution of the individual dynamics, whereby $s(k+1) = F(s(k))$. The linear stability of synchronization can be studied through the following variational equation, obtained by linearizing equation (5.1) in the neighborhood of the synchronization manifold:

$$\xi(k+1) = [F'(s(k)) - d(k)]\,\xi(k), \tag{5.2}$$

where prime indicates differentiation, $d(k) = \varepsilon_1(k) + \varepsilon_2(k)$ is the net coupling, and $\xi(k) = x_1(k) - x_2(k)$ is the synchronization error at time step k. Equation (5.2) defines the linear transverse dynamics of the coupled oscillators, measured with respect to the difference between their states $\xi(k)$. This quantity is zero when the two oscillators are synchronized. Equation (5.2) rests on the assumption that the mapping governing the individual dynamics, F, is differentiable everywhere. This assumption can be relaxed, however, to functions that

are differentiable almost everywhere [112].

Only the sum of the two coupling gains $\varepsilon_1(k)$ and $\varepsilon_2(k)$ affects the transverse dynamics, thereby only the statistics of the random variable $d(k)$ modulate the linear stability of the synchronization manifold. To simplify the treatment of the variational problem in equation (5.2), we can rescale the time variable with respect to the switching period as follows:

$$\tilde{\xi}(k+1) = \prod_{i=0}^{m-1} (F'(s(mk+i)) - \tilde{d}(k))\tilde{\xi}(k), \tag{5.3}$$

where $\tilde{\xi}(k) = \xi(mk)$ and $\tilde{d}(k) = \tilde{\varepsilon}_1(k) + \tilde{\varepsilon}_2(k)$. Equation (5.3) casts the variational dynamics in the form of a first order time-dependent Markov chain, generated by a linear time-varying stochastic finite difference equation [54, 89].

It is important to emphasize that the synchronization manifold $x_1(k) = x_2(k)$ is an invariant set of the stochastic equation (5.1). Therefore, the dynamics of the synchronization manifold is governed by an attractor of the mapping function $F(s(k))$.

5.2.2 Mean Square Stability of Synchronization

In determining the stability of the synchronous state, various criteria can be considered, such as almost sure, in probability, and mean square [54, 89]. The concept of mean square stability is particularly attractive, due to its practicality of implementation and its inclusiveness with respect to other criteria. Mean square stability of the synchronous state is ascertained through the analysis of the temporal evolution of the second moment of the error $\mathrm{E}[\tilde{\xi}^2]$, where $\mathrm{E}[\cdot]$ indicates expectation with respect to the σ-algebra generated by the switching. By taking the square of each side of equation (5.3) and computing the expectation, we obtain

$$\mathrm{E}\left[\tilde{\xi}^2(k+1)\right] = \mathrm{E}\left[\prod_{i=0}^{m-1} (F'(s(mk+i)) - \tilde{d}(k))^2\right] \mathrm{E}\left[\tilde{\xi}^2(k)\right]. \tag{5.4}$$

The above recursion is a linear, time-varying, deterministic finite difference equation

whose initial condition is $\tilde{\xi}^2(0)$, which is treated as a given value and not as a random variable. We say that equation (5.3) is mean square asymptotically stable if equation (5.4) is asymptotically stable, that is, if the Lyapunov exponent λ of equation (5.4) is negative. This implies that any small difference between the states of the oscillators will converge to zero in the mean square sense as time increases.

The Lyapunov exponent is a function of the switching period m and can be computed from equation (5.4) as follows [112]:

$$\lambda(m) = \lim_{k\to\infty} \frac{1}{k} \ln \prod_{j=0}^{k-1} \mathrm{E}\left[\prod_{i=0}^{m-1} (F'(s(mj+i)) - \tilde{d}(j))^2\right]. \tag{5.5}$$

In general, the stability of the synchronization manifold depends on the underlying synchronous solution, whereby $\lambda(m)$ in equation (5.5) explicitly depends on $s(k)$. In what follows, we focus on the case where $s(k)$ is a fixed point of the individual map or a chaotic trajectory. We comment that our approach is based on the linearized dynamics in equation (5.2), which describes small perturbations from the synchronous state. Thus, our analysis is only applicable to the study of local stability of the synchronization manifold, and initial conditions cannot be arbitrarily selected in the basin of attraction.

5.3 Main Results

5.3.1 Preliminary Claims

We assume that $\tilde{d}(k)$ takes values on a finite sample space $D = \{d_1, d_2, \ldots, d_n\}$ of cardinality n. For $l = 1, \ldots, n$, the probability that the net coupling is equal to d_l is chosen to be equal to p_l. For example, in the case of simple on-off connections, the individual coupling gains take values 0 and ε with corresponding probabilities p and $1-p$. Therefore, the net coupling gain $\tilde{d}(k)$ takes values $d_1 = 0, d_2 = \varepsilon$, and $d_3 = 2\varepsilon$ with corresponding probabilities $p_1 = p^2, p_2 = 2p(1-p)$ and $p_3 = (1-p)^2$.

From the individual values of the net coupling and their probabilities, we can evaluate

the Lyapunov exponent in equation (5.5) as

$$\lambda(m) = \lim_{k\to\infty} \frac{1}{k} \sum_{j=0}^{k-1} \ln \left[\sum_{l=1}^{n} p_l \prod_{i=0}^{m-1} (F'(s(mj+i)) - d_l)^2 \right]. \tag{5.6}$$

One of the central objectives of this study is to understand the relationship between the synchronizability of the coupled maps when statically coupled through the net coupling gains in D and their stochastic synchronizability when the net coupling randomly switches at a period m. Toward this aim, we adjust equation (5.6) to the case of statically coupled maps with a net coupling $d^\star$

$$\lambda^{\mathrm{st}}(d^\star) = \lim_{k\to\infty} \frac{1}{k} \sum_{j=0}^{k-1} \ln \left[(F'(s(j)) - d^\star)^2 \right]. \tag{5.7}$$

For convenience, we write $\lambda_l^{\mathrm{st}} = \lambda^{\mathrm{st}}(d_l)$ for $l = 1, \ldots, n$. Depending on the value of d_l, the statically coupled systems may synchronize or not, that is, the corresponding error dynamics may be asymptotically stable or unstable.

If all of the Lyapunov exponents of the statically coupled systems are finite, then we can establish the following relationship between the Lyapunov exponent of the stochastic error dynamics (5.6) and $\{\lambda_r^{\mathrm{st}}\}_{r=1}^n$:

$$\lambda(m) = m\lambda_r^{\mathrm{st}} + \lim_{k\to\infty} \frac{1}{k} \sum_{j=0}^{k-1} \ln \left[\frac{\sum_{l=1}^{n} p_l \prod_{i=0}^{m-1} (F'(s(mj+i)) - d_l)^2}{\prod_{i=0}^{m-1} (F'(s(mj+i)) - d_r)^2} \right]. \tag{5.8}$$

Equation (5.8) is derived from equation (5.6) by: i) dividing and multiplying the argument of the logarithm by $\prod_{i=0}^{m-1}(F'(s(mj+i)) - d_r)^2$; ii) using the product rule of logarithms; and iii) applying equation (5.7) upon rescaling of the time variable by the period m.

By multiplying both sides of equation (5.8) by p_r and summing over r, we obtain the following compact relationship between the Lyapunov exponent of the stochastic dynamics

and the individual Lyapunov exponents for statically coupled maps:

$$\lambda(m) = m \sum_{l=1}^{n} p_l \lambda_l^{\mathrm{st}} + \lim_{k\to\infty} \frac{1}{k} \sum_{j=0}^{k-1} \ln \frac{\sum_{l=1}^{n} p_l \zeta_l(j)}{\prod_{l=1}^{n} \zeta_l^{p_l}(j)}. \tag{5.9}$$

Here, we have introduced:

$$\zeta_l(j) = \prod_{i=0}^{m-1} (F'(s(mj+i)) - d_l)^2, \tag{5.10}$$

which we assume to be different than zero to ensure that the Lyapunov exponent stays finite.

The first summand on the right-hand side of equation (5.9) is linearly proportional to the switching period m and the "effective" Lyapunov exponent $\bar{\lambda} = \sum_{l=1}^{n} p_l \lambda_l^{\mathrm{st}}$, which corresponds to the average of the Lyapunov exponents associated with the statically coupled maps, weighted by the probability of the corresponding switching. The second summand is a residual quantity, which is always nonnegative and encapsulates the complex dependence of the transverse dynamics on the switching period beyond the linear dependence associated with the first summand.

5.3.2 Necessary Condition for Mean Square Synchronization

Proposition 5.1 *The synchronization of the stochastic system (5.1) is mean square stable only if the effective Lyapunov exponent $\bar{\lambda}$ is negative.*

Proof. *A lower bound for the Lyapunov exponent $\lambda(m)$ can be obtained by applying the weighted arithmetic-geometric mean inequality [31]*

$$\prod_{l=1}^{n} \zeta_l^{p_l} \leqslant \sum_{l=1}^{n} p_l \zeta_l. \tag{5.11}$$

From inequality (5.11), it follows that the argument of the logarithm in equation (5.9) is larger than or equal to 1. As a result, we obtain

$$\lambda(m) \geqslant m\bar{\lambda}. \tag{5.12}$$

This inequality establishes that for $\lambda(m)$ to be negative, $\bar{\lambda}$ must also be negative.

□

Remark 4 *From the previous claim, we posit if none of the Lyapunov exponents $\{\lambda_r^{\mathrm{st}}\}_{r=1}^n$ are negative, synchronization is not feasible for any selection of m and $\{p_r\}_{r=1}^n$. Thus, stochastic synchronization cannot be achieved without at least one coupling configuration to support synchronization. This is in contrast with observations from continuous-time systems which indicate the possibility of stable synchronization even if none of the coupling configurations support synchronization [79, 80].*

Remark 5 *The weighted arithmetic and geometric mean, introduced in (5.11), are equal if and only if $\zeta_1 = \zeta_2 = \ldots = \zeta_n$. Thus, inequality (5.12) reduces to an equality if and only if*

$$\prod_{i=0}^{m-1}(F'(s(mj+i))-d_1)^2 = \prod_{i=0}^{m-1}(F'(s(mj+i))-d_2)^2 = \ldots = \prod_{i=0}^{m-1}(F'(s(mj+i))-d_n)^2 \tag{5.13}$$

holds for any $j \in \mathbb{Z}^+$. For the case of chaotic dynamics, where $s(k)$ does not evolve periodically in time, this condition cannot be satisfied and (5.13) *is a strict inequality.*

For continuous-time systems [19, 68, 124, 125, 118, 119, 120, 122, 123], it was shown that under fast switching conditions the synchronizability of stochastically switching system can be assessed from the synchronizability of the averaged system. Here, we re-examine this limit in the case of coupled maps, whereby the averaged system is obtained by replacing the switching gain by its expected values. The synchronizability of the averaged system is ascertained by studying the Lyapunov exponent obtained by replacing $d^\star$ with $\mathrm{E}[d]$ in equation (5.7), that is,

$$\lambda^{\mathrm{aver}} = \lim_{k\to\infty}\frac{1}{k}\sum_{j=0}^{k-1}\ln\left[(F'(s(j))-\mathrm{E}[d])^2\right]. \tag{5.14}$$

In what follows, we demonstrate through examples that the weighted average Lyapunov exponent $\bar{\lambda}$ can be positive or negative, *independent* of the value of λ^{aver}. Therefore, the

averaged system does not offer valuable insight on the stability of the synchronization manifold of the stochastically coupled maps. For the sake of illustration, we consider the case in which the individual dynamics corresponds to the identity, such that

$$\begin{bmatrix} x_1(k+1) \\ x_2(k+1) \end{bmatrix} = \begin{bmatrix} x_1(k) + \varepsilon_1(k)(x_2(k) - x_1(k)) \\ x_2(k) + \varepsilon_2(k)(x_1(k) - x_2(k)) \end{bmatrix}. \tag{5.15}$$

In this case, the transverse dynamics in (5.2) takes the simple form

$$\xi(k+1) = [1 - d(k)]\,\xi(k). \tag{5.16}$$

Statically coupled identity maps should have a Lyapunov exponent given by (5.7) with $F'(s(j)) = 1$, that is,

$$\lambda^{\mathrm{st}}(d^\star) = \ln\left[(1-d^\star)^2\right]. \tag{5.17}$$

Suppose that the net switching gain is a random variable that takes values $d_1 = 1$ and $d_2 = -1$ with equal probabilities 0.5. Then, using equation (5.17) we compute

$$\bar{\lambda} = \frac{1}{2}\left(\lambda^{\mathrm{st}}(1) + \lambda^{\mathrm{st}}(-1)\right) = -\infty, \tag{5.18a}$$

$$\lambda^{\mathrm{aver}} = \lambda^{\mathrm{st}}(0) = 0 > \bar{\lambda}. \tag{5.18b}$$

Thus, the average coupling does not support synchronization, even though the effective Lyapunov exponent is negative.

Now, we assume $d_1 = 0$ and $d_2 = 2$ with the same probability 0.5, which yields

$$\bar{\lambda} = \frac{1}{2}\left(\lambda^{\mathrm{st}}(0) + \lambda^{\mathrm{st}}(2)\right) = 0, \tag{5.19a}$$

$$\lambda^{\mathrm{aver}} = \lambda^{\mathrm{st}}(1) = -\infty < \bar{\lambda}. \tag{5.19b}$$

This posits that the stochastically coupled maps cannot synchronize for any selection of the period m, even though the average coupling affords synchronization in a single time step.

If the difference between the possible values of the net coupling gain in D is sufficiently small, the stability of the stochastic system can be related to the stability of the error dynamics of the averaged system. In this case, if for all $l = 1, \ldots, n$, we can write $F'(x) - d_l$ as $F'(x) - \Delta d_l + \mathrm{E}[d]$, where $|\Delta d_l| \ll |F'(x) - \mathrm{E}[d]|$ is the deviation of the stochastic switching with respect to their expected value. Thus, we obtain

$$\bar{\lambda} = \sum_{l=1}^{n} p_l \lim_{k\to\infty} \frac{1}{k} \sum_{j=0}^{k-1} \ln\left[(F'(s(j)) - \mathrm{E}[d] + \Delta d_l)^2\right] \approx$$
$$\lim_{k\to\infty} \frac{1}{k} \sum_{j=0}^{k-1} \left(\ln\left[(F'(s(j)) - \mathrm{E}[d])^2\right]\right) + \sum_{l=1}^{n} \lim_{k\to\infty} \sum_{j=0}^{k-1} \frac{2p_l \Delta d_l}{F'(s(j) - E[d]} = \lambda^{\mathrm{aver}}, \quad (5.20)$$

where we have expanded the logarithm in series in the neighborhood of $F'(s(j)) - \mathrm{E}[d]$ and we have used the fact that $\sum_{l=1}^{n} p_l \Delta d_l = 0$ by construction.

5.3.3 The Case of Fixed Points

We start the analysis by considering synchronization at a fixed point s_0, that is, $s_0 = F(s_0)$. In this case, the computation of the Lyapunov exponent for the stochastically coupled system in equation (5.6) can be simplified as

$$\lambda(m) = \ln\left[\sum_{l=1}^{n} p_l e^{m\lambda_l^{\mathrm{st}}}\right], \quad (5.21)$$

where the Lyapunov exponents of the statically coupled maps are given by equation (5.7), which takes the following form:

$$\lambda_l^{\mathrm{st}} = \ln\left[(F'(s_0) - d_l)^2\right]. \quad (5.22)$$

Depending on the value of the Lyapunov exponents of the statically coupled maps (5.22) and the probabilities of occurrence of the corresponding gains, we classify three distinct behaviors of the function $e^{\lambda(m)} = \sum_{l=1}^{n} p_l e^{m\lambda_l^{\mathrm{st}}}$, given by the argument of the logarithm in (5.21), as shown in Fig. 5.1. The existence of these three behaviors can be demonstrated by

considering m as a real variable. First, we note that $e^{\lambda(m)}$ is a convex function in m, since its second derivative with respect to m is nonnegative. As m goes to 0, $e^{\lambda(m)}$ tends to 1 and its slope approaches $\overline{\lambda}$. As m goes to infinity $e^{\lambda(m)}$ will grow unbounded if there is a net coupling gain with nonzero probability that would not support synchronization.

Thus, if the coupling switches between states such that $\lambda_l^{\text{st}} < 0$ for all $l = 1, 2, \ldots, n$, $\lambda(m)$ will decrease with m and will always be negative (Fig. 5.1(top)). This corresponds to a system that stochastically switches between coupling gains which would individually lead to synchronization for statically coupled maps. In the case of maps of a higher dimension, a similar finding should not be expected given the possibility of complex, non-commuting eigenstructures [150]. On the other hand, if the coupling switches between values such that $\overline{\lambda} > 0$, $\lambda(m)$ will always be positive and will increase with m (Fig. 5.1(middle)).

Finally, if the system has at least one coupling gain corresponding to $\lambda_l^{\text{st}} > 0$, but $\overline{\lambda} < 0$, we may observe a window of opportunity. Specifically, if $e^{\lambda(1)} < 1$, the stochastically coupled maps will synchronize for $m = 1, \ldots, m^{\text{cr}} - 1$, where m^{cr} is the lowest integer such that $e^{\lambda(m^{\text{cr}})} > 1$, and will not synchronize for larger switching periods (Fig. 5.1(bottom)). Notably, such a window of opportunity must encompass the fast switching limit, $m = 1$, and disconnected windows are not feasible. For chaotic dynamics, we demonstrate that both these constraints can be relaxed, with disconnected windows of opportunity extending beyond the fast switching limit.

5.3.4 The Case of Chaotic Dynamics

Direct computation of the Lyapunov exponent as a limit of a time series from equation (5.6) or (5.9) may be challenging or even not feasible; for example, if $F'(x)$ is undefined on a finite set of points x. Following the approach of [71], we replace the summation with integration using Birkhoff's ergodic theorem [32].

Toward this aim, we introduce $\rho(x)$ as the probability density function of the map $F(x)$, defined on a set B and continuously differentiable on B except for a finite number of points. The probability density function of each map can be found analytically or numerically [24,

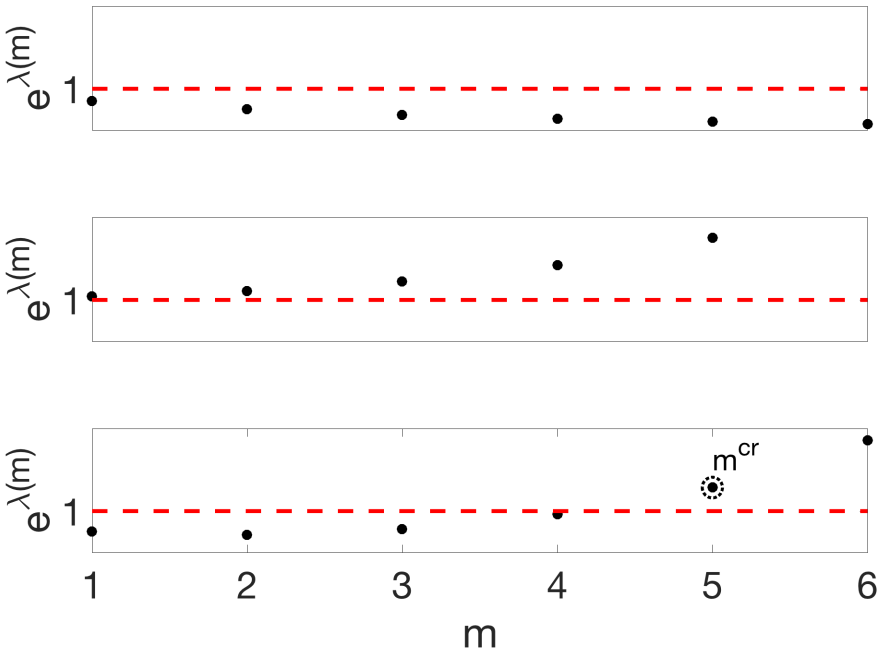

Figure 5.1 Stability analysis for fixed points. Lyapunov exponent for the stochastically coupled maps about a fixed point (5.21), where the net coupling switches between values such that: (top) $\lambda_l^{\mathrm{st}} < 0$ for $l = 1, 2, \ldots, n$; (middle) $\overline{\lambda} > 0$; and (bottom) $\overline{\lambda} < 0$ and $e^{\lambda(1)} < 1$.

30]. Using Birkhoff's ergodic theorem, equations (5.6), (5.7), and (5.9) can be written as

$$\lambda_l^{\mathrm{st}} = \int_B \ln\left[(F'(t) - d_l)^2\right]\rho(t)dt, \tag{5.23a}$$

$$\lambda(m) = \int_B \ln \sum_{l=1}^{n} p_l Y_l(t,m)\rho(t)dt, \tag{5.23b}$$

$$\lambda(m) = m\sum_{l=1}^{n} p_l \lambda_l^{\mathrm{st}} + \int_B \ln \frac{\sum_{l=1}^{n} p_l Y_l(t,m)}{\prod_{l=1}^{n} Y_l^{p_l}(t,m)}\rho(t)dt. \tag{5.23c}$$

Here, we have introduced the function of time and switching period

$$Y_l(t,m) = \prod_{i=0}^{m-1} (F'(F^i(t)) - d_l)^2, \tag{5.24}$$

where $F^i(t) = [F \circ F \circ \ldots \circ F](t)$ is the composite function of order i.

If the analytical expression of the probability density function is known, the Lyapunov

exponents can be found explicitly as further detailed in what follows when we study coupled tent maps. Numerical analysis can also benefit from the above formulation, which obviates with computational challenges related to uncertainties in rounding variables in equations (5.6), (5.7), and (5.9) for large values of k. This may be especially evident for large curvatures of the individual map, which could result in sudden changes in the synchronization dynamics.

Remark 6 *Equation set (5.23) can be used to explore the synchronizability of an N-periodic trajectory $s(Nk+i) = s_i$, where $i = 0, 1, \ldots, N-1, k \in \mathbb{Z}^+$, and $N \in \mathbb{Z}^+/\{0\}$, by using the appropriate probability density function [30] $\rho(s) = \frac{1}{N}\sum_{i=0}^{N-1} \delta(s - s_i)$, where $\delta(\cdot)$ denotes the Dirac delta distribution. Specifically, from (5.23a) and (5.23b), we establish*

$$\lambda(m) = \frac{1}{N}\sum_{i=0}^{N-1} \ln \sum_{l=1}^{n} p_l Y_l(s_i, m), \tag{5.25}$$

which reduces to the fixed point analysis presented in Section 5.3.3 for the case $N = 1$.

5.4 The Paradigm of the Coupled Sigmoid Maps

Here, we illustrate our approach for the analysis of stochastic synchronization of coupled chaotic maps by focusing on the so-called modified sigmoid function $S : [0, 1] \to [0, 1]$, see further details in Appendix C. The sigmoid map is a continuously differentiable function, which can be used to proxy the classical logistic and tent maps by varying a single control parameter, see Appendix C.1.

Lyapunov exponents are computed from equations (5.6) and (5.7) for stochastically or statically coupled maps by using a nominal trajectory $s(k)$ generated by initializing a sigmoid map with initial conditions, chosen randomly from the unit interval. In all computations, the argument of the logarithm in (5.6) and (5.7) is monitored at each time step to ensure it was above numerical precision.

We should comment that the direct computation of the Lyapunov exponent from the time series of the two coupled maps poses further technical challenges [112], related to: i) the varying size of the invariant manifold as a function of the coupling gain and the switching

period; ii) potential numerical overflow for diverging trajectories; and iii) false reading for trajectories converging within numerical precision.

The latter possibility should also be contemplated when studying synchronization from the error dynamics rather than the Lyapunov exponent [79] in the case of stochastic switching. For large values of the switching period, it may be possible that the error dynamics reaches values before numerical precision in correspondence of a coupling gain which would support synchronization in case of static coupling. As a result, the two trajectories become identical for all times, irrespective of the sequence of coupling gains. This possibility would lead to incorrectly identifying windows of opportunity.

5.4.1 Statically Coupled Maps

As a first step, we investigate the synchronizability of statically coupled maps in terms of the Lyapunov function for their transverse dynamics in (5.7). Specifically, we evaluate equation (5.7) for different values of the net coupling $d^\star$, ranging from -4 to 4, using a step of 0.0001. Simulations are run for 10,000 times steps, the first 10% of the data points are discarded, and the remaining 90% are averaged to estimate the Lyapunov exponent.

Figure 5.2 illustrates the dependence of the Lyapunov exponent on the net coupling gain for different values of the control parameter γ, ranging from 1 to 1000. As further elaborated in Appendix C.2, the selected range of the control parameter γ spans the case of logistic maps ($\gamma = 1$) and approximates the case of tent maps ($\gamma = 1000$). Figure 5.2(top) indicates the existence of disjoint intervals of $d^\star$, where the Lyapunov exponent is negative and synchronization is attained, similar to the tent map [71]. The existence, location, and extent of these intervals depend on the parameter γ. For $\gamma = 1$, these intervals do not exist, indicating that logistic maps do not synchronize for any selection of the coupling gains. As γ increases to approximately 10, we observe the formation of two narrow intervals where the maps synchronize.

Such intervals are generally not symmetric with respect to $d^\star = 0$, except for the limit cases of the logistic and tent map, due to the asymmetry in the probability density

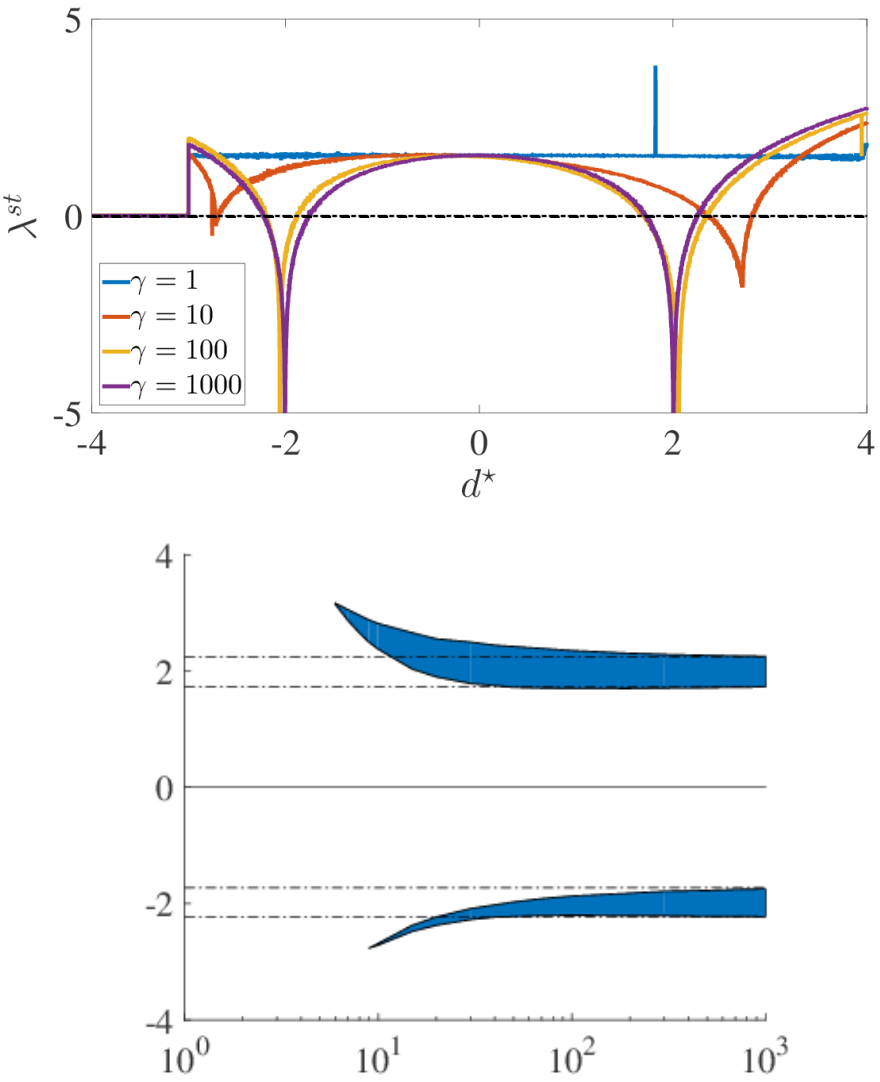

Figure 5.2 Synchronizability of statically coupled maps. (top) Lyapunov exponent of the transverse dynamics of two statically coupled sigmoid maps as a function of the net coupling $d^\star$ for different values of the parameter γ. Data are restricted to the interval $[-4, 4]$ for improved legibility. The dashed line identifies the limit of synchronization $\lambda^{\mathrm{st}} = 0$; and (bottom) range of the net coupling gain $d^\star$ that is supporting synchronization of the statically coupled sigmoid maps, as a function of the control parameter γ. The dashed line identifies the tent map solution [71].

function, which is elucidated in Appendix C.1. For the considered cases, we specifically find that the Lyapunov exponent is negative in the following approximate intervals for $\gamma = 10$, 100, and 1000, respectively: $(-2.72, -2.69)$ and $(2.37, 2.82)$; $(-2.20, -1.87)$ and $(1.70, 2.35)$; and $(-2.23, -1.75)$ and $(1.72, 2.25)$. Figure 5.2(bottom) also shows that the range of the Lyapunov exponent in these intervals is a function of the control parameter γ. Specifically, as γ increases we widen the range of variation of the Lyapunov exponent, which becomes infinitely large as γ goes to infinity and the sigmoid map approaches the tent map. In this case, synchronization may be possible within a single time step.

The role of γ on synchronizability is further illustrated in Fig. 5.2(bottom), where we depict the dependence of these intervals on the control parameter γ, which varies with a step of 1 for $\gamma \in [1, 10]$, 10 for $[10, 100]$, and 100 for $[100, 1000]$. Figure 5.2 suggests that synchronization becomes feasible for $\gamma = 6$, and that until $\gamma = 9$ only positive values of the net coupling gains ensure synchronization. As γ further increases, we observe that the intervals converge to theoretical predictions from the tent map, that is, $(-\sqrt{5}, -\sqrt{3}) \cup (\sqrt{3}, \sqrt{5})$. In these intervals, the Lyapunov exponent for the tent map is given by [71][a]

$$\lambda^{\mathrm{st}} = \ln|2 - d^{\star}| + \ln|2 + d^{\star}|. \tag{5.26}$$

5.4.2 Stochastically Coupled Maps

To elucidate synchronizability of stochastically coupled sigmoid maps, we assume that the net coupling gain d takes values d_1 and d_2 with corresponding probabilities p_1 and $p_2 = 1 - p_1$. The numerical computation of the Lyapunov exponent in (5.6) is performed for different values of d_2 from -4 to 4 with a step of 0.01 and m from 1 to 25 with a step of 1. The probability p_1 is held fixed to 0.5 and the net coupling gain d_1 to -1.90. Further, we consider the same four different values of γ as in Fig. 5.2.

This wide parameter selection allows for exploring the connection between the stabil-

[a]Note that equation (5.26) differs from equation (4.13) in [71] in a factor of 2 which is due to our analysis of mean square error dynamics.

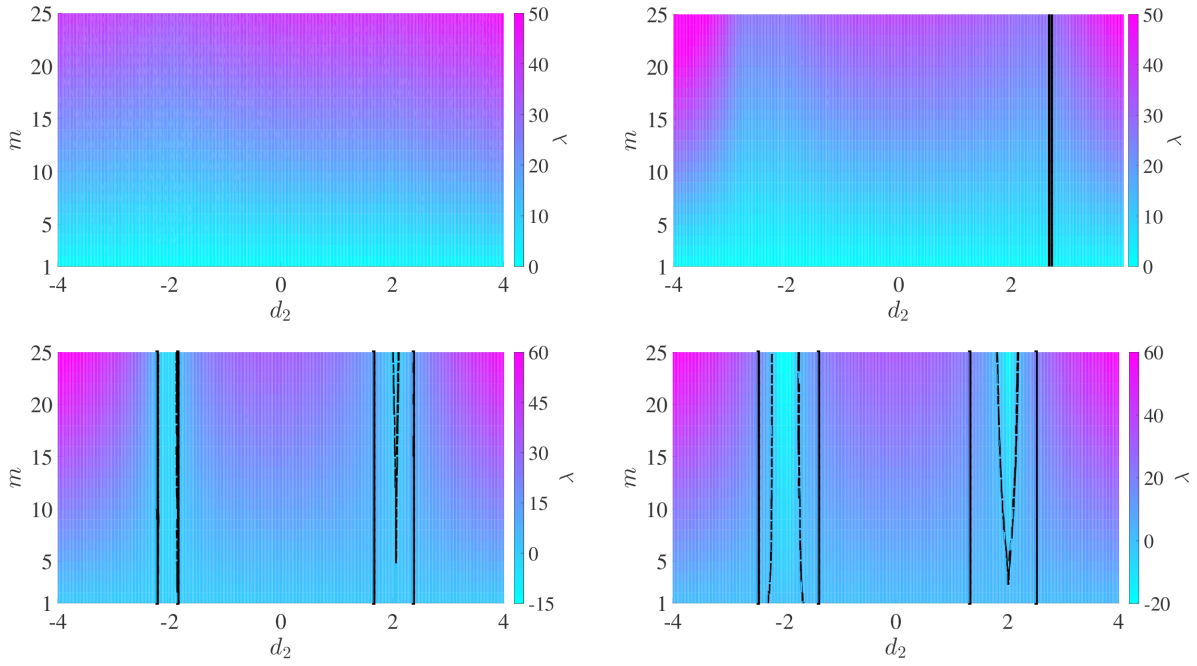

Figure 5.3 Synchronizability of stochastically coupled maps. Lyapunov exponent of two stochastically coupled sigmoid maps, where the net coupling is switching with equal probability between $d_1 = -1.90$ and d_2 at a period m. Each subfigure refers to a specific value of the control parameter γ, which is varied to elucidate the response of the sigmoid map ($\gamma = 1$) from the logistic to the tent map approximation ($\gamma = 1000$). The color bar illustrates the range of Lyapunov exponents attained for each value of γ. The dashed line identify the values of d_2 and m for which the Lyapunov exponent is zero; the regions within such contours correspond to negative values of the Lyapunov exponent and thus stochastic synchronization. The solid lines refer to the values of d_2 and m for which the effective Lyapunov exponent is zero, calculated analytically from statically coupled sigmoid maps. The vertical bands identified by such solid lines correspond to regions where stochastic synchronization is feasible, as predicted by Proposition 5.1. (For interpretation of the references to color in this figure legend, the reader is referred to the digital version of this chapter.)

ity of synchronization for static coupling and the resulting stochastic synchronization. We consider different cases, where stochastic switching is implemented on coupling gains which could individually support or hamper synchronization for statically coupled maps. Specifically, we contemplate the case in which: none (case I), one (case II), or both (case III) of the coupling gains yield synchronization. Simulations are run for $10^3 \times m$ times steps, the first 10% of the data points are discarded, and the remaining 90% are averaged to estimate the Lyapunov exponent.

Figure 5.3 demonstrates the dependence of the Lyapunov exponent on m and d_2 and the selected values of γ, including the logistic map ($\gamma = 1$) and the tent map approximation ($\gamma = 1000$). Therein, the dashed contour identifies the combination of m and d_2 for which the Lyapunov exponent is zero and synchronization initiates. The solid lines depict the values of d_2 for which the effective Lyapunov exponent is zero and synchronization may begin to be feasible based on the necessary condition in Proposition 5.1. The effective Lyapunov exponent is analytically calculated from the static Lyapunov exponents depicted in Fig. 5.2 for any value of d_2 and γ. Figure 5.4 illustrates the interplay between stochastic synchronization and the stability of synchronization for static coupling, grouped into cases I, II, and III. The possible combinations are identified through different colors, where darker colors (blue and green) mark windows of opportunity and lighter colors (yellow, orange, and red) correspond to asynchronous states.

For $\gamma = 1$, the Lyapunov exponent of the statically coupled logistic maps is positive for any value of the coupling gain (Fig. 5.2), which corresponds to case I where the switching is implemented between two configurations that would not support synchronization. As a result, there is no value of m which affords synchronization of the coupled logistic maps as shown in Figs. 5.3(a) and 5.4(a).

For $\gamma = 10$, we encompass both cases I and II, depending on the value of d_2, since $\lambda_1^{\text{st}} \approx 1.59$ and λ_2^{st} can be negative, as shown in Fig. 5.2. When applying our necessary condition, we cannot dismiss the possibility of stochastic synchronization, whereby we could attain a negative effective Lyapunov exponent for d_2 between 2.66 and 2.73, as shown in Fig. 5.3(b). However, the maps do not stochastically synchronize, since the Lyapunov exponent of the stochastically coupled maps is positive for all $m = 1, 2, \ldots, 25$, as displayed in Figs. 5.3(b) and and 5.4(b).

For $\gamma = 100$ and $\gamma = 1000$, we encompass cases II and III, depending on the value of d_2, since λ_1^{st} is negative ($\lambda_1^{\text{st}} \approx -0.08$ for $\gamma = 100$ and $\lambda_1^{\text{st}} \approx -0.83$ for $\gamma = 1000$). For both values of γ, we find two intervals of d_2 where the effective Lyapunov exponent, analytically calculated through Proposition 5.1, is negative. Specifically, it is negative when

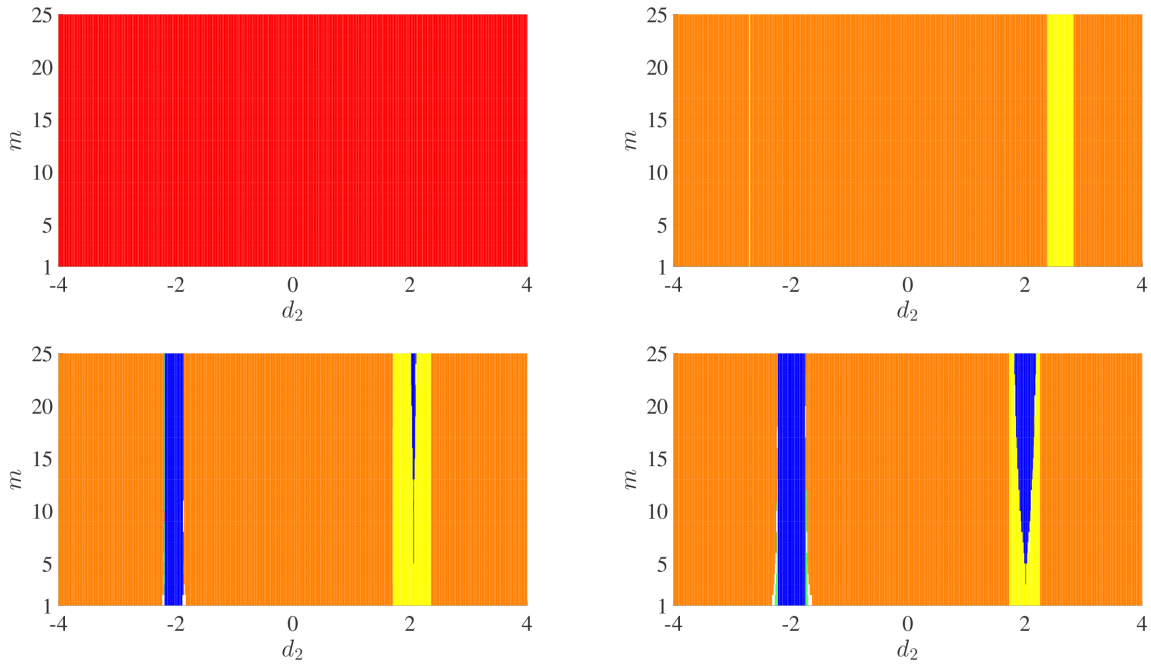

Figure 5.4 Interplay between synchronization in stochastically and statically coupled maps as in Fig. 5.3. The stochastic stability of the synchronization manifold for each pair d_2 and m is ascertained from the sign of the Lyapunov exponent in Fig. 5.3. The partition into cases I, II, and III is based on the sign of the Lyapunov exponent in Fig. 5.2, corresponding to the net couplings d_1 and d_2. The regions are colored as follows: red (case I); orange (case II without stochastic synchronization); yellow (case III without stochastic synchronization); green (case II with stochastic synchronization); and blue (case III with stochastic synchronization). White coloring identifies pairs of d_2 and m, for which synchronization cannot be precisely assessed due to oscillations in the Lyapunov exponent within ± 0.025. Note that case I prevents the possibility of stochastic synchronization. (For interpretation of the references to color in this figure legend, the reader is referred to the digital version of this chapter.)

$(-2.21, -1.88)$ and $(1.67, 2.37)$ for $\gamma = 100$, and $(-2.45, -1.40)$ and $(1.34, 2.49)$ for $\gamma = 1000$, as shown in Figs. 5.3(c) and (d). Regions of stochastic synchronization are located within these intervals as shown in Figs. 5.3(c) and (d). For $\gamma = 100$, the effective Lyapunov exponent provides a very close estimate of the region of synchronization in the vicinity for negative values of d_2.

As illustrated in Figs. 5.4(c) and (d), synchronization may be attained by switching between a coupling gain which supports synchronization and another which does not, as described by case II. This is particularly evident for $\gamma = 1000$, where we observe two thin triangular regions depicted in green where the instability of one of the coupling configurations does not hamper stochastic synchronization. For example, fast switching at $m = 1$ ensures synchronization for d_2 between approximately -2.29 and -1.67, which contains the range where λ_2^{st} is negative, that is, $(-2.23, -1.75)$.

Numerical results in Figs. 5.4(c) and (d) also indicate that case III, where each coupling configuration would independently lead to synchronization, *does not* guarantee stochastic stability of synchronization for any choice of the switching period. Specifically, for $d_2 > 0$, the region of stochastic synchronization has wedge-like shape, for which synchronization may only be possible for sufficiently large values of m. Notably, the wedges do not touch the $m = 1$ axis, whereby the stochastic Lyapunov exponents are found to be always positive for m less than 5 and 3 for $\gamma = 100$ and $\gamma = 1000$, respectively. Thus, fast switching between two coupling gains that would individually support synchronization does not produce stochastic synchronization. By increasing the value of m, we confirm our intuition that slowly switching in case III would favor stochastic synchronization, whereby we would trap the trajectory in a static coupling configuration which supports synchronization. By hypothesizing uniform stability of the synchronization manifold for each of the individual values of the net coupling gains, this claim could be proved in the context of the theory of dwell time [150][b].

Increasing the value of m in the numerical simulations to illustrate the role of slow

[b] While the stability of fixed points could be properly addressed by using dwell time theory, chaotic orbits pose further challenges associated with the existence of a common Lyapunov function.

switching is not feasible, due to the excessive lengths of the time series and resulting challenges in estimating the Lyapunov exponents. To address this issue and offer further validation for our claims, we focus on the case $\gamma \to \infty$, which corresponds to the tent map as further elaborated in Appendix C.1. Not only does the analytical treatment of the tent map addresses the issue of numerical overflow for long trajectories, but also it enables a closed-form solution of the stochastic Lyapunov exponents. Such an analytical result is critical for accurately resolving the transition between the regions shown in Fig. 5.4, which can be only approximately predicted through numerical computations.

A closed-form expression for the Lyapunov exponent of coupled tent maps can be derived from equation (5.23b) using the probability density function $\rho(t) = 1$, see Appendix C.2 for a precise derivation,

$$\lambda(m) = \frac{1}{2^m} \sum_{i=0}^{m} \binom{m}{i} \ln \left(\sum_{l=1}^{n} p_l (2 - d_l)^{2(m-i)} (2 + d_l)^{2i} \right). \tag{5.27}$$

We comment that for large m the binomial coefficient grows as $2^m/\sqrt{m}$ according to Stirling's formula, which ensures that the summation is well behaved in the slow switching limit [105].

Figure 5.5(left) extends the results presented in Fig. 5.3(d) by an order of magnitude in m through equation (5.27) specialized to binary switching. The effective Lyapunov exponent is directly computed from equation (5.26), which for the select parameters, $p_1 = p_2 = 0.5$ and $d_1 = -1.90$, yield the following intervals for d_2: $\left(-\sqrt{4 + \frac{1}{0.39}}, -\sqrt{4 - \frac{1}{0.39}}\right) \cup \left(\sqrt{4 - \frac{1}{0.39}}, \sqrt{4 + \frac{1}{0.39}}\right)$. Analytical results are in excellent agreement with numerical predictions for $\gamma = 1000$, offering compelling evidence for the accuracy of the proposed closed-form expression and the validity of our computational approach to estimate Lyapunov exponents. Importantly, analytical results for large periods in Fig. 5.5(right) confirm that slow switching in case III favors stochastic synchronization, whereby we observe that the blue regions vertically extends beyond $m = 25$ as numerically shown in Fig. 5.4(d). Figure 5.5(right) also confirms the existence of a thin green zone surrounding the blue bands, where synchronization is stable even though one of the coupling gains does not support synchronization (case

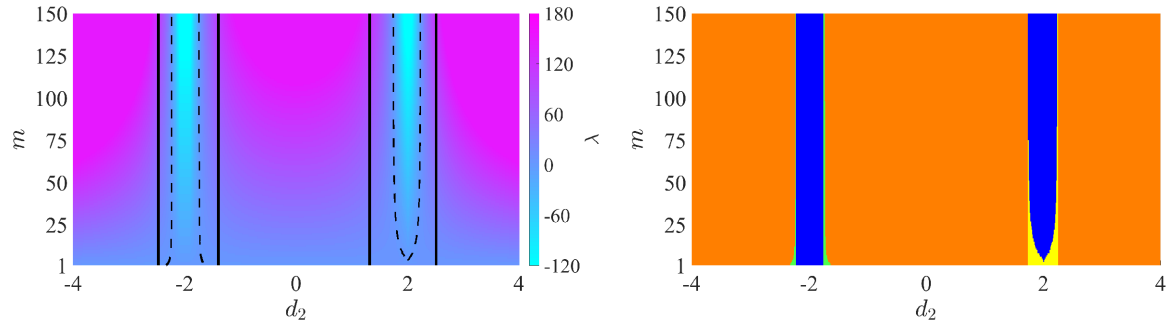

Figure 5.5 Analytical demonstration of slow switching synchronization. (left) Lyapunov exponent of two stochastically tent maps, where the net coupling is switching with equal probability between $d_1 = -1.90$ and d_2 at a period m, analytically computed from equation (5.27). The color bar illustrates the range of Lyapunov exponents attained for each value of γ. The dashed line identifies the values of d_2 and m for which the Lyapunov exponent is zero; the regions within such contours correspond to negative values of the Lyapunov exponent and thus stochastic synchronization. The solid lines refer to the values of d_2 and m for which the effective Lyapunov exponent is zero. The vertical bands identified by such solid lines correspond to regions where stochastic synchronization is feasible, as predicted by Proposition 5.1. (right) Interplay between synchronization in stochastically and statically coupled tent maps. The partition into cases I, II, and III is based on the sign of the Lyapunov exponent in equation (5.26), corresponding to the net couplings d_1 and d_2. The regions are colored as follows: orange (case II without stochastic synchronization); yellow (case III without stochastic synchronization); green (case II with stochastic synchronization); and blue (case III with stochastic synchronization). (For interpretation of the references to color in this figure legend, the reader is referred to the digital version of this chapter.)

II). For example, in the case of fast switching, $m = 1$, these regions are $(-2.33, -2.24)$ and $-1.73, 1.64$ from the closed-form expressions in equations (5.26) and (5.27).

The analytical solution in equation (5.27) allows for shedding further light on the possibility of synchronizing coupled maps in case II. Specifically, we consider switching between coupling gains $d_1 = -1.9999$ and $d_2 = 1.7000$, which are associated with $\lambda_1^{\text{st}} = -7.82$ (strongly stable synchronization) and $\lambda_2^{\text{st}} = 0.10$ (weakly unstable synchronization). We systematically vary the probability of switching p_1 from 0.6 to 1 with a step 0.001, so that when the coupled maps spend most of the time with the coupling gain that would support synchronization. In this case, the effective Lyapunov exponent is always negative, and synchronization may be attained everywhere in the parameter space.

Surprisingly, under fast switching conditions, synchronization is not attained if $p_1 \lessapprox 1$

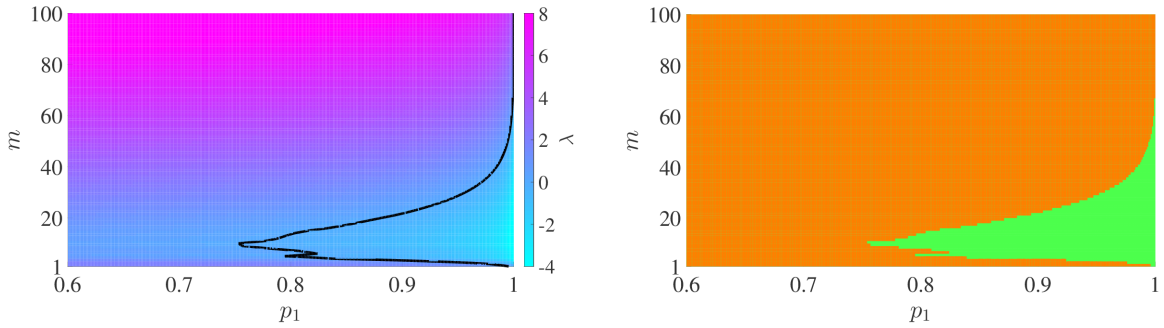

Figure 5.6 Analytical demonstration of emergence of windows of opportunity. (left) Lyapunov exponent of two stochastically tent maps as a function of the switching probability p_1 and the period m, analytically computed from equation (5.27) with $d_1 = -1.9999$ and $d_2 = 1.7000$. The color bar illustrates the range of Lyapunov exponents attained for each value of γ. The dashed line identify the values of d_2 and m for which the Lyapunov exponent is zero; the regions within such contours correspond to negative values of the Lyapunov exponent and thus stochastic synchronization. (right) Interplay between synchronization in stochastically and statically coupled tent maps. For the select values of the net couplings, $\lambda_1^{\text{st}} = -7.82$ and $\lambda_2^{\text{st}} = 0.10$, which correspond to case II. The regions are colored as follows: orange (case II without stochastic synchronization) and green (case II with stochastic synchronization). (For interpretation of the references to color in this figure legend, the reader is referred to the web version of this chapter.)

as shown in Fig. 5.6. Although the maps spend most of the time in a configuration that would strongly support synchronization, the sporadic ($p_2 \approx 0$) occurrence of a coupling gain which would lead to weak instability hampers stochastic synchronization under fast switching. Increasing the switching period, synchronization may be attained for $p_1 > 0.995$ (see the "Pinocchio nose" in Fig. 5.6(right)). For $0.753 < p_1 < 0.795$, we observe a single window of opportunity, whereby synchronization is achieved in a compact region around $m = 10$. For $0.795 \lessapprox p_1 \lessapprox 0.824$, a second window of opportunity emerges for smaller values of m around 5. The two windows ultimately merge for $p_1 \approx 0.83$ in a larger window that grows in size as p_1 approaches 1.

5.5 Chapter Summary

While the study of synchronization in evolving dynamical networks has been recently gaining significant momentum, the vast majority of rigorous mathematical investigations fo-

cus on the case of fast switching network topology as compared to the individual, intrinsic, node dynamics. In this chapter, we have made a first step towards understanding synchronization in stochastically switching networks of coupled maps beyond the fast switching limit.

To isolate the delicate mechanisms underpinning stochastic synchronization, we have considered two coupled maps with independent identically distributed stochastic switching and studied the stability of synchronization as a function of the switching period. We have studied the stochastic stability of the transverse dynamics using the notion of mean square stability, establishing a mathematically-tractable form for the Lyapunov exponent of the error dynamics. We have demonstrated the computation of the stochastic Lyapunov exponent from the knowledge of the probability density function. A necessary condition for stochastic synchronization has been established, aggregating the Lyapunov exponents associated with each static coupling configuration into an effective Lyapunov exponent for the stochastic dynamics. We have focused on the sigmoid map, which bridges the logistic and tent maps as a function of a single control parameter. For tent maps, we have established a closed-form expression for the stochastic Lyapunov exponent, which helps dissecting the contribution of the coupling gains, switching probabilities, and switching period on stochastic synchronization.

We have demonstrated the central role of non-fast switching, which may provide opportunity for stochastic synchronization in a range of switching periods where fast switching fails to synchronize the maps. More specifically, non-fast switching may promote synchronization of maps whose coupling alternates between one configuration where synchronization is unstable and another where synchronization is stable (case II). These windows of opportunity for the selection of the switching period may be disconnected and located away from the fast switching limit, where the coupling is allowed to change at each time step.

In contrast to one's expectations, fast switching may not even be successful in synchronizing maps that are coupled by switching between two configurations that would support synchronization (case III). However, a sufficiently slow switching that allows the maps to

spend more time in one of the two stable synchronization states will induce stochastic synchronization. The emergence of a lower limit for the switching period to ensure stochastic synchronization is highly non-trivial, while the stabilization of synchronization by slow switching in the dwell time limit should be expected as the maps will spend the time necessary to synchronize in one of the stable configurations, before being re-wired to the other stable configuration.

The proposed necessary condition demonstrates that switching between two unstable states (case I) cannot stabilize synchronization for any switching frequencies, in contrast with networks of continuous-time oscillators where windows of opportunity appear as a result of switching between two unstable (saddle) states. These windows of opportunity for synchronization in continuous-time Rössler and Duffing oscillators [79] and tritrophic Rosenzweig-MacArthur food-chain models [80] were reported earlier, but the derivation of explicit conditions for the emergence of these windows in the continuous-time case is more challenging and remains a subject of future study.

Not only will the continuous-time setting challenge the use of a power expansion in the mean square stability analysis, but also it will increase the dimensionality of the problem. The latter research direction should also be pursued when expanding the framework to large networks, where the relationship between the eigenstructures of the switching Laplacian graphs will likely play a major role. Focusing on a discrete-time setting and scalar maps has enabled us to undertake a first, necessary step toward the prediction and quantification of windows of opportunity for stochastic synchronization beyond fast switching.

CHAPTER 6

NETWORK SYNCHRONIZATION THROUGH STOCHASTIC BROADCASTING

Building on our results in the previous chapter on the stochastic synchronization of two intermittently coupled maps, in this chapter, we approach a more complicated network synchronization problem. Synchronization is often observed in interacting dynamical systems, comprising natural and technological networks; however, seldom do we have precise knowledge and control over the synchronous trajectory. In this chapter, we investigate the possibility of controlling the synchronization of a network by broadcasting from a single reference node. We consider the general case in which broadcasting is not static, but stochastically switches in time. Through an analytical treatment of the Lyapunov exponents of the error dynamics between the network and the reference node, we obtain an explicit dependence of synchronization on the strength of the broadcasting signal, the eigenvalues of the network Laplacian matrix, and the switching probabilities of broadcasting. For coupled chaotic tent maps, we demonstrate that: (i) time averaging fails to predict the onset of controlled synchronization and (ii) the success of broadcasting depends on the network topology, where the more heterogeneous the network is, the more difficult it is to control.

6.1 Introduction

In this chapter, we study the feasibility of broadcasting from a common reference node to control synchronization of a network of coupled dynamical systems. Within this approach, every node in the network has access to the same information from the reference node at a given time, but we allow for this information to stochastically change in time. For example, the reference node could share information with the network only sporadically in time or could alternate between several conflicting messages. With respect to schooling fish, for

example, leaders may use sudden changes in swimming direction as a visual cue to elicit followership of the group [87].

The problem of controlled synchronization through broadcasting shares similarities with the literature on pinning control, where a control action is applied to a small selected subset of nodes to tame the dynamics of the entire network on the trajectory of a reference node [34, 152]. Building on the standard approach developed a decade ago [117, 143, 39], most of the literature considers the case in which pinning control is statically applied to the network, such that control gains are held constant in time. This is in contrast with the broadcasting approach, in which all nodes are controlled but for a limited fraction of time and with a varying gain. Only few studies have explored the possibility of time-varying pinning control, but we still have limited analytical insight into the interplay between the internal nonlinear dynamics of the nodes, the evolution of the control gains, and the network structure [34].

Here, we seek to close this gap in the context of stochastic broadcasting. Toward this aim, we extend our recent work [61, 116], where we established a rigorous methodology for assessing the mean square stability of the synchronous solution in a pair of coupled discrete-time oscillators. Specifically, we derive a master equation for the mean square stability of the error dynamics, parametrized in terms of the eigenvalues of the graph Laplacian of the network. We apply ergodic theory [9] to study the Lyapunov exponent of the master equation, which we specialize to chaotic tent maps. In an effort to compare our analysis with the state of the art on switching networks [110], we also challenge the practical use of time-averaging to predict the onset of stochastic synchronization of discrete-time oscillators.

6.2 Problem Formulation

We study the synchronization of a network of N coupled discrete-time oscillators ($y_i \in \mathbb{R}$, where $i = 1, 2, \ldots, N$), interacting with a reference oscillator ($x \in \mathbb{R}$) that broadcasts to the entire network, as shown in Fig. 6.1. The network nodes are interconnected by an arbitrary, undirected and unweighted, topology, which is represented by the graph $\mathcal{G} = (\mathcal{V}, \mathcal{E})$, where $\mathcal{V}$ is the vertex set and $\mathcal{E}$ is the edge set. The evolution of all the oscillators (network and

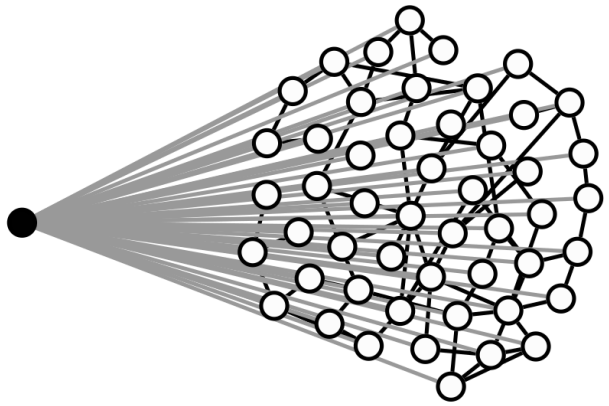

Figure 6.1 Illustration of the problem: the reference oscillator, x, (black) stochastically broadcasts to a network of N oscillators, $y_1, \ldots, y_N$ (white).

reference nodes) is governed by the same nonlinear function $F : \mathbb{R} \to \mathbb{R}$. That is, in the absence of coupling, $y_i(k+1) = F(y_i(k))$ and $x(k+1) = F(x(k))$. The broadcasting process is independent and identically distributed (i.i.d.) in time, such that, at each time step k, the control gain of the reference node, $\varepsilon(k)$, is randomly drawn from a set $\{\varepsilon_1, \varepsilon_2, \ldots, \varepsilon_m\}$ with probabilities $p_1, p_2, \ldots, p_m$, respectively (with $\sum_{i=1}^{m} p_i = 1$). As broadcasting is global, the value of the switching gain is common to all nodes. We say that the reference node and the network are synchronized if $y_1(k) = y_2(k) = \cdots = y_N(k) = x(k)$ for $k \in \mathbb{Z}^+$.

To summarize the setup of the problem, the system of equations governing the discrete-time evolution is

$$\begin{aligned} x(k+1) &= F(x(k)), \\ y_i(k+1) &= F(y_i(k)) + \varepsilon(k)(x(k) - y_i(k)) + \sum_{j=1, ij \in \mathcal{E}}^{N} \mu(y_j(k) - y_i(k)), \end{aligned} \tag{6.1}$$

for $i = 1, 2, \ldots N$, where μ is a network coupling used to scale the node-to-node interactions versus the strength of the broadcasting signal. System (6.1) is a stochastic dynamical system whose study requires tools from both stability and ergodic theories [9]. More specifically, system (6.1) describes a switched nonlinear linear system, with an underlying memoryless switching.

In general, the network dynamics can be written in the following vector form

$$\mathbf{y}(k+1) = \mathbf{F}(\mathbf{y}(k)) - \mu L\mathbf{y}(k) - \varepsilon(k) I_N \left(\mathbf{y}(k) - x(k)\mathbf{1}_N\right), \tag{6.2}$$

where $\mathbf{y}(k)$ is the vector comprised of all the network states, $\mathbf{F}(\mathbf{y})$ is the vector-valued extension of the mapping function $F(y)$, $\mathbf{1}_N$ is the vector of ones of length N, and L is the Laplacian matrix of $\mathcal{G}$ [60], that is,

$$L = \begin{cases} L_{ij} = -1 & ij \in \mathcal{E} \\ L_{ii} = \sum\limits_{j} 1 & i = 1, 2, \ldots, N, \end{cases}$$

with eigenvalues $\gamma_1 = 0 \leq \gamma_2 \leq \cdots \leq \gamma_N$.

To understand the role of broadcasting in inducing synchronization with the reference trajectory $x(k)$, we look at the evolution of the error dynamics $\xi(k) = x(k)\mathbf{1}_N - \mathbf{y}(k)$. To study the stability of synchronization, we linearize the system about the reference trajectory:

$$\xi(k+1) = \left[DF(x(k))\, I_N - \mu L - \varepsilon(k)\, I_N\right] \xi(k), \tag{6.3}$$

where I_N is the $N \times N$ identity matrix and $DF(x(k))$ is the Jacobian of F at $x(k)$. In (6.3), we have assumed infinitesimal perturbations $\xi(k)$ in the directions transversal to the synchronous solution thereby, allowing for the linearization and application of the Jacobian DF. The linearized discrete-time system in (6.3) is a first order Markov chain, due to the presence of the switching gain $\varepsilon(k)$. Although $\varepsilon(k)$ is drawn from an i.i.d. distribution, (6.3) describes a linear time-varying switching system, since the reference trajectory $x(k)$ generally varies in time. Stochasticity and time-dependence, however, only appear as a compound multiplier of the identity matrix, thereby affording the possibility of diagonalizing the system in terms of the eigenspaces of the Laplacian matrix. In other words, to a first linear approximation, the error dynamics on the eigenspaces of the Laplacian evolve independently of each other, allowing for the use of a single stochastic master equation.

Specifically, diagonalizing (6.3), we obtain

$$\zeta(k+1) \;=\; [I_N DF(x(k)) - \mu\gamma - \varepsilon(k) I_N]\,\zeta(k), \tag{6.4}$$

where $\gamma \in \{\gamma_1, \ldots, \gamma_N\}$ encapsulates the role of the network topology on the evolution of the error dynamics along the eigenvectors of L, identified by $\zeta(k)$. Master equation (6.4) can be parametrically studied as a function of $\mu\gamma$ to illuminate the influence of the strength of the broadcasting signal and the switching probabilities of broadcasting on the stability of synchronization along each eigenvector of L. This equation reduces to the traditional, deterministic master stability equation in [109] in the absence of stochastic broadcasting ($\varepsilon(k) = 0$).

6.3 Master Stability Function

While there are many criteria that one can contemplate when examining stochastic stability of a network about a synchronous solution, we use the lens of mean square stability for its practicality of implementation and inclusiveness with other criteria [89, 54]. For example, as shown in [101], mean square asymptotic stability of switching linear systems with an underlying time-homogenous finite-state Markov chain is equivalent to exponential second moment stability and implies almost sure stability. Several studies have demonstrated the feasibility of using mean square stability in the study of synchronization of discrete-time systems, and we build on this literature toward an analytical treatment of broadcasting [159, 114]. Through this lens, the error dynamics is controlled by both the mean and the variance of the switching signal, different from fast-switching approaches in continuous-time systems that only rely on the mean [124, 79]. We discuss different types of stability and their relationships in Appendix D.

Definition 6.1. *The synchronous solution* $y_1(k) = y_2(k) = \ldots = y_N(k) = x(k)$ *in the stochastic system (6.1) is locally asymptotically mean-square stable, if* $\lim_{k\to\infty} \mathrm{E}[\xi^2(k)] = 0$ *for any initial condition* $\xi(0)$ *of* (6.3)*, where* $\mathrm{E}[\cdot]$ *denotes expectation with respect to the* σ*-algebra*

generated by the stochastic process of switching.

Analyzing mean square stability of the stochastic system (6.3), and therefore of the master equation (6.4), corresponds to studying the deterministic evolution of the second moment of $\zeta(k)$ toward the derivation of a rigorous convergence criterion. To this end, we take the expectation of the square of both sides in (6.4), to obtain

$$\mathrm{E}[\zeta^2(k+1)] = \big[\,(DF(x(k)) - \mu\gamma)^2 + 2(\mu\gamma - DF(x(k)))\mathrm{E}[\varepsilon(k)] + \mathrm{E}[\varepsilon^2(k)]\big]\mathrm{E}[\zeta^2(k)]. \quad (6.5)$$

The stability of the deterministic system in (6.5) can be inferred through the study of its Lyapunov exponent [112]. If the limit exists, the Lyapunov exponent is computed from the error dynamics for a non-zero initial condition $\zeta(0)$ as

$$\lambda = \lim_{k\to\infty} \frac{1}{k} \ln \left[\frac{\mathrm{E}[\zeta^2(k)]}{\zeta^2(0)}\right] = \lim_{j\to\infty} \frac{1}{j} \sum_{k=1}^{j} \ln \mathrm{E}[\zeta^2(j)]. \quad (6.6)$$

The study of the stochastic stability of the N-dimensional error dynamics in (6.3) reduces to monitoring the sign of λ as a function of γ.

Lemma 6.1. *The synchronous solution $x(k)$ of the nonlinear stochastic system (6.1) is locally asymptotically mean-square stable if the Lyapunov exponent λ in (6.6) is negative for every $\gamma \in \{\gamma_1, \ldots, \gamma_N\}$.*

Proof. *The proof is trivial. The negativenesses of the Lyapunov exponent implies the convergence of* $\mathrm{E}[\zeta^2(k)]$ *to zero, and therefore guarantees local asymptotic mean-square stability, according to Definition 1.* □

Given the strength of the node-to-node interaction μ, the mean and variance of the broadcasting signal $\mathrm{E}[\varepsilon(k)]$ and $\mathrm{E}[\varepsilon^2(k)]$, and the individual dynamics F, one can numerically compute λ for a range of values of γ to generate a so-called master stability function. From the master stability function, one can then infer which network topology will support synchronization to the reference trajectory.

Remark 1. *For a linear system, $F(x) = \alpha x$, where $\alpha \in \mathbb{R}$, the Lyapunov exponents can be*

easily computed from the limit in (6.6)*, such that*

$$\lambda = \ln\left[\,(\alpha-\mu\gamma)^2 + 2(\mu\gamma-\alpha)\mathrm{E}[\varepsilon(k)] + \mathrm{E}[\varepsilon^2(k)]\right]. \tag{6.7}$$

Remark 2. *For nonlinear discrete-time systems, numerical computation of Lyapunov exponents may be a challenging task, potentially leading to false predictions on stochastic synchronization. For example, stable dynamics may lead to* $\mathrm{E}[\zeta^2(k)]$ *attaining values below numerical precision in a few steps, thereby hampering the evaluation of the Lyapunov exponent; and similarly, unstable dynamics may lead to sudden numerical overflow.*

Toward overcoming potential confounds associated with numerical computation of (6.6), we adopt Birkoff's ergodic theorem [9] to derive the main general statement of this chapter.

Proposition 6.1. *The synchronous solution* $s(k)$ *of the stochastic system (6.1) with the invariant density* $\rho(x)$ *of* F *is locally mean square stable if*

$$\lambda \quad = \quad \int_B \ln\left[\,(DF(z)-\mu\gamma_i)^2 \;+\; 2(\mu\gamma \;-\; DF(z))\mathrm{E}[\varepsilon(k)] \;+\; \mathrm{E}[\varepsilon^2(k)]\right]\rho(z)\mathrm{d}z, \tag{6.8}$$

where $B \subseteq \mathbb{R}$ *is where the invariant density* $\rho(x)$ *is defined.*

Proof. *The key step in the proof lies in the introduction of the invariant density function of* F*, which measures the probability that a typical trajectory will visit a neighborhood of the state* x *– for example, for a periodic trajectory of period two, such that* $x(k) = x(k+2)$*, the invariant density* $\rho(x)$ *will correspond to two Delta distributions of equal intensity at* $x(0)$ *and* $x(1)$ *and for more complex, possibly chaotic, systems the invariant density may become a continuous function. By virtue of Birkoff's ergodic theorem [9], using* $\rho(x)$*, one can replace the summation over time in* (6.6) *with the integration over the probability space in* (6.8)*, following the line of argument in [61, 116].* □

Remark 3. *With knowledge of the invariant density,* (6.8) *can be analytically or numerically evaluated to establish a master stability function for controlled stochastic synchronization through broadcasting, without incurring in the computational challenges indicated*

in Remark 2.

For non-switching broadcasting, such that the switching gain ε is constant in time and equal to $\bar{\varepsilon}$, (6.8) *reduces to*

$$\lambda = 2 \int_B \ln \left| DF(t) - \mu\gamma - \bar{\varepsilon} \right| \rho(z)\, dz. \tag{6.9}$$

Notice that the dependence of the argument of the logarithm on γ is linear, different from (6.8)*, where we find linear and quadratic dependencies. Equation* (6.9) *will be used to elucidate the predictive power, or lack thereof, of the averaged system on stochastic synchronization. Specifically, we will examine the sign of the Lyapunov exponent in* (6.9) *with $\bar{\varepsilon} = \mathrm{E}[\varepsilon(k)]$ and compare with* (6.8)*.*

Remark 4. *Since* 0 *is necessarily an eigenvalue of the Laplacian matrix (due to the zero row-sum property), one of the Lyapunov exponents is always given by $\lambda_1 = \int_B \ln \left[DF(z)^2 - 2DF(z)\mathrm{E}[\varepsilon(k)] + \mathrm{E}[\varepsilon^2(k)] \right] \rho(z)\, dz$. This Lyapunov exponent indicates that the stability of synchronization of an individual oscillator to the reference oscillator is necessary for the stability of synchronization of the entire network to broadcasting. Therefore, the network can not facilitate synchronization as it introduces further constraints on the switching gain beyond those implied by a direct one-to-one coupling between an isolated node and the reference node.*

6.4 Application to Chaotic Tent Maps

To illustrate the implications of (6.8), we consider the case of the chaotic tent map [71] with parameter equal to 2, which has a known density function $\rho(x) = 1$ on the interval $B = [0, 1]$. We limit the analysis to two control gains for the broadcasting signal, $\varepsilon_i \in \{\varepsilon_1, \varepsilon_2\}$. These gains could exemplify a single broadcasting message (if $\varepsilon_2 = 0$), or two conflicting messages (if $\varepsilon_1 \neq \varepsilon_2$). In our numerical demonstrations, we parametrically vary ε_1 and μ, with $\varepsilon_2 = 2.2$ and $p_1 = p_2 = 0.5$. The value of ε_2 is chosen such that a single, isolated map would synchronize to a non-switching broadcasting signal [71]. At the same time, ε_1

may take a value such that it would destabilize synchronization in the non-switching case. Therefore, ε_1 and ε_2 can be assimilated to conflicting messages broadcasted by the reference node to the network.

6.4.1 Master Stability Function

Substituting the invariant density function into the integral in (6.8), we can compute in closed-form the Lyapunov exponent for the mean square stability of the error dynamics, thereby arriving at the following application of Proposition 6.1 to the chaotic tent maps.

Corollary 6.1. *The Lyapunov exponent for the mean square stability of the synchronous solution in the system (6.1) of chaotic tent maps is*

$$\lambda = \ln\left[(2-\mu\gamma)^2+2(\mu\gamma-2)\mathrm{E}[\varepsilon(k)]+\mathrm{E}[\varepsilon^2(k)]\right]\cdot\left[(-2-\mu\gamma)^2+2(\mu\gamma+2)\mathrm{E}[\varepsilon(k)]+\mathrm{E}[\varepsilon^2(k)]\right], \tag{6.10}$$

where $\mathrm{E}[\varepsilon(k)] = p_1\varepsilon_1 + p_2\varepsilon_2$ *and* $\mathrm{E}[\varepsilon^2(k)] = p_1\varepsilon_1^2 + p_2\varepsilon_2^2$.

This Lyapunov exponent demonstrates the explicit dependence of the stability of stochastic synchronization on the node-to-node coupling strength, the eigenvalues of the Laplacian matrix, and the stochastically switching coupling strengths along with their respective probabilities.

Figure 6.2 illustrates the dependence of λ on ε_1 and $\mu\gamma$. The dashed curve in Fig. 6.2 indicates the boundary between positive and negative Lyapunov exponents, identifying the onset of mean square stability of the error dynamics. In order for the network to synchronize to the reference node, the point $(\varepsilon_1, \mu\gamma)$ must fall within the dashed curve for *every* eigenvalue in the spectrum of the Laplacian matrix. In agreement with our predictions, we find that as $\mu\gamma$ increases the range of values of ε_1 which affords stable synchronization becomes smaller and smaller. This suggests that the resilience of the network to synchronize improves with $\mu\gamma$.

Remark 5. *While the nonlinear dependence of the stability boundary on* ε_1 *and* $\mu\gamma$ *is modu-*

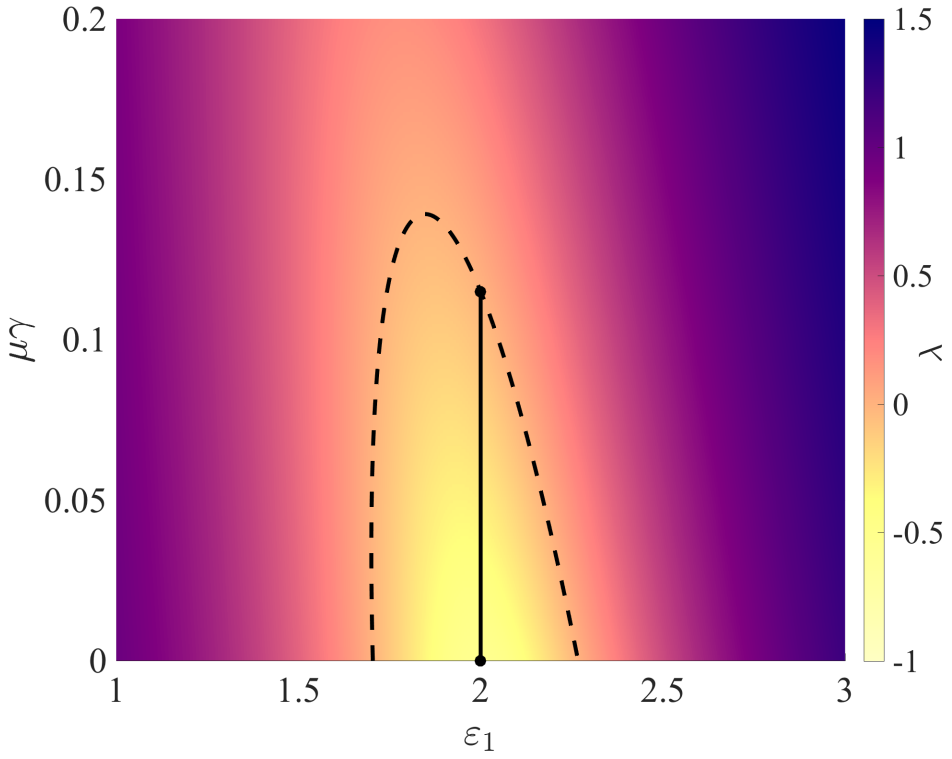

Figure 6.2 Master stability function for stochastic synchronization of chaotic tent maps, for $\varepsilon_2 = 2.2$ and $p_1 = p_2 = 0.5$. For synchronization to be stable, each eigenvalue of the Laplacian matrix must correspond to a negative Lyapunov exponent (indicated by the yellow color, isolated by the black dashed curve). For example, the black vertical line shows the range of admissible values of $\mu\gamma$ that would guarantee stability at $\varepsilon_1 = 2$.

lated by the nonlinearity in the individual dynamics, it should not be deemed as a prerogative of nonlinear systems. As shown in Remark 1, the stochastic stability of synchronization in the simplest case of a linear system is also nonlinearly related to the spectrum of the Laplacian matrix and to the expectation and variance of the broadcasting signal – even for classical consensus with $\alpha = 1$ [34].

Remark 6. *In this example of a chaotic tent map, the stability boundary is a single curve, defining a connected stability region. To ensure stable synchronization of a generic network, it is thus sufficient to monitor the largest eigenvalue of the Laplacian matrix, γ_N, such that $(\varepsilon_1, \mu\gamma)$ will fall within the stability region. This is in contrast with the master stability function for uncontrolled, spontaneous synchronization [109], which would typically require the consideration of the second smallest eigenvalue, often referred to as the algebraic connectivity [60]. However, similar to master stability functions for uncontrolled, spontaneous synchronization [145], we would expect that for different maps, one may find several disjoint regions in the $(\varepsilon_1, \mu\gamma)$-plane where stable stochastic synchronization can be attained.*

6.4.2 Comparing the Static and Stochastic Systems

Next, we wish to gain insight into the ability of the averaged system to predict the onset of synchronization on the broadcasting trajectory. From (6.9), we obtain the following closed-form for the Lyapunov exponent:

$$\lambda = \ln \left| \left(2 - \mu\gamma - \mathrm{E}[\varepsilon(k)]\right) \left(-2 - \mu\gamma - \mathrm{E}[\varepsilon(k)]\right) \right|. \tag{6.11}$$

In Fig. 6.3, we summarize predictions on the stability of stochastic synchronization for a ring of 100 nodes, gathered through the master stability function depicted in Fig. 6.2 and the averaged system described through (6.11). Figure 6.3 identifies distinct regions of the parameter space spanned by μ and ε_1, where predictions from the averaged system with respect to the exact result from the master stability function should be considered valid or invalid.

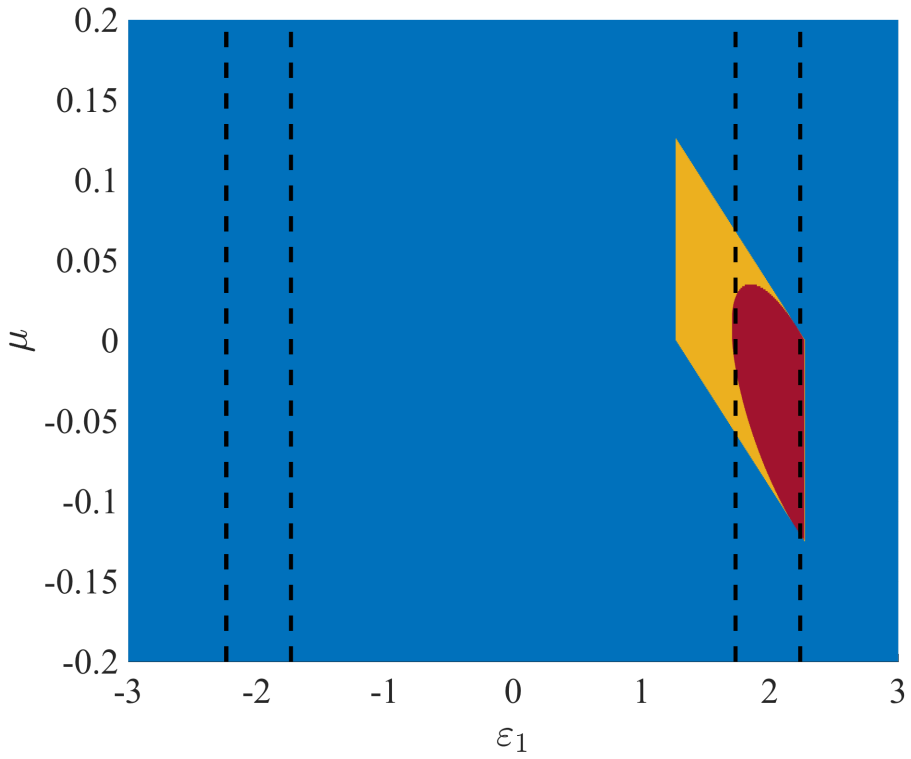

Figure 6.3 Verification of predictions from the averaged system on the stochastic synchronization of a ring of 100 chaotic tent maps, for $\varepsilon_2 = 2.2$ and $p_1 = p_2 = 0.5$. The red region indicates when averaged system correctly identifies the stability of synchronization, the yellow region indicates when the averaged system predicts stability of synchronization against the master stability function that posits unstable synchronization, and the blue region indicates when the averaged system correctly anticipates unstable synchronization. The regions enclosed by the dashed vertical lines identifies the values of ε_1 that could support stable synchronization of an isolated node, that is, $\mu = 0$.

Remark 7. *Our results suggest the presence of a wide region of the parameter space in which the averaged system fails to predict the stability of synchronization, while we find no evidence of invalid predictions on the instability of synchronization by the averaged system. Hence, in this particular example, the averaged system seems to provide a necessary condition. Care should be placed in extending this claim to other settings, whereby, as shown in [61, 116], one can construct examples for* $N = 1$ *in which unstable synchronization in the averaged system does not imply unstable synchronization for stochastically coupled systems.*

6.4.3 Role of Network Topology

The master stability function in Fig. 6.2 shows that both μ and γ contribute to the resilience of the network to synchronization induced by stochastic broadcasting. For a given value of the node-to-node coupling strength μ, different networks will exhibit different residences based on their topology. Based on the lower bound by Grone and Merris [66] and the upper bound by Anderson and Morley [4], for a graph with at least one edge, we can write $\max\{d_i, \quad i = 1, \ldots, N\} + 1 \leq \gamma_N \leq \max\{d_i + d_j, \quad ij \in \mathcal{E}\}$, where d_i is the degree of node $i = 1, \ldots, N$. While these bounds are not tight, they suggest that the degree distribution has a key role on γ_N. For a given number of edges, one may expect that networks with highly heterogeneous degree distribution, such as scale-free networks [29], could lead to stronger resilience to broadcasting as compared to regular or random networks, with more homogenous degree distributions [29].

In Fig. 6.4, we illustrate this proposition by numerically computing the largest eigenvalue of the graph Laplacian for three different network types:

(i) A $2K$-regular network, in which each node is connected to $2K$ nearest neighbors, such that the degree is equal to $2K$. As K increases, the network approaches a complete graph.

(ii) A scale-free network which is grown from a small network of q nodes. At each iteration of the graph generation algorithm, a node is added with q edges to nodes already in

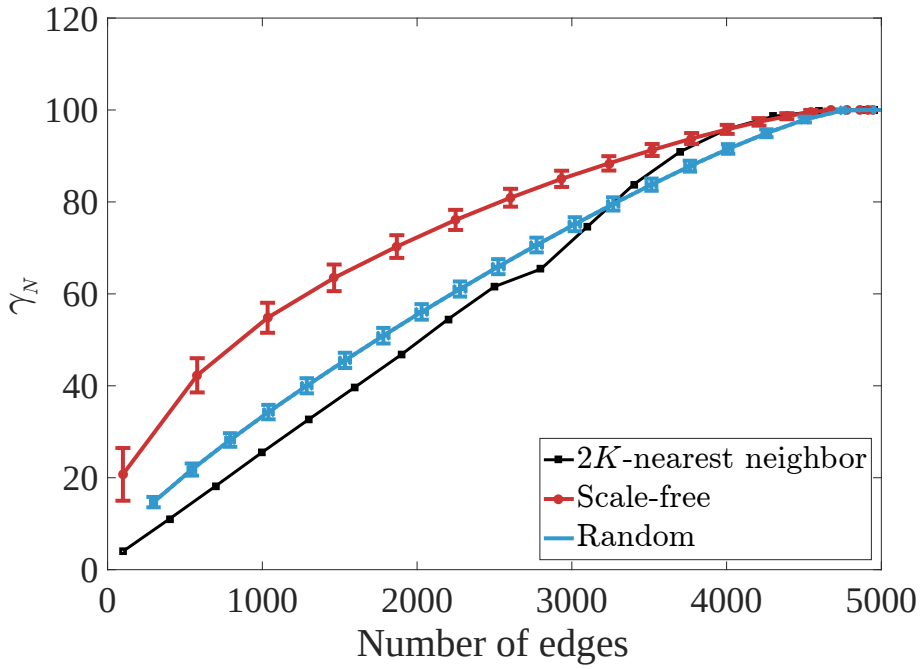

Figure 6.4 Largest eigenvalue γ_N of the Laplacian matrix as a function of the number of edges for three different types of networks of 100 nodes: a $2K$-regular network (black curve with square markers), scale-free (red curve with circle markers), and random Erdös-Renyi (blue curve) networks. Scale-free and random networks are run 10000 times to compute means and standard deviations, reported herein – note that error bars are only vertical for scale-free networks since the number of edges is fully determined by q, while for random networks also horizontal error bars can be seen due to the process of network assembly.

the network. The probability that an edge will be connected to a specific node is given by the ratio of its degree to the total number of edges in the network. Nodes are added until there are N nodes in the network. When q is small, there are a few hub nodes that have a large degree and many secondary nodes with small degree, whereas when q is large, the scale-free network is highly connected and similar to a complete graph.

(iii) A random Erdös-Renyi network which takes as input the probability, p, of an edge between any two nodes. When p is small, the network is almost surely disconnected, and when p approaches 1, it is a complete graph.

We fix N to 100 and vary K, q, and p in (i), (ii), and (iii), respectively, to explore the role of the number of edges.

As expected from the bounds in [66, 4], for a given number of edges, the scale-free network tends to exhibit larger values of γ_N. This is particularly noticeable for networks of intermediate size, whereby growing the number of edges will cause the three network types to collapse on a complete graph of N nodes. As the largest eigenvalue of the Laplacian matrix fully controls the resilience of the network to broadcasting-induced synchronization (in the case of linear and chaotic tent maps), we may argue that, given a fixed number of edges, the network can be configured such that it is either more conducive (regular graph) or resistant (scale-free graph) to synchronization. The increased resilience of scale-free networks should be attributed to the process of broadcasting-induced synchronization, which globally acts on all nodes simultaneously, without targeting critical nodes (low or high degree) like in pinning control [34, 152].

6.5 Chapter Summary

Much attention recently has been placed on controlling the synchronization networks, though the vast majority of the literature considers cases in which the control is continuously applied on selected network sites. Here, we have taken a different approach, by addressing the problem of broadcasting-induced synchronization of a network of oscillators, using a single,

external, reference node. The reference node is stochastically coupled with the network, such that control actions are intermittently applied over time, switching over a set of potentially conflicting messages.

In the context of mean square convergence, we have examined the stochastic stability of the error dynamics of the network oscillators with respect to the reference trajectory. By decomposing the error dynamics on independent components along the eigenvectors of the Laplacian matrix, we have established a master stability equation to predict the onset of stable synchronization. From the Lyapunov exponent of the master stability equation, we posit a master stability function, which can be used to systematically study the role of the mean and variance of the broadcasting control gain on synchronization. In a principled manner, we have applied elements of ergodic theory to cast the computation of the Lyapunov exponent in terms of an integration in a probability space, which is amenable to analytical and numerical treatments. We have illustrated the approach for chaotic tent maps, for which we have clarified the predictive power of time-averaging and systematically analyzed the role of network topology.

Our general approach is not limited to one-dimensional maps but directly applicable to higher dimensional node dynamics, provided that the invariant ergodic measure of the given map can be calculated. In rare cases which include Anosov maps (two-dimensional diffeomorphisms on tori) [72], invariant density functions can be assessed analytically. In some examples of two- and higher-dimensional chaotic maps, the invariant density can be calculated numerically and approximated by an explicit continuous function. Known examples of such numerically-assisted approximations include volume-preserving two-dimensional standard maps and the four-dimensional Froeschlé map [93].

In contrast to classical master stability functions for uncontrolled, spontaneous synchronization, where both the algebraic connectivity and the largest eigenvalue of the Laplacian matrix determine the onset of synchronization, we report that the algebraic connectivity has no role on broadcasting-induced synchronization of linear maps and chaotic tent maps. Specifically, the resilience of the network to broadcasting synchronization increases with the

value of the largest eigenvalue of the Laplacian matrix. Heterogenous topologies with hubs of large degree should be preferred over homogenous topologies, when designing networks that should be resilient to influence from a broadcasting oscillator. On the contrary, homogenous topologies, such as regular or random topologies, should be preferred when seeking networks that could be easily tamed through an external broadcasting oscillator. Interestingly, these predictions would be hampered by a simplified analysis based on averaging, which could lead to false claims regarding the stability of synchronous solutions.

Two of the key assumptions of the current setup are the lack of a memory in switching and the need for switching at every time step. Both these assumptions could be relaxed by building on our recent work on synchronization of two coupled maps [61, 116], where we have demonstrated potential advantages of memory and non-fast switching. The analysis presented therein corresponds to broadcasting-induced synchronization for $N = 1$. We anticipate that combining those findings with the methodology proposed in this work could lay the foundation for a general theory of non-fast broadcasting with memory, which could translate into control strategies with improved energy efficiency and performance.

CHAPTER 7

CONCLUSIONS

Inherent randomness and unpredictability is an underlying property in most realistic phenomena that scientists would want to model. In an effort to improve our collective ability to model systems with these fundamental random properties, we present a new framework for describing stochastically switching dynamical systems. Traditionally in continuous-time dynamical systems, stochasticity is incorporated through a "noise" term $\xi(t)$ which is randomly chosen from some continuous distribution at every time step. This type of stochasticity is fairly arbitrarily introduced into systems (either as driving noise, or causing parameters to jitter about some value) and needlessly challenging to approach on a technical level. We offer an alternative dynamical strategy in which the system is deterministic at any given step, but the system switches between deterministic regimes randomly. This can account for random changes to the environment of a system (like unpredictable periods of extreme weather) or random adaptation/evolution of a social or technological network. This framework builds on [69] and [70] in regard to continuous-time dynamical systems and [54, 55] and [114] in discrete-time systems.

In continuous-time dynamical we first introduced a simple example to motivate the use of these switching dynamical systems, and to familiarize the reader with both the existing theory in the fast switching limit as well as the types of non-intuitive behaviors that are possible when switching is not almost instantaneous. We show that it can be proven that if the switching period is sufficiently fast, the dynamics of the switching system closely follows the dynamics of the average system (obtained by replacing the stochastic variables with their expectations). Beyond fast switching, we show that even in this simple example, the switching system can hop between attraction basins to converge to the wrong attractor against all odds. With these ideas in mind, we then extend our framework to stochastically

switching networks that change topology every τ units of time (as well as change dynamics on the nodes). We specifically present an example of a network of randomly connected ecological metacommunities that are only connected by unpredictable events (like erratic rainfall or strong winds). We prove conditions for which these networks can synchronize, even if they are disconnected at nearly every time step (which prevents the ability to synchronize in static networks). Surprisingly, we find "Windows of Opportunity," or bounded ranges of optimal, intermediate switching frequencies for which a network can synchronize despite switching between a disconnected network and a network with destabilizing coupling (with an average coupling value that is also destabilizing). This phenomenon is similar in spirit to stochastic resonance, from which systems can be stabilized by intermediate levels of noise, or Kapitza's pendulum, in which an upright pendulum can be stabilized by intermittent vertical oscillations. While it certainly has a similar spirit to both of these phenomena, it arises in a different dynamical setting, and has a different underlying mechanism.

To understand some of the observed behavior at intermediate switching frequency, we reduce the complexity of the problem and consider the case of two stochastically switching discrete-time dynamical systems. For this scaled-down example, we were able to analytically derive a formula for the stochastic Lyapunov exponent indicating the mean-square stability of two coupled maps. This formula reduces even further if the dynamics of the individual maps are ergodic (so that they Lyapunov exponent can be computed from averaging over space, instead of time). Using sigmoid maps, we showed the relationships between the static and stochastic maps, as well as the interplay between the different parameters for the switching process (the switching probabilities, coupling strengths, and switching period). Then, for the first time, we analytically showed the existence of a bounded region for which intermediate switching periods favor synchrony when both fast and slow switching do not. Adding some layers of complexity to this example, we then consider the control problem of stochastically broadcasting a signal from a reference node to a network connected through an arbitrary topology. When switching is fast, the network topology only adds more conditions for the system to be mean-square stable (the nodes in the network converging to the trajectory of

the reference node). Indeed, each node synchronizing to the reference node in that absence of a network is a necessary condition for the new broadcasting problem. However, we find that for both fast-switching and arbitrary switching periods, the network can be altered in minor ways that will allow for the network to be synchronized.

Even with the strides we have made and the phenomena we have discovered and studied, we have hardly scratched the surface of stochastically switching dynamical systems. To conclude, we will examine some of the natural directions in which this work can be extended. Firstly, all of this work was done assuming that the stochastic variables are independent and identically distributed. While a recent work [116] extended some of our work with discrete-time dynamical systems to a more general Markov switching process, the i.i.d assumption can be relaxed in general, and will likely unveil an entirely new set of phenomena. Technically, even the behavior in the fast switching limit has not been proven for other stochastic processes, so there are immediate rigorous gaps in the literature that need filling. Another direction that follows immediately from the work presented in continuous-time would be to rigorously analyze these systems for intermediate switching periods. This is motivated by the "Windows of Opportunity" phenomenon, by which a system can switch between unstable states with an unstable average and reliably converge to a stable state. This has not been observed in any other context, and is more than a mathematical curiosity: it could be quite useful in physics and engineering. Likely this analysis would first be completed for a periodic switching process, eliminating the random element would hopefully expose the underlying dynamical mechanism for this behavior. Lastly for continuous-time systems, it would be interesting to see these types of systems used for modeling to fit some kind of data, for example by modeling a stochastically switching neuronal network. Also, to see what other behaviors are possible when incorporating this type of stochasticity into classical dynamical systems problems.

In discrete-time systems with stochastic switching, it would be interesting to develop a theory beyond fast switching *outside* of the networks/control paradigm. The current state-of-the-art only focuses on finite-state Markov processes applied to linear switching systems.

It is not clear what happens in non-linear systems, or when switching does not occur at every time instant. In the contexts of network control, it would be interesting to explore less restrictive control schemes than the broadcasting we have studied. It would also be worth investigating what type of behavior is possible for higher dimensional problems.

The framework presented here is highly adaptive and presents a significant advancement in creating more realistic models by virtue of better incorporating stochasticity into models.

REFERENCES

[1] Nicole Abaid and Maurizio Porfiri. Consensus over numerosity-constrained random networks. *IEEE Transactions on Automatic Control*, 56(3):649–654, 2011.

[2] VS Afraimovich, NN Verichev, and Ml I Rabinovich. Stochastic synchronization of oscillation in dissipative systems. *Radiophysics and Quantum Electronics*, 29(9):795–803, 1986.

[3] Réka Albert and Albert-László Barabási. Statistical mechanics of complex networks. *Reviews of modern physics*, 74(1):47, 2002.

[4] William N Anderson Jr and Thomas D Morley. Eigenvalues of the laplacian of a graph. *Linear and multilinear algebra*, 18(2):141–145, 1985.

[5] V Anishchenko, S Nikolaev, and J Kurths. Peculiarities of synchronization of a resonant limit cycle on a two-dimensional torus. *Physical Review E*, 76(4):046216, 2007.

[6] Vadim S Anishchenko and Alexander B Neiman. Stochastic synchronization. In *Stochastic Dynamics*, pages 154–166. Springer, 1997.

[7] Vadim Semenovich Anishchenko, Arkady B Neiman, F Moss, and L Shimansky-Geier. Stochastic resonance: noise-enhanced order. *Physics-Uspekhi*, 42(1):7–36, 1999.

[8] VS Anishchenko, AB Neiman, and MA Safanova. Stochastic resonance in chaotic systems. *Journal of statistical physics*, 70(1):183–196, 1993.

[9] Ludwig Arnold. *Random dynamical systems*. Springer Science & Business Media, 2013.

[10] Abdennasser Azzouz and Martin Hasler. Uniqueness of the asymptotic behaviour of autonomous and non-autonomous, switched and non-switched, linear and non-linear systems of dimension 2. *International journal of circuit theory and applications*, 16(2):191–226, 1988.

[11] R. Bellman. Limiting theorems for non-commutative operators. *Duke Mathematics Journal*, 21:456, 1960.

[12] I Belykh, V Belykh, K Nevidin, and M Hasler. Persistent clusters in lattices of coupled nonidentical chaotic systems. *Chaos: An Interdisciplinary Journal of Nonlinear Science*, 13(1):165–178, 2003.

[13] Igor Belykh, Vladimir Belykh, and Martin Hasler. Generalized connection graph method for synchronization in asymmetrical networks. *Physica D: Nonlinear Phenomena*, 224(1):42–51, 2006.

[14] Igor Belykh, Vladimir Belykh, Russell Jeter, and Martin Hasler. Multistable randomly switching oscillators: The odds of meeting a ghost. *The European Physical Journal Special Topics*, 222(10):2497–2507, 2013.

[15] Igor Belykh, Douglas Carter, and Russell Jeter. Synchronization in multilayer networks: when good links go bad. *Physical Review X*, (Submitted).

[16] Igor Belykh, Mario Di Bernardo, Jürgen Kurths, and Maurizio Porfiri. Evolving dynamical networks. *Physica D*, 267(1):1–6, 2014.

[17] Igor Belykh, Russell Jeter, and Vladimir Belykh. Foot force models of crowd dynamics on a wobbly bridge. *Science advances*, 3(11):e1701512, 2017.

[18] Igor Belykh, Carlo Piccardi, and Sergio Rinaldi. Synchrony in tritrophic food chain metacommunities. *Journal of biological dynamics*, 3(5):497–514, 2009.

[19] Igor V Belykh, Vladimir N Belykh, and Martin Hasler. Blinking model and synchronization in small-world networks with a time-varying coupling. *Physica D: Nonlinear Phenomena*, 195(1):188–206, 2004.

[20] Igor V Belykh, Russell Jeter, and Vladimir N Belykh. Bistable gaits and wobbling induced by pedestrian-bridge interactions. *Chaos: An Interdisciplinary Journal of Nonlinear Science*, 26(11):116314, 2016.

[21] Vladimir N Belykh, Igor V Belykh, and Martin Hasler. Hierarchy and stability of partially synchronous oscillations of diffusively coupled dynamical systems. *Physical Review E*, 62(5):6332, 2000.

[22] Vladimir N Belykh, Igor V Belykh, and Martin Hasler. Connection graph stability method for synchronized coupled chaotic systems. *Physica D: nonlinear phenomena*, 195(1):159–187, 2004.

[23] J. E. Bertram and P. E. Sarachik. Stability of circuits with randomly time-varying parameters. *Transactions of IRE, PGIT-5*, Special issue(260), 1959.

[24] L Billings and EM Bollt. Probability density functions of some skew tent maps. *Chaos, Solitons & Fractals*, 12(2):365–376, 2001.

[25] Frede Blaabjerg, Remus Teodorescu, Marco Liserre, and Adrian V Timbus. Overview of control and grid synchronization for distributed power generation systems. *IEEE Transactions on industrial electronics*, 53(5):1398–1409, 2006.

[26] Andrew E Blanchard and Ting Lu. Bacterial social interactions drive the emergence of differential spatial colony structures. *BMC systems biology*, 9(1):59, 2015.

[27] Bernd Blasius, Amit Huppert, and Lewi Stone. Complex dynamics and phase synchronization in spatially extended ecological systems. *Nature*, 399(6734):354–359, 1999.

[28] Stefano Boccaletti, Jürgen Kurths, Grigory Osipov, DL Valladares, and CS Zhou. The synchronization of chaotic systems. *Physics reports*, 366(1):1–101, 2002.

[29] Stefano Boccaletti, Vito Latora, Yamir Moreno, Martin Chavez, and D-U Hwang. Complex networks: Structure and dynamics. *Physics reports*, 424(4):175–308, 2006.

[30] Erik M Bollt and Naratip Santitissadeekorn. *Applied and Computational Measurable Dynamics*. SIAM, 2013.

[31] Peter S Bullen, Dragoslav S Mitrinovic, and M Vasic. *Means and their Inequalities*, volume 31. Springer Science & Business Media, 2013.

[32] LA Bunimovich, SG Dani, RL Dobrushin, MV Jakobson, IP Kornfeld, NB Maslova, Ya B Pesin, J Smillie, Yu M Sukhov, and AM Vershik. *Dynamical systems, ergodic theory and applications*, volume 100. Springer Science & Business Media, 2000.

[33] Stephen Cantrell, Chris Cosner, and Shigui Ruan. *Spatial ecology*. CRC Press, 2009.

[34] Yongcan Cao, Wenwu Yu, Wei Ren, and Guanrong Chen. An overview of recent progress in the study of distributed multi-agent coordination. *IEEE Transactions on Industrial informatics*, 9(1):427–438, 2013.

[35] Isabella Cattadori, Peter Hudson, Stefano Merler, Annapaola Rizzoli, et al. Synchrony, scale and temporal dynamics of rock partridge (alectoris graeca saxatilis) populations in the dolomites. *Journal of Animal Ecology*, 68(3):540–549, 1999.

[36] Bernard Cazelles and Gérard Boudjema. The moran effect and phase synchronization in complex spatial community dynamics. *The American Naturalist*, 157(6):670–676, 2001.

[37] Jérôme Chave. The problem of pattern and scale in ecology: what have we learned in 20 years? *Ecology Letters*, 16(s1):4–16, 2013.

[38] Maoyin Chen, Yun Shang, Changsong Zhou, Ye Wu, and Jürgen Kurths. Enhanced synchronizability in scale-free networks. *Chaos: An Interdisciplinary Journal of Nonlinear Science*, 19(1):013105, 2009.

[39] Tianping Chen, Xiwei Liu, and Wenlian Lu. Pinning complex networks by a single controller. *IEEE Transactions on Circuits and Systems I: Regular Papers*, 54(6):1317–1326, 2007.

[40] Alessandro Colombo, Fabio Dercole, and Sergio Rinaldi. Remarks on metacommunity synchronization with application to prey-predator systems. *The American Naturalist*, 171(4):430–442, 2008.

[41] Oswaldo Luiz Valle Costa, Marcelo Dutra Fragoso, and Ricardo Paulino Marques. *Discrete-time Markov jump linear systems*. Springer Science & Business Media, 2006.

[42] Pietro De Lellis, Mario di Bernardo, and Franco Garofalo. Synchronization of complex networks through local adaptive coupling. *Chaos: An Interdisciplinary Journal of Nonlinear Science*, 18(3):037110, 2008.

[43] Pietro DeLellis, Mario Di Bernardo, and Franco Garofalo. Adaptive pinning control of networks of circuits and systems in lur'e form. *IEEE Transactions on Circuits and Systems I: Regular Papers*, 60(11):3033–3042, 2013.

[44] Pietro DeLellis, Mario Di Bernardo, Thomas E Gorochowski, and Giovanni Russo. Synchronization and control of complex networks via contraction, adaptation and evolution. *IEEE Circuits and Systems Magazine*, 10(3):64–82, 2010.

[45] Pietro DeLellis, Franco Garofalo, Maurizio Porfiri, et al. Evolution of complex networks via edge snapping. *IEEE Transactions on Circuits and Systems I: Regular Papers*, 57(8):2132–2143, 2010.

[46] Jordi Delgado and Ricard V Solé. Noise induced transitions in fluid neural networks. *Physics Letters A*, 229(3):183–189, 1997.

[47] Bo Deng and Gwendolen Hines. Food chain chaos due to shilnikov's orbit. *Chaos: An Interdisciplinary Journal of Nonlinear Science*, 12(3):533–538, 2002.

[48] William L Ditto, Steven N Rauseo, and Mark L Spano. Experimental control of chaos. *Physical Review Letters*, 65(26):3211, 1990.

[49] Sergey N Dorogovtsev and Jose FF Mendes. Evolution of networks. *Advances in physics*, 51(4):1079–1187, 2002.

[50] David JD Earn, Simon A Levin, and Pejman Rohani. Coherence and conservation. *Science*, 290(5495):1360–1364, 2000.

[51] Charles Elton and Mary Nicholson. The ten-year cycle in numbers of the lynx in canada. *The Journal of Animal Ecology*, pages 215–244, 1942.

[52] Charles S Elton. Periodic fluctuations in the numbers of animals: their causes and effects. *Journal of Experimental Biology*, 2(1):119–163, 1924.

[53] Y Fang, KA Loparo, and X Feng. Stability of discrete time jump linear systems. *Journal of Mathematical Systems, Estimation and Control*, 5(3):275–321, 1995.

[54] Yuguang Fang. *Stability analysis of linear control systems with uncertain parameters*. PhD thesis, Case Western Reserve University, 1994.

[55] Yuguang Fang and Kenneth A Loparo. On the relationship between the sample path and moment lyapunov exponents for jump linear systems. *IEEE transactions on automatic control*, 47(9):1556–1560, 2002.

[56] Yuguang Fang and Xiangbo Loparo, K. A.and Feng. Almost sure and δmoment stability of jump linear systems. *International Journal of Control*, 59(5):1281–1307, 1994.

[57] Herta Flor, Christoph Braun, Thomas Elbert, and Niels Birbaumer. Extensive reorganization of primary somatosensory cortex in chronic back pain patients. *Neuroscience letters*, 224(1):5–8, 1997.

[58] Mattia Frasca, Arturo Buscarino, Alessandro Rizzo, Luigi Fortuna, and Stefano Boccaletti. Synchronization of moving chaotic agents. *Physical review letters*, 100(4):044102, 2008.

[59] Hu Gang and Qu Zhilin. Controlling spatiotemporal chaos in coupled map lattice systems. *Physical Review Letters*, 72(1):68, 1994.

[60] Chris Godsil and Gordon F Royle. *Algebraic graph theory*, volume 207. Springer Science & Business Media, 2013.

[61] Olga Golovneva, Russell Jeter, Igor Belykh, and Maurizio Porfiri. Windows of opportunity for synchronization in stochastically coupled maps. *Physica D: Nonlinear Phenomena*, 340:1–13, 2017.

[62] Thomas E Gorochowski, Mario Di Bernardo, and Claire S Grierson. Evolving dynamical networks: a formalism for describing complex systems. *Complexity*, 17(3):18–25, 2012.

[63] Thomas E Gorochowski, Mario di Bernardo, and Claire S Grierson. Evolving enhanced topologies for the synchronization of dynamical complex networks. *Physical Review E*, 81(5):056212, 2010.

[64] BT Grenfell, K_ Wilson, BF Finkenstädt, TN Coulson, Stuart Murray, SD Albon, JM Pemberton, TH Clutton-Brock, and MJ Crawley. Noise and determinism in synchronized sheep dynamics. *Nature*, 394(6694):674–677, 1998.

[65] RO Grigoriev, MC Cross, and HG Schuster. Pinning control of spatiotemporal chaos. *Physical Review Letters*, 79(15):2795, 1997.

[66] Robert Grone and Russell Merris. The laplacian spectrum of a graph ii. *SIAM Journal on Discrete Mathematics*, 7(2):221–229, 1994.

[67] Ilkka Hanski and Ian P Woiwod. Spatial synchrony in the dynamics of moth and aphid populations. *Journal of Animal Ecology*, pages 656–668, 1993.

[68] Martin Hasler and Igor Belykh. Blinking long-range connections increase the functionality of locally connected networks. *IEICE Transactions on Fundamentals of Electronics, Communications and Computer Sciences*, 88(10):2647–2655, 2005.

[69] Martin Hasler, Vladimir Belykh, and Igor Belykh. Dynamics of stochastically blinking systems. part i: Finite time properties. *SIAM Journal on Applied Dynamical Systems*, 12(2):1007–1030, 2013.

[70] Martin Hasler, Vladimir Belykh, and Igor Belykh. Dynamics of stochastically blinking systems. part ii: Asymptotic properties. *SIAM Journal on Applied Dynamical Systems*, 12(2):1031–1084, 2013.

[71] Martin Hasler and Yuri L Maistrenko. An introduction to the synchronization of chaotic systems: Coupled skew tent maps. *IEEE Transactions on Circuits and Systems I: Fundamental Theory and Applications*, 44(10):856–866, 1997.

[72] Boris Hasselblatt and Anatole Katok. *Handbook of dynamical systems*. Elsevier, 2002.

[73] Daihai He, Lewi Stone, and Bernard Cazelles. Noise-induced synchronization in multitrophic chaotic ecological systems. *International Journal of Bifurcation and Chaos*, 20(06):1779–1788, 2010.

[74] Kevin Higgins, Alan Hastings, Jacob N Sarvela, and Louis W Botsford. Stochastic dynamics and deterministic skeletons: population behavior of dungeness crab. *Science*, 276(5317):1431–1435, 1997.

[75] Yunxin Huang and Odo Diekmann. Predator migration in response to prey density: what are the consequences? *Journal of mathematical biology*, 43(6):561–581, 2001.

[76] Junji Ito and Kunihiko Kaneko. Spontaneous structure formation in a network of chaotic units with variable connection strengths. *Physical Review Letters*, 88(2):028701, 2001.

[77] R. Jeter, M. Porfiri, and I. Belykh. Network synchronization through stochastic broadcasting. *IEEE Control Systems Letters*, 2(1):103–108, Jan 2018.

[78] Russell Jeter and Igor Belykh. Dynamical networks with on-off stochastic connections: Beyond fast switching. In *Circuits and Systems (ISCAS), 2014 IEEE International Symposium on*, pages 1788–1791. IEEE, 2014.

[79] Russell Jeter and Igor Belykh. Synchronization in on-off stochastic networks: windows of opportunity. *IEEE Transactions on Circuits and Systems I: Regular Papers*, 62(5):1260–1269, 2015.

[80] Russell Jeter and Igor Belykh. Synchrony in metapopulations with sporadic dispersal. *International Journal of Bifurcation and Chaos*, 25(07):1540002, 2015.

[81] Russell Jeter, Maurizio Porfiri, and Igor Belykh. Stochastic network synchronization: Overcoming network resistance via stochastic broadcasting. *Chaos*, (Submitted).

[82] Derek M Johnson, Andrew M Liebhold, Ottar N Bjørnstad, and Michael L Mcmanus. Circumpolar variation in periodicity and synchrony among gypsy moth populations. *Journal of Animal Ecology*, 74(5):882–892, 2005.

[83] Dominic Jordan and Peter Smith. *Nonlinear ordinary differential equations: an introduction for scientists and engineers*, volume 10. Oxford University Press on Demand, 2007.

[84] Peter Leonidovich Kapitza. A pendulum with oscillating suspension. *Uspekhi Fizicheskikh Nauk*, 44:7–20, 1951.

[85] I. I. Kats and N. N. Krasovskii. On the stability of systems with random parameters. *Journal of Applied Mathematics and Mechanics*, 24:1225–1246, 1960.

[86] Ljupčo Kocarev, Predrag Janjić, Ulrich Parlitz, and Toni Stojanovski. Controlling spatio-temporal chaos in coupled oscillators by sporadic driving. *Chaos, Solitons & Fractals*, 9(1):283–293, 1998.

[87] Dieter Köhler. The interaction between conditioned fish and naive schools of juvenile carp (Cyprinus carpio, pisces). *Behavioural Processes*, 1(3):267–275, 1976.

[88] F. Kozin. A survey of stability of stochastic systems. *Automatica*, 5(1):95–112, 1969.

[89] Harold Joseph Kushner. *Introduction to stochastic control*. Holt, Rinehart and Winston New York, 1971.

[90] Yu A Kuznetsov, Oscar De Feo, and Sergio Rinaldi. Belyakov homoclinic bifurcations in a tritrophic food chain model. *SIAM Journal on Applied Mathematics*, 62(2):462–487, 2001.

[91] Sean D Lawley, Jonathan C Mattingly, and Michael C Reed. Sensitivity to switching rates in stochastically switched odes. *Communications in Mathematical Sciences*, 12(7), 2014.

[92] Simon A Levin. The problem of pattern and scale in ecology: the robert h. macarthur award lecture. *Ecology*, 73(6):1943–1967, 1992.

[93] Zoran Levnajić and Igor Mezić. Ergodic theory and visualization. i. mesochronic plots for visualization of ergodic partition and invariant sets. *Chaos: An Interdisciplinary Journal of Nonlinear Science*, 20(3):033114, 2010.

[94] R Lima and M Rahibe. Exact lyapunov exponent for infinite products of random matrices. *Journal of Physics A: Mathematical and General*, 27(10):3427, 1994.

[95] Yang-Yu Liu, Jean-Jacques Slotine, and Albert-László Barabási. Controllability of complex networks. *Nature*, 473(7346):167, 2011.

[96] Jinhu Lu and Guanrong Chen. A time-varying complex dynamical network model and its controlled synchronization criteria. *IEEE Transactions on Automatic Control*, 50(6):841–846, 2005.

[97] Wenlian Lu. Adaptive dynamical networks via neighborhood information: Synchronization and pinning control. *Chaos: An Interdisciplinary Journal of Nonlinear Science*, 17(2):023122, 2007.

[98] M. Mariton. *Jump Linear Systems in Automatic Control*. Marcel Dekker, New York, USA, 1988.

[99] Renato E Mirollo and Steven H Strogatz. Synchronization of pulse-coupled biological oscillators. *SIAM Journal on Applied Mathematics*, 50(6):1645–1662, 1990.

[100] Arghya Mondal, Sudeshna Sinha, and Juergen Kurths. Rapidly switched random links enhance spatiotemporal regularity. *Physical Review E*, 78(6):066209, 2008.

[101] Toader Morozan. Optimal stationary control for dynamic systems with markov perturbations. *Stochastic Analysis and Applications*, 1(3):299–325, 1983.

[102] Mark EJ Newman and Duncan J Watts. Renormalization group analysis of the small-world network model. *Physics Letters A*, 263(4-6):341–346, 1999.

[103] M Ogura and CF Martin. Generalized joint spectral radius and stability of switching systems. *Linear Algebra and its Applications*, 439(8):2222–2239, 2013.

[104] Bernt Øksendal. Stochastic differential equations. In *Stochastic differential equations*, pages 65–84. Springer, 2003.

[105] FWJ Olver, DW Lozier, RF Boisvert, and CW Clark. Nist handbook of mathematical functions, cambridge uni. *Press, Cambridge*, 2010.

[106] Edward Ott. *Chaos in dynamical systems*. Cambridge university press, 2002.

[107] Edward Ott, Celso Grebogi, and James A Yorke. Controlling chaos. *Physical review letters*, 64(11):1196, 1990.

[108] Louis M Pecora. Synchronization conditions and desynchronizing patterns in coupled limit-cycle and chaotic systems. *Physical Review E*, 58(1):347, 1998.

[109] Louis M Pecora and Thomas L Carroll. Master stability functions for synchronized coupled systems. *Physical review letters*, 80(10):2109, 1998.

[110] Carmen Pedicini, Francesco Vasca, Luigi Iannelli, and Ulf Jonsson. An overview on averaging for pulse-modulated switched systems. In *Decision and Control and European Control Conference (CDC-ECC), 2011 50th IEEE Conference on*, pages 1860–1865. IEEE, 2011.

[111] Alan S Perelson, Denise E Kirschner, and Rob De Boer. Dynamics of hiv infection of cd4+ t cells. *Mathematical biosciences*, 114(1):81–125, 1993.

[112] Arkady Pikovsky and Antonio Politi. *Lyapunov exponents: a tool to explore complex dynamics*. Cambridge University Press, 2016.

[113] Steve Pincus. Strong laws of large numbers for products of random matrices. *Transactions of the American Mathematical Society*, 287(1):65–89, 1985.

[114] Maurizio Porfiri. A master stability function for stochastically coupled chaotic maps. *EPL (Europhysics Letters)*, 96(4):40014, 2011.

[115] Maurizio Porfiri. Stochastic synchronization in blinking networks of chaotic maps. *Physical Review E*, 85(5):056114, 2012.

[116] Maurizio Porfiri and Igor Belykh. Memory matters in synchronization of stochastically coupled maps. *SIAM Journal on Applied Dynamical Systems*, 16(3):1372–1396, 2017.

[117] Maurizio Porfiri and Mario Di Bernardo. Criteria for global pinning-controllability of complex networks. *Automatica*, 44(12):3100–3106, 2008.

[118] Maurizio Porfiri and Francesca Fiorilli. Global pulse synchronization of chaotic oscillators through fast-switching: theory and experiments. *Chaos, Solitons & Fractals*, 41(1):245–262, 2009.

[119] Maurizio Porfiri and Francesca Fiorilli. Node-to-node pinning control of complex networks. *Chaos: An Interdisciplinary Journal of Nonlinear Science*, 19(1):013122, 2009.

[120] Maurizio Porfiri and Francesca Fiorilli. Experiments on node-to-node pinning control of chua's circuits. *Physica D: Nonlinear Phenomena*, 239(8):454–464, 2010.

[121] Maurizio Porfiri, Russell Jeter, and Igor Belykh. Windows of opportunity for the stability of jump linear systems: almost sure versus moment convergence. (Submitted).

[122] Maurizio Porfiri and Roberta Pigliacampo. Master-slave global stochastic synchronization of chaotic oscillators. *SIAM Journal on Applied Dynamical Systems*, 7(3):825–842, 2008.

[123] Maurizio Porfiri and Daniel J Stilwell. Consensus seeking over random weighted directed graphs. *IEEE Transactions on Automatic Control*, 52(9):1767–1773, 2007.

[124] Maurizio Porfiri, Daniel J Stilwell, and Erik M Bollt. Synchronization in random weighted directed networks. *IEEE Transactions on Circuits and Systems I: Regular Papers*, 55(10):3170–3177, 2008.

[125] Maurizio Porfiri, Daniel J Stilwell, Erik M Bollt, and Joseph D Skufca. Random talk: Random walk and synchronizability in a moving neighborhood network. *Physica D: Nonlinear Phenomena*, 224(1):102–113, 2006.

[126] Kestutis Pyragas. Continuous control of chaos by self-controlling feedback. *Physics letters A*, 170(6):421–428, 1992.

[127] Pasko Rakic. Progress: Neurogenesis in adult primate neocortex: an evaluation of the evidence. *Nature Reviews Neuroscience*, 3(1):65, 2002.

[128] Esa Ranta, Veijo Kaitala, Jan Lindström, and Eero Helle. The moran effect and synchrony in population dynamics. *Oikos*, pages 136–142, 1997.

[129] Esa Ranta, Veijo Kaitala, Jan Lindstrom, and Harto Linden. Synchrony in population dynamics. *Proceedings of the Royal Society of London B: Biological Sciences*, 262(1364):113–118, 1995.

[130] O Ravera. Caratteristiche chimiche e fisiche delle acque del lago di lugano. *Quaderni di geologia e geofisica applicata*, 2:137–148, 1977.

[131] Sergio Rinaldi. Synchrony in slow–fast metacommunities. *International journal of bifurcation and chaos*, 19(07):2447–2453, 2009.

[132] Sergio Rinaldi. Recurrent and synchronous insect pest outbreaks in forests. *Theoretical population biology*, 81(1):1–8, 2012.

[133] Sergio Rinaldi, Fabio Della Rossa, and Pietro Landi. A mathematical model of "gone with the wind". *Physica A: Statistical Mechanics and its Applications*, 392(15):3231 – 3239, 2013.

[134] A. Rosembloom. Analysis of linear systems with randomly time-varying parameters. *Proceedings of the Symposium on Information Nets*, 3:145, 1954.

[135] Michael L Rosenzweig and Robert H MacArthur. Graphical representation and stability conditions of predator-prey interactions. *The American Naturalist*, 97(895):209–223, 1963.

[136] Rajarshi Roy, TW Murphy Jr, TD Maier, Z Gills, and ER Hunt. Dynamical control of a chaotic laser: Experimental stabilization of a globally coupled system. *Physical Review Letters*, 68(9):1259, 1992.

[137] Kelvin Rozier and Vladimir E Bondarenko. Distinct physiological effects of β1-and β2-adrenoceptors in mouse ventricular myocytes: insights from a compartmentalized mathematical model. *American Journal of Physiology-Cell Physiology*, 312(5):C595–C623, 2017.

[138] Kelvin Rozier and Vladimir E Bondarenko. Mathematical modeling physiological effects of the overexpression of β2-adrenoceptors in mouse ventricular myocytes. *American Journal of Physiology-Heart and Circulatory Physiology*, 314(3):H643–H658, 2017.

[139] Michael K Schwartz, L Scott Mills, Kevin S McKelvey, Leonard F Ruggiero, and Fred W Allendorf. Dna reveals high dispersal synchronizing the population dynamics of canada lynx. *Nature*, 415(6871):520–522, 2002.

[140] Joseph D Skufca and Erik M Bollt. Communication and synchronization in disconnected networks with dynamic topology: Moving neighborhood networks. *arXiv preprint nlin/0307010*, 2003.

[141] Paul So, Bernard C Cotton, and Ernest Barreto. Synchronization in interacting populations of heterogeneous oscillators with time-varying coupling. *Chaos: An Interdisciplinary Journal of Nonlinear Science*, 18(3):037114, 2008.

[142] Ricard V Solé and Octavio Miramontes. Information at the edge of chaos in fluid neural networks. *Physica D: Nonlinear Phenomena*, 80(1-2):171–180, 1995.

[143] Francesco Sorrentino, Mario di Bernardo, Franco Garofalo, and Guanrong Chen. Controllability of complex networks via pinning. *Physical Review E*, 75(4):046103, 2007.

[144] Francesco Sorrentino and Edward Ott. Adaptive synchronization of dynamics on evolving complex networks. *Physical review letters*, 100(11):114101, 2008.

[145] Andrzej Stefański, Przemyslaw Perlikowski, and Tomasz Kapitaniak. Ragged synchronizability of coupled oscillators. *Physical Review E*, 75(1):016210, 2007.

[146] Toni Stojanovski, Ljupco Kocarev, Ulrich Parlitz, and Richard Harris. Sporadic driving of dynamical systems. *Physical Review E*, 55(4):4035, 1997.

[147] Steven H Strogatz. Exploring complex networks. *Nature*, 410(6825):268–276, 2001.

[148] Steven H Strogatz. *Nonlinear dynamics and chaos: with applications to physics, biology, chemistry, and engineering*. Hachette UK, 2014.

[149] Rob Sturman and Jean-Luc Thiffeault. Lyapunov exponents for the random product of two shears. *arXiv preprint arXiv:1706.03398*, 2017.

[150] Zhendong Sun. *Switched linear systems: control and design*. Springer Science & Business Media, 2006.

[151] Yang Tang, Huijun Gao, Jürgen Kurths, and Jian-an Fang. Evolutionary pinning control and its application in uav coordination. *IEEE Transactions on Industrial Informatics*, 8(4):828–838, 2012.

[152] Yang Tang, Feng Qian, Huijun Gao, and Jürgen Kurths. Synchronization in complex networks and its application–a survey of recent advances and challenges. *Annual Reviews in Control*, 38(2):184–198, 2014.

[153] John N Tsitsiklis and Vincent D Blondel. The lyapunov exponent and joint spectral radius of pairs of matrices are hard when not impossible to compute and to approximate. *Mathematics of Control, Signals, and Systems (MCSS)*, 10(1):31–40, 1997.

[154] Duncan J Watts and Steven H Strogatz. Collective dynamics of 'small-world'networks. *nature*, 393(6684):440, 1998.

[155] Kurt Wiesenfeld and Frank Moss. Stochastic resonance and the benefits of noise: from ice ages to crayfish and squids. *Nature*, 373(6509):33–36, 1995.

[156] Paul David Williams and Alan Hastings. Stochastic dispersal and population persistence in marine organisms. *The American Naturalist*, 182(2):271–282, 2013.

[157] Wenwu Yu, Pietro DeLellis, Guanrong Chen, Mario Di Bernardo, and Jürgen Kurths. Distributed adaptive control of synchronization in complex networks. *IEEE Transactions on Automatic Control*, 57(8):2153–2158, 2012.

[158] Damián H Zanette and Alexander S Mikhailov. Dynamical systems with time-dependent coupling: clustering and critical behaviour. *Physica D: Nonlinear Phenomena*, 194(3):203–218, 2004.

[159] Jing Zhou and Qian Wang. Convergence speed in distributed consensus over dynamically switching random networks. *Automatica*, 45(6):1455–1461, 2009.

Appendix A

APPENDIX FOR CHAPTER 2

In this appendix, we give the details for the calculation of upper bounds (2.10) for the first and second derivatives of Lyapunov functions W_Φ and W_F.

The upper bound for the first derivative of Lyapunov function $\dot{W}_\Phi$ (2.8) on $R : 0 \le \rho \le 3$ falls on the endpoint $r = 3$ and equals

$$B_{W\Phi} = \max_{0\le r\le 3} \left|\dot{W}\right| = \max_{0\le r\le 3} \lambda r^2(r-1)^2(r-2)^2 = 36\lambda. \tag{A.1}$$

The second derivative $\ddot{W}(r) \equiv D^2_\Phi W$ (see the notation in [70]) reads as

$$\ddot{W}_\Phi = 2\lambda^2(3r^2-6r+2)r^2(r-1)^2(r-2)^2 = 2\lambda(3r^2-6r+2)\left|\dot{W}_\Phi\right|.$$

Hence, the absolute value of its bound on R, also at $r = 3$, is

$$LB_{W\Phi} = \max_{0\le r\le 3} \left|\ddot{W}_\Phi\right| < 2\lambda \cdot 11 \cdot \max_{0\le r\le 3} \left|\dot{W}_\Phi\right| = 792\lambda^2. \tag{A.2}$$

Similarly, we calculate the first derivative of Lyapunov function W_F (2.9) for the switching system (2.1)-(2.2)

$$\dot{W}_F = \operatorname{grad} W \cdot F = W_\rho\left(\rho_x\dot{x} + \rho_y\dot{y}\right) = -\lambda\rho^2(\rho-1)(\rho-2)(\rho^2-2(2-s)\rho+7-10s).$$

Note that $\dot{W}_F$ depends on a particular sequence of $s(t) = 0$ and $s(t) = 1$, generated by the i.i.d. stochastic switching. In terms of notation in [70], $\dot{W}_F \equiv D_F W(x, s)$.

The absolute value of its bound on R can be estimated by

$$\begin{aligned} B_{WF} = \max_{s\in\{0,1\}} \max_{0\le r\le 3} \left|\dot{W}_F\right| < \lambda \max_{0\le\rho\le 3} |\rho(\rho-1)(\rho-2)| \times \\ \times \max_{s\in\{0,1\}} \max_{0\le r\le 3} |.\rho(\rho^2 - 2(2-s)\rho + 7 - 10s)| \,. \end{aligned} \tag{A.3}$$

The maximum of the first co-factor in (A.3), $|\rho(\rho-1)(\rho-2)|$, on R is reached at the endpoint $r = 3$ and equals 6. The second co-factor $|\rho(\rho^2 - 2(2-s)\rho + 7 - 10s)|$ depends on s which may take on values 0 and 1. When the switch is on and $s = 1$, it becomes $|\rho(\rho^2 - 2\rho - 3)|$, whereas when the switch is off and $s = 0$, it takes the form $|\rho(\rho^2 - 4\rho + 7)|$. Simple analysis shows that the maximum of the latter function for $s = 0$ on R is larger than that of the former function for $s = 0$. It is reached at $\rho = 3$ and therefore equals 12. Hence, the upper bound for estimate (A.3) becomes

$$B_{WF} = \lambda \cdot 6 \cdot 12 = 72\lambda. \tag{A.4}$$

Finally, we calculate the second derivative $\ddot{W}_F(\rho) \equiv D_F^2 W$ (see the notation in [70]):

$$\begin{aligned} \ddot{W}_F = \operatorname{grad} \dot{W}_F \cdot F = -\lambda\rho^2(\rho-1)(\rho-2)(\rho^2 - 2(2-s)\rho + 7 - 10s) \times \\ \times \left(-\lambda\rho(\rho^2 - 2(2-\tilde{s})\rho + 7 - 10\tilde{s})\right), \end{aligned} \tag{A.5}$$

where s and $\tilde{s}$ are taken from two different stochastic sequences, corresponding to $\dot{W}_F$ and the switching system (2.1)-(2.2) (via F). Depending on the combination of random values $s = 0, 1$ and $\tilde{s} = 0, 1$, function (A.5) has four different expressions for $(s = 1, \tilde{s} = 1)$, $(s = 1, \tilde{s} = 0)$, $(s = 0, \tilde{s} = 1)$, and $(s = 0, \tilde{s} = 0)$. Our analysis indicates that the maximum value of $\ddot{W}_F$ on R is produced by the combination $s = 0, \tilde{s} = 0$, generating the following function:

$$\max_{s,\tilde{s}\in\{0,1\}} \ddot{W}_F = \lambda^2(6\rho^5 - 35\rho^4 + 84\rho^3 - 87\rho^2 + 28\rho)(\rho(\rho^2 - 4\rho + 7). \tag{A.6}$$

The first co-factor polynomial $P_1 = 6\rho^5 - 35\rho^4 + 84\rho^3 - 87\rho^2 + 28\rho$ can be bounded from

above as follows: $\max_{0\le r\le 3}|P_1| < \max_{0\le r\le 3}|6\rho^5 - 35\rho^4| + \max_{0\le r\le 3}|84\rho^3 - 87\rho^2 + 28\rho|$. The latter two maximum values are reached at the endpoint $\rho = 3$ so that $\max_{0\le r\le 3}|P_1| < 1377 + 1395 = 2772$. The second co-factor polynomial $P_2 = (\rho(\rho^2 - 4\rho + 7)$ in (A.6) was estimated above (cf. (A.4)) and is bounded by 12. Thus,

$$LB_{WF} = \max_{s\in\{0,1\}} \max_{0\le r\le 3} \left|\ddot{W}_F\right| = \lambda^2 \max_{0\le r\le 3}|P_1| \max_{0\le r\le 3}|P_2| = 33264\lambda^2. \tag{A.7}$$

Collecting (A.1),(A.2),(A.4), and (A.7) yields bounds (2.10).

Appendix B

DERIVATION OF THE BOUND FROM THEOREM 4.2

In this appendix, we present the calculations of the constants used in the statement of Theorem 4.2. As we consider the two-patch network, we can rewrite the Lyapunov function (4.10) for the different variables $X = x_2 - x_1$, $Y = y_2 - y_1$, $Z = z_2 - z_1$ as

$$W = \frac{1}{2}\left(X^2 + Y^2 + Z^2\right). \tag{B.1}$$

To apply Theorem 9.1 in [70] to the global stability of approximate synchronization in the two-patch x, y, z-coupled network (4.2) with $\varepsilon = \varepsilon_x = \varepsilon_y = \varepsilon_z$, we need to calculate upper bounds on the first and second time derivatives of the Lyapunov function W, calculated along solutions of the averaged and switching networks. As in the main text, we use the same notation for the Lyapunov functions and their derivatives as in [70]. The required derivatives are

$$\begin{aligned} B_{W\Phi} &= \max_{\mathbf{x}\in\mathbb{R}} |D_\Phi W(\mathbf{x})| \\ LB_{W\Phi} &= \max_{\mathbf{x}\in\mathbb{R}} |D^2_\Phi W(\mathbf{x})| \\ B_{WF} &= \max_{\mathbf{s}\in 0,1^M} \max_{x\in\mathbb{R}} |D_F W(\mathbf{x},\mathbf{s})| \\ LB_{WF} &= \max_{\mathbf{s},\bar{\mathbf{s}}\in 0,1^M} \max_{x\in\mathbb{R}} |D^2_F W(\mathbf{x},\bar{\mathbf{s}},\mathbf{s})|, \end{aligned} \tag{B.2}$$

where $\mathbf{x}$ is the vector of $\mathbf{x}_i = \{x_i, y_i, z_i\}, i = 1, 2$, $\mathbb{R}$ is the systems' absorbing domain, $\mathbf{s}$ is a set of stochastic sequences corresponding to the connections between patches and the switching of the parameter a_1; similarly, $\bar{\mathbf{s}}$ corresponds to another set of stochastic switching sequences. We start with $B_{W\Phi}$, which requires the first time derivative of the Lyapunov function of the averaged system:

$$D_\Phi W(x) = X\dot{X} + Y\dot{Y} + Z\dot{Z}.$$

Here, the derivatives $\dot{X}$, $\dot{Y}$, and $\dot{Z}$ are given by the following difference system, obtained by subtracting the corresponding equations of the averaged network

$$\begin{aligned} \dot{X} &= [(f(x_2) - f(x_1)) - (g(x_2)y_2 - g(x_1)y_1)] - 2p\varepsilon X \\ \dot{Y} &= [(g(x_2)y_2 - g(x_1)y_1) - (h(y_2)z_2 - h(y_1)z_1)] - (m_1 + 2p\varepsilon)\, Y \\ \dot{Z} &= [h(y_2)z_2 - h(y_1)z_1] - (m_2 + 2p\varepsilon)\, Z \end{aligned} \tag{B.3}$$

with $f(\eta) = r\eta\left(1 - \frac{\eta}{K}\right)$, $g(\eta) = \frac{a_1^*\eta}{1+a_1^*b_1\eta}$, where $\eta = x_1, x_2$ and $a_1^* = [1 + \Delta a \cdot p]a_1$ and $h(\xi) = \frac{a_2\xi}{1+a_2b_2\xi}$ with $\xi = y_1, y_2$.

Recall that $0 \leq x_i,y_i,z_i < \psi = \frac{K}{4rm_2}\left(r + m_2\right)^2$ (cf. (4.9)). We use this bound to find $B_{W\Phi} = \max_{\mathbf{x}\in\mathbb{R}}|D_\Phi W(\mathbf{x})|$ by substituting either 0 or ψ for each x_i,y_i, z_i $(i = 1, 2)$, depending on which will maximize each term. While this may not give the tightest bound, it simplifies the derivation of the bound, and makes the final bound a little more manageable:

$$\begin{aligned} \max|D_\Phi W(x)| = \; & \Big[\psi\left(r\psi + p\varepsilon\psi + \tfrac{r\psi^2}{K} + a_1^*\psi + p\varepsilon\psi\right) + \psi\big(a_1^*\psi^2 + p\varepsilon\psi + m_1\psi + a_2\psi^2 \\ & + p\varepsilon\psi\big) + \psi\big(a_2\psi^2 + p\varepsilon\psi + m_2\psi + p\varepsilon\psi\big)\Big], \end{aligned}$$

which reduces to

$$B_{W\Phi} = \psi^2\big(r + \tfrac{r\psi}{K} + 2a_1^*\psi + m_1 + 2a_2\psi + m_2 + 6p\varepsilon\big). \tag{B.4}$$

Next, we repeat this process for $LB_{W\Phi} = \max_{\mathbf{x}\in\mathbb{R}}|D_\Phi^2 W(\mathbf{x})|$ which requires the second time derivative of the Lyapunov function of the averaged system, $D_\Phi^2 W(\mathbf{x})$. Taking the second time derivative of W_Φ, we get:

$$D_\Phi^2 W(\mathbf{x}) = \dot{X}^2 + X\ddot{X} + \dot{Y}^2 + Y\ddot{Y} + \dot{Z}^2 + Z\ddot{Z},$$

where $\ddot{X}$, $\ddot{Y}$, and $\ddot{Z}$ are defined by the system

$$\begin{aligned}
\ddot{X} &= \left[\dot{f}(x_2) - \dot{f}(x_1)\right] - \left[\dot{g}(x_2)y_2 + g(x_2)\dot{y}_2 - \dot{g}(x_1)y_1 - g(x_1)\dot{y}_1\right] - 2p\varepsilon\dot{X} \\
\ddot{Y} &= \left[\dot{g}(x_2)y_2 + g(x_2)\dot{y}_2 - \dot{g}(x_1)y_1 - g(x_1)\dot{y}_1\right] - \left[\dot{h}(y_2)z_2 + h(y_2)\dot{z}_2 - \dot{h}(y_1)z_1 - h(y_1)\dot{z}_1\right] \\
&\quad - (m_1 + 2p\varepsilon)\,\dot{Y} \\
\ddot{Z} &= \dot{h}(y_2)z_2 + h(y_2)\dot{z}_2 - \dot{h}(y_1)z_1 - h(y_1)\dot{z}_1 - (m_2 + 2p\varepsilon)\,\dot{Z}.
\end{aligned} \tag{B.5}$$

Then, using the same methods as before, we replace all of the variables with either ψ or 0, depending on which helps maximize the equation term by term. Using *Mathematica*, we simplify the tedious expression to get:

$$\begin{aligned}
LB_{W\Phi} &= \max|D^2_{\Phi}W(\mathbf{x})| \\
&= \psi^2\Big[4(a_1^*)^2\psi^2 + 6a_2^2\psi^2 + 2m_1^2 + m_2 + 2m_2^2 + 2p\varepsilon + 7pm_1\varepsilon + 5p\varepsilon m_2 + 20p^2\varepsilon^2 + \\
&\quad a_2\psi\,(1 + 5m_1 + a_1^*\psi\,(4 + m_1) + 4m_2 + 17p\varepsilon + m_1p\varepsilon) + 6\tfrac{r\varepsilon\psi}{K} + 6p\varepsilon r + 2p\varepsilon\psi r + \\
&\quad 3\tfrac{\psi^2r^2}{K} + 2\tfrac{\psi r^2}{K} + r^2 + \tfrac{a_1^*\psi}{K}\,(3Km_1 + 16p\varepsilon K + 5\psi r + 3Kr)\Big].
\end{aligned} \tag{B.6}$$

After finding these bounds for the averaged network, we must do the same thing for the stochastic system. We start by finding

$$\max|D_FW(\mathbf{x},\mathbf{s})| = X\dot{X} + Y\dot{Y} + Z\dot{Z},$$

where the derivatives $\dot{X}$, $\dot{Y}$, and $\dot{Z}$ are governed by the difference system which is identical to (B.19), when p is replaced with $s_{12}(t)$ and a_1^* with $[1+\Delta a\cdot\xi_1]a_1$ and a_1^* with $[1+\Delta a\cdot\xi_2]a_1$ in the functions $g(x_1)$ and $g(x_2)$, respectively. Similarly to the calculations of $B_{W\Phi}$, the expression for $\max|D_FW(\mathbf{x},\mathbf{s})|$ can be simplified using the same bounds. It is worth mentioning that in choosing the favorable bound term by term, the inequalities will be maximized for $s_{12} = 1$,

i.e when the switch is 'on' and $\xi_1 = \xi_2 = 1$ such that

$$\begin{aligned} B_{WF} &= \max |D_F W(\mathbf{x}, \mathbf{s})| \\ &= \Big[\psi\left(r\psi + \varepsilon\psi + \tfrac{r\psi^2}{K} + \hat{a}_1\psi + \varepsilon\psi\right) + \psi\big(\hat{a}_1\psi^2 + \varepsilon\psi + m_1\psi + \\ &\quad a_2\psi^2 + \varepsilon\psi\big) + \psi\left(a_2\psi^2 + \varepsilon\psi + m_2\psi + \varepsilon\psi\right)\Big], \end{aligned}$$

where $\hat{a}_1 = [1 + \Delta a]a_1$. The bound further reduces as follow

$$B_{WF} = \psi^2\big(r + \tfrac{r\psi}{K} + 2\hat{a}_1\psi + m_1 + 2a_2\psi + m_2 + 6\varepsilon\big). \tag{B.7}$$

Then, we take the second time derivative of W_F to get

$$D_F^2 W(\mathbf{x}, \mathbf{s}, \bar{\mathbf{s}}) \;=\; \dot{X}^2 + X\ddot{X} + \dot{Y}^2 + Y\ddot{Y} + \dot{Z}^2 + Z\ddot{Z},$$

with $\ddot{X}$, $\ddot{Y}$, and $\ddot{Z}$ defined in difference system (B.19), when p is replaced with $\bar{s}_{12}(t)$ and a_1^* with $[1 + \Delta a \cdot \bar{\xi}_1]a_1$ and a_1^* with $[1 + \Delta a \cdot \bar{\xi}_2]a_1$ in the functions $g(x_1)$ and $g(x_2)$, respectively. The reader should notice the additional stochastic variables $\bar{s}_{12}$, $\bar{\xi}_1$, and $\bar{\xi}_2$. This is another realization of the stochastic sequence that does not match the realization given by s_{12}, ξ_1, and ξ_2. However, after substituting the bounds on the state variables, we observe that the maximum is obtained when $s_{12} = \bar{s}_{12} = 1$, $\xi_1 = \bar{\xi}_1 = 1$, and $\xi_2 = \bar{\xi}_2 = 1$. Therefore, the bound simplifies to

$$\begin{aligned} LB_{WF} &= \max |D_F^2 W(x)| \\ &= \psi^2\Big[4\hat{a}_1^2\psi^2 + 6a_2^2\psi^2 + 2\varepsilon + 20\varepsilon^2 + 7\varepsilon m_1 + 2m_1^2 + m_2 + 5\varepsilon m_2 + 2m_2^2 + a_2\psi \cdot \\ &\quad \cdot (1 + 5m_1 + \hat{a}_1\psi\,(4 + m_1) + \varepsilon\,(17 + m_1) + 4m_2) + 6\tfrac{\psi\varepsilon r}{K} + 6\varepsilon r + 2\psi\varepsilon r + \\ &\quad 3\tfrac{\psi^2 r^2}{K^2} + 2\tfrac{\psi r^2}{K} + r^2 + \tfrac{\hat{a}_1\psi}{K}\,(16\varepsilon K + 5\psi r + 3K\,(m_1 + r))\Big]. \end{aligned} \tag{B.8}$$

The next step in deriving the bound τ^* of Theorem 4.2 is to define the size of the δ-neighborhood of the ghost synchronization solution of the stochastic system (4.2). To do

this, we choose a level curve of the Lyapunov function W_Φ for the averaged system (4.3):

$$V_0 : W = \frac{1}{2}\left(\delta_X^2 + \delta_Y^2 + \delta_Z^2\right). \tag{B.9}$$

We let $\delta = \max\{\delta_X, \delta_Y, \delta_Z\}$, which simplifies the level to

$$V_0 : W_\Phi \leq \frac{3}{2}\delta^2. \tag{B.10}$$

We define another level, V_1 as the absorbing domain of the Lyapunov function, which we obtain by replacing each difference variable with its maximum value, subject to the constraints on $\mathbf{x}$. We get:

$$V_1 : W_\Phi = \frac{1}{2}\left(\psi^2 + \psi^2 + \psi^2\right) = \frac{3}{2}\psi^2. \tag{B.11}$$

These level curves allow us to define the following quantity used in the general Theorem 9.1 [70]:

$$\gamma = \min_{\mathbf{x}\in\mathbf{R}, V_0 \leq W_\Phi \leq V_1} |D_\Phi W(x)|.$$

We can see that $|D_\Phi W(X)|$ is minimized at the level V_0, which corresponds to the δ-neighborhood. Hence, we calculate γ as:

$$\gamma = \min_{\mathbf{x}\in\mathbb{R}, V_0 \leq W_\Phi \leq V_1} |D_\Phi W(x)| = |\delta^2\left(r - \tfrac{r}{K}\delta - m_1 - m_2 - 6p\varepsilon\right)|. \tag{B.12}$$

We must also define the following constants that are used in the theorem:

$$\begin{aligned} c &= \tfrac{1}{64(LB_{WF} + LB_{W\Phi})B_{WF}^2} \\ D &= 8(LB_{WF} + LB_{W\Phi}) \\ U_0 &= \left\{x | W(x) < V_0 + \tfrac{4\gamma^2}{D}\right\}, \end{aligned} \tag{B.13}$$

where U_0 is a neighborhood of the synchronization solution of the averaged system (4.3), and is slightly larger than V_0, which corresponds to the δ-neighborhood of the ghost synchronization solution in the stochastic system (4.2). After substituting the values for B_{WF},

LB_{WF}, and $LB_{W\Phi}$ we obtain

$$\begin{aligned} c &= K^4 \cdot \Big[64\psi^4\big(2\hat{a}_1\psi K + 2a_2\psi K + Km_1 + Km_2 + 6Kp\varepsilon + \psi r + Kr\big)^2\big(\tfrac{1}{K^2\psi^2}\big(6a_2^2\psi^2K^2 + \\ &\quad 4(\hat{a}_1)^2\psi^2K^2 + 2K^2m_1^2 + K^2m_2 + 2K^2m_2^2 + 2p\varepsilon K^2 + 7p\varepsilon K^2m_1 + 5p\varepsilon K^2m_2 + 20p^2\varepsilon^2K^2 + \\ &\quad a_2\psi K^2\big(15m_1 + \hat{a}_1\psi\,(4 + m_1) + 4m_2 + 17p\varepsilon + p\varepsilon m_1\big) + 6\psi pKr\varepsilon + 6p\varepsilon K^2r + 2\psi p\varepsilon rK^2 + \\ &\quad 3\psi^2r^2 + 2\psi r^2K + K^2r^2 + \hat{a}_1\psi K\big(3Km_1 + 16p\varepsilon K + 5\psi r + 3Kr\big)\big) + \tfrac{1}{K^2\psi^2}\big(6a_2^2\psi^2K^2 + \\ &\quad a_2\psi K^2\big(1 + 4m_2 + 4a_1^*\psi + 17p\varepsilon + m_1\big(5 + a_1^*\psi + p\varepsilon\big)\big) + 3\psi^2r^2 + \psi Kr\big(5a_1^*\psi + 6p\varepsilon + 2r\big) + \\ &\quad K^2\big(2m_1^2 + m_2 + 2m_2^2 + 2p\varepsilon + 3a_1^*\psi m_1 + 7p\varepsilon m_1 + 5p\varepsilon m_2 + 4(a_1^*)^2\psi^2 + 16a_1^*\psi p\varepsilon + 20p^2\varepsilon^2 + \\ &\quad 3a_1^*\psi r + 6rp\varepsilon + 2\psi rp\varepsilon + r^2\big)\big)\big)\Big]^{-1} \end{aligned} \tag{B.14}$$

and

$$\begin{aligned} D &= 8\psi^2\Big(12a_2^2\psi^2 + 4(a_1^*)^2\psi^2 + 4\hat{a}_1^2\psi^2 + a_2\psi\big((\hat{a}_1\psi + a_1^*\psi)\,(4 + m_1) + 2\big(1 + 5m_1 + 4m_2 + \\ &\quad 17p\varepsilon + m_1p\varepsilon\big)\big) + \tfrac{(a_1^* + \hat{a}_1)\psi}{K}\big(5\psi r + K\big(3m_1 + 16p\varepsilon + 3r\big)\big) + 2\big(\tfrac{1}{K}\big(3\psi^2r^2 + 2\psi Kr\,(3p\varepsilon + r) \\ &\quad + 2m_1^2 + m_2 + 2m_2^2 + r^2 + p\varepsilon\big(2 + 7m_1 + 5m_2 + 20p\varepsilon + 6r + 2\psi r\big)\big)\Big). \end{aligned} \tag{B.15}$$

With C_1 being defined as $\frac{4\gamma}{D}$, we get

$$\begin{aligned} C_1 &= \delta^4\left(r - \tfrac{r}{K}\delta - m_1 - m_2 - 6p\varepsilon\right)^2\tfrac{1}{2}\Big[\psi^2\Big(12a_2^2\psi^2 + 4(a_1^*)^2\psi^2 + 4\hat{a}_1^2\psi^2 + \\ &\quad a_2\psi\big((\hat{a}_1\psi + a_1^*\psi)\,(4 + m_1) + 2\big(1 + 5m_1 + 4m_2 + 17p\varepsilon + m_1p\varepsilon\big)\big) + \tfrac{(a_1^* + \hat{a}_1)\psi}{K}\big(5\psi r + \\ &\quad K\big(3m_1 + 16p\varepsilon + 3r\big)\big) + 2\big(\tfrac{1}{K}\big(3\psi^2r^2 + 2\psi Kr\,(3p\varepsilon + r) + 2m_1^2 + m_2 + 2m_2^2 + r^2 + \\ &\quad p\varepsilon\big(2 + 7m_1 + 5m_2 + 20p\varepsilon + 6r + 2\psi r\big)\big)\Big)\Big]^{-1}. \end{aligned} \tag{B.16}$$

The desired bound on the switching period τ^* in Theorem 4.2 comes from the bound in Theorem 9.1 [70] such that

$$\tau < \tau* = \frac{c\gamma^3}{\ln\left[D\frac{(V_1 - V_0)}{\gamma^2}\right]} \tag{B.17}$$

Plugging the constants c (B.14), γ (B.12), D (B.15), V_0 (B.10), V_1 (B.11) into the

general expression (B.17) yields the final bound used in Theorem 4.2:

$$\begin{aligned}\tau < \tau* = \; & K^4|\delta^2\left(r-\tfrac{r}{K}\delta-m_1-m_2-6p\varepsilon\right)|^3\cdot\Big(64\psi^4\big(2\hat{a}_1\psi K+2a_2\psi K+Km_1+\\ & Km_2+6Kp\varepsilon+\psi r+Kr\big)^2\big(\tfrac{1}{K^2\psi^2}\big(6a_2^2\psi^2K^2+4\hat{a}_1^2\psi^2K^2+2K^2m_1^2+K^2m_2+\\ & 2K^2m_2^2+2p\varepsilon K^2+7p\varepsilon K^2m_1+5p\varepsilon K^2m_2+20p^2\varepsilon^2K^2+a_2\psi K^2\big(15m_1+\\ & \hat{a}_1\psi\left(4+m_1\right)+4m_2+17p\varepsilon+p\varepsilon m_1\big)+6\psi pKr\varepsilon+6p\varepsilon K^2r+2\psi p\varepsilon rK^2+\\ & 3\psi^2r^2+2\psi r^2K+K^2r^2+\hat{a}_1\psi K\big(3Km_1+16p\varepsilon K+5\psi r+3Kr\big)\big)+\tfrac{1}{K^2\psi^2}\cdot\\ & \big(6a_2^2\psi^2K^2+a_2\psi K^2\big(1+4m_2+4a_1^*\psi+17p\varepsilon+m_1\big(5+a_1^*\psi+p\varepsilon\big)\big)+3\psi^2r^2+\\ & \psi Kr\big(5a_1^*\psi+6p\varepsilon+2r\big)+K^2\big(2m_1^2+m_2+2m_2^2+2p\varepsilon+3a_1^*\psi m_1+7p\varepsilon m_1+\\ & 5p\varepsilon m_2+4(a_1^*)^2\psi^2+16a_1^*\psi p\varepsilon+20p^2\varepsilon^2+3a_1^*\psi r+6rp\varepsilon+2\psi rp\varepsilon+r^2\big)\big)\big)\Big)\cdot\\ & \ln\Big[8\psi^2\Big(12a_2^2\psi^2+4(a_1^*)^2\psi^2+4\hat{a}_1^2\psi^2+a_2\psi\big(\left(a_1^*\psi+\hat{a}_1\psi\right)\left(4+m_1\right)+2\big(1+\\ & 5m_1+4m_2+17p\varepsilon+m_1p\varepsilon\big)\big)+\tfrac{(a_1^*+\hat{a}_1)\psi}{K}\big(5\psi r+K\big(3m_1+16p\varepsilon+3r\big)\big)+\\ & 2\big(\tfrac{1}{K}\big(3\psi^2r^2+2\psi Kr\left(3p\varepsilon+r\right)+2m_1^2+m_2+2m_2^2+r^2+p\varepsilon\big(2+7m_1+\\ & 5m_2+20p\varepsilon+6r+2\psi r\big)\big)\Big)\tfrac{\frac{3}{2}\left(\psi^2-\delta\right)}{\delta^4\left(r-\frac{r}{K}\delta-m_1-m_2-6p\varepsilon\right)^2}\Big)\Big]^{-1},\end{aligned} \tag{B.18}$$

where once again $\psi = \frac{K}{4rm_2}\left(r+m_2\right)^2$ is the absorbing domain bounds (cf. (4.9)), $a_1^* = [1+\Delta a\cdot p]a_1$, and $\hat{a}_1 = [1+\Delta a]a_1$. Note that the bound τ^* is explicit in the parameter of the stochastic network. The size of the neighborhood U_0 used in Theorem 4.2 is given by $U_0 = V_0 + C_1$, where $V_0 = \frac{3}{2}\delta^2$ (cf. (B.10)) and C_1 is given in (B.16). The constant δ defines the required precision of synchronization and can be chosen arbitrarily.

This completes the calculation of the bounds are necessary to apply general theorem Theorem 9.1 [70] on the convergence near the ghost attractor in a stochastically switching dynamical system to formulate Theorem 4.2 for approximate synchronization in the stochastic ecological network (4.2).

$$
\begin{aligned}
\ddot{X} &= [f'(x_2,\dot{x}_2) - f'(x_1,\dot{x}_1)] - \left[g'(x_2,\dot{x}_2)y_2 + g(x_2)\dot{y}_2 - g'(x_1,\dot{x}_1)y_1 - g(x_1)\dot{y}_1\right] - 2p\varepsilon\dot{X} \\
\ddot{Y} &= [g'(x_2,\dot{x}_2)y_2 + g(x_2)\dot{y}_2 - g'(x_1,\dot{x}_1)y_1 - g(x_1)\dot{y}_1] - \left[h'(y_2,\dot{y}_2)z_2 + h(y_2)\dot{z}_2 - h'(y_1,\dot{y}_1)z_1 - \right. \\
&\quad \left. h(y_1)\dot{z}_1\right] - (m_1 + 2p\varepsilon)\,\dot{Y} \\
\ddot{Z} &= h'(y_2,\dot{y}_2)z_2 + h(y_2)\dot{z}_2 - h'(y_1,\dot{y}_1)z_1 - h(y_1)\dot{z}_1 - (m_2 + 2p\varepsilon)\,\dot{Z}.
\end{aligned}
\tag{B.19}
$$

Appendix C

THE SIGMOID MAP AND THE LYAPUNOV EXPONENT FOR STOCHASTICALLY COUPLED SIGMOID MAPS

C.1 Sigmoid map

The sigmoid map is described by the following equation:

$$S(x) = \frac{-\gamma\frac{x}{2} - \ln\left(1 + e^{-\gamma(x-0.5)}\right) + \ln\left(1 + e^{0.5\gamma}\right)}{-\frac{\gamma}{4} - \ln 2 + \ln\left(1 + e^{\gamma/2}\right)}, \tag{C.1a}$$

where γ is a parameter that controls the shape of the map. The map is constructed to be an endomorphism in the unit interval. Fig. C.1 shows the sigmoid map and its first derivative for a few selected values of the parameter γ.

For values of γ on the order of 1, the first derivative of S is approximately linear, similar to a logistic map with parameter equal to 4, see for example [30]. As γ increases, the curvature of S in the vicinity of $x = 0.5$ increases, and the map approaches the classical tent map, see for example [30]. Specifically, in the limit $\gamma \to \infty$, the sigmoid map can be approximated by the tent map

$$f(x) = \begin{cases} 2x, & x \leqslant 0.5 \\ 2(1-x), & x \geqslant 0.5 \end{cases} \tag{C.2}$$

and in the limit $\gamma \to 1$ we recover

$$4x(1-x), \tag{C.3}$$

the logistic map with parameter equal to 4.

From the time series of the sigmoid map for different values of γ, we can estimate the probability density function $\rho(x)$ associated with the chaotic dynamics. The positive Lyapunov exponents for each of these cases can be obtained from Fig. 5.2(top) for $d^\star = 0$. From simulation data over 100000 time steps and binning with a bin size of 0.05, we obtain the probability density functions in Fig. C.2. Therein, we also report closed form results for the tent ($\rho(x) = 1$) and the logistic map ($\rho(x) = 1/(\pi\sqrt{x(1-x)})$), see for example [30]. Numerical results confirm analytical predictions for $\gamma = 1$ and indicate close agreement between the sigmoid map and the tent map for $\gamma = 1000$. For intermediate values of γ, we observe a nonsymmetric probability density function with respect to $x = 0.5$.

C.2 Lyapunov exponent for stochastically coupled tent maps

Here, we present the derivation of the closed-form expression for the Lyapunov exponent of the stochastically coupled tent maps (5.27). By using the probability density function $\rho(x) = 1$, equation (5.23b) becomes

$$\lambda(m) = \int_0^1 \ln\left(\sum_{l=1}^{n} p_l Y_l(t,m)\right) dt, \tag{C.4}$$

where F is given by equation (C.2) and $Y_l(t,m)$ is defined in (5.24). For convenience, we introduce the 2^m subintervals of $[0,1]$ of length $\frac{1}{2^m}$: $\tau_1 = \left[0, \frac{1}{2^m}\right), \tau_2 = \left(\frac{1}{2^m}, \frac{1}{2^{m-1}}\right), \ldots, \tau_{2^m-1} = \left(\frac{2^m-1}{2^{m-1}}, \frac{2^m-1}{2^m}\right), \tau_{2^m} = \left(\frac{2^m-1}{2^m}, 1\right]$. These subintervals constitute a partition of the unit interval up to a set of measure zero, where $Y^l(t,m)$ is not uniquely defined as detailed below.

For each of these subintervals, we can determine the sequence of composite functions that is needed for calculating $Y_l(t,m)$ in the following way. For $t \in \tau_1$ we find $F^0(t) = t < \frac{1}{2^m}$. This quantity is less than 0.5, thereby from (5.27), we find $F^1(t) = 2F^0(t)$, which is, in turn, less than $2\frac{1}{2^m}$. The latter quantity is again less than 0.5 and the argument above can be iterated for any composite function up to the $(m-1)$-th order. As a result, within τ_1, $F'(F^i(t))$ will be equal to 2 for $i = 0, 1, \ldots, m-1$, and $Y_l(t,m)$ reduces to $(2-d_l)^{2m}$.

Following a similar line of arguments, we can study the sequence of composite functions

for $t \in \tau_2$. In this case, we find $F^i(t) < 0.5$ for $i = 0, 1, \ldots, m-2$ and $F^{m-1}(t) > 0.5$. Thus, $F'(F^i(t))$ will be equal to 2 for $i = 0, 1, \ldots, m-2$ and -2 for $i = m-1$, which imply that $Y_l(t, m) = (2 - d_l)^{2(m-1)}(2 + d_l)^2$. Note that this value is different from the value attained in τ_1, confirming that $Y_l(t, m)$ jumps between two contiguous subintervals.

By carrying out this procedure for all of the considered 2^m subintervals, we find that $Y_l(t, m)$ is constant in each subinterval and equal to one of the following values: $Y_l^{(0,m)} = (2 - d_l)^{2m}, Y_l^{(1,m)} = (2 - d_l)^{2(m-1)}(2 + d_l)^2, \ldots, Y_l^{(i,m)} = (2 - d_l)^{2(m-i)}(2 + d_l)^{2i}, \ldots, Y_l^{(m,m)} = (2 + d_l)^{2m}$. Each of these values occurs $\binom{m}{i}$ times, corresponding to the number of possible ways to obtain $(2 - d_l)^{2i}(2 + d_l)^{2(m-i)}$ from the product of m quantities each taking values in $\{(2 - d_l)^2, (2 + d_l)^2\}$.

By partitioning the integral in equation (C.4) in 2^m integrals over $\tau_1, \ldots, \tau_{2^m}$, we obtain

$$\lambda(m) = \sum_{i=1}^{2^m} \int_{\tau_i} \ln \left(\sum_{l=1}^{n} p_l Y_l(t, m) \right) dt = \frac{1}{2^m} \sum_{i=0}^{m} \binom{m}{i} \ln \left(\sum_{l=1}^{n} p_l Y_l^{(i,m)} \right), \tag{C.5}$$

which implies equation (5.27).

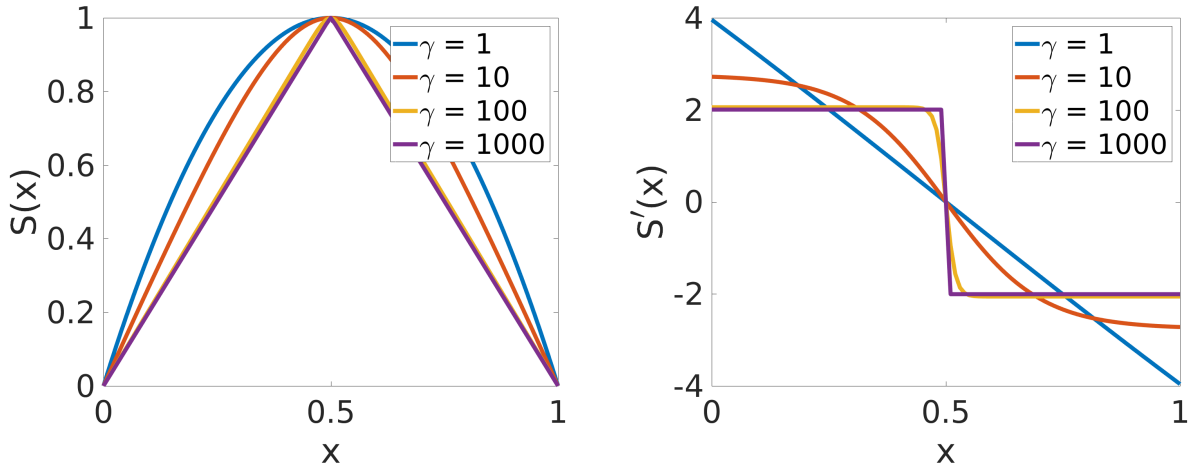

Figure C.1 **Sigmoid map (left) and its derivative (right) for different values of γ.**

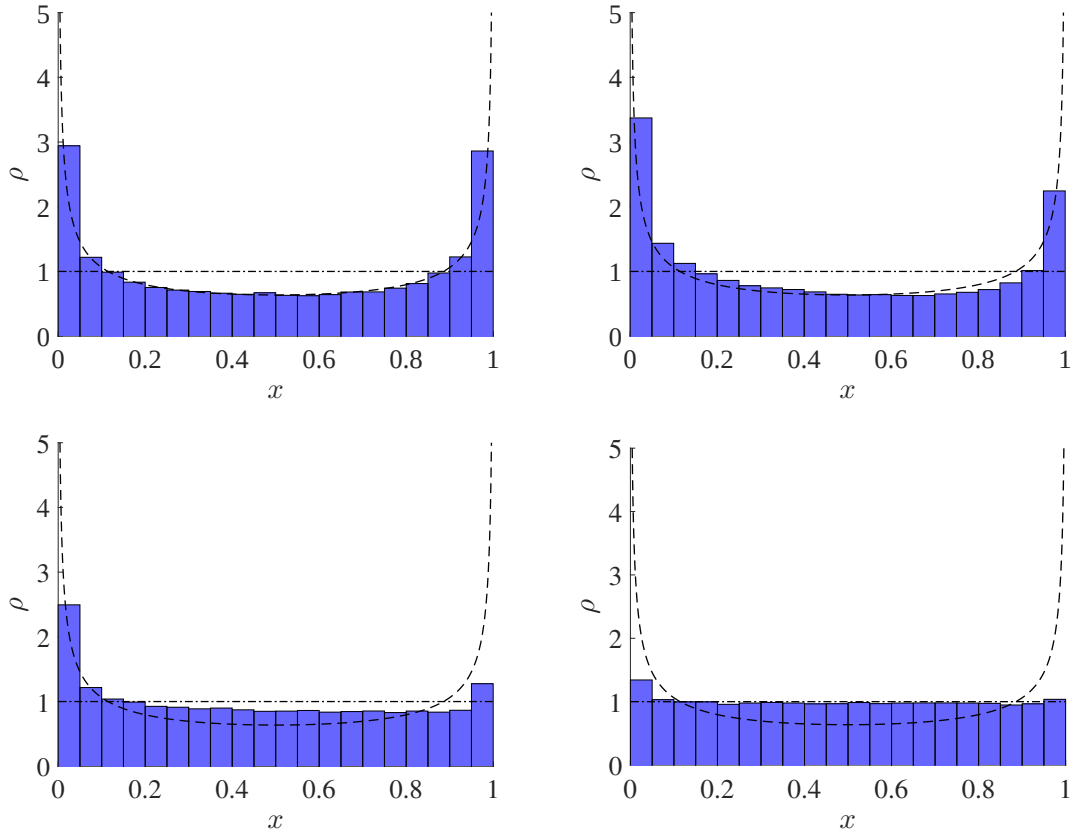

Figure C.2 **Asymmetric ergodic behavior of the sigmoid map.** Probability density functions of the sigmoid map (C.1a) for different values of the control parameter γ: (a) $\gamma = 1$, (b) $\gamma = 10$, (c) $\gamma = 100$, and (d) $\gamma = 1000$. Probability density function of the tent and logistic maps are shown as dot-dashed and dashed lines, respectively.

Appendix D

WINDOWS OF OPPORTUNITY FOR THE STABILITY OF JUMP LINEAR SYSTEMS: ALMOST SURE VERSUS MOMENT CONVERGENCE

In this appendix, we examine the role of the switching period on the stochastic stability of jump linear systems. More specifically, we consider a jump linear system in which the state matrix switches every m time steps randomly within a finite set of realizations, without a memory of past switching instances. Through the computation of the Lyapunov exponents, we study δ-moment and almost sure stability of the system. For scalar systems, we demonstrate that almost sure stability is independent of m, while δ-moment stability can be modulated through the selection of the switching period. For higher-dimensional problems, we discover a richer influence of m on stochastic stability, quantified in an almost sure or δ-moment sense. Through the detailed analysis of a two-dimensional problem, we illustrate the existence of a disconnected window of opportunity where the system becomes unstable, even though it switches between two asymptotically stable states.

This appendix represents submitted, but currently unpublished work [121].

D.1 Introduction

Assessing stochastic stability is a critical problem in the study of jump linear systems, with important applications in modeling biological systems, formulating hybrid control algorithms, and designing power electronics, see, for example, [**?**]. An excellent review of the history of research on stochastic stability of jump linear systems can be found in [56] . Rosembloom [134] was the first to study moment stability of jump linear systems and Bellman [11] was the first to tackle moment stability through Kronecker algebra. Kats and Krasovskii [85] and Bertram and Sarachick [23] put forward criteria based on Lyapunov's second method to study moment and almost sure stability.

Building on these seminal papers over sixty years back, several breakthroughs have been made in the study of stochastic stability of jump linear systems, summarized in a number of comprehensive books, doctoral dissertations, and review papers [89, 41, 88, 56, 98] While there is not a general consensus on the most desirable stability property for a jump linear system, almost sure stability seems to be the most useful criterion for practical applications and mean-square stability the simplest criterion to implement. Moment stability implies almost sure stability, but the converse is generally false, as shown by Kozin [88]. In an almost sure stability context, one seeks to ensure the stability of the system for any realization of the underlying stochastic process, with the exception of a set of measure zero. Moment stability, instead, pertains to the deterministic dynamics of the moments, with mean-square stability specifically referring to the second moment of the state.

In this appendix, we examine a specific class of jump linear systems in which the state matrix switches every $m \in \mathbb{Z}^+$ time steps, within a finite set of realizations, without a memory of past switching instances. As a result, in each time interval of length m, the state matrix is constant and the dynamics progresses analogously to a time-invariant system. Schur-stable matrices, whose spectrum is contained in the unit circle, will tend to steer the dynamics toward the origin, while unstable matrices will push the dynamics away from it. Every m time steps, the state matrix switches following an independent and identically distributed (i.i.d.) random process, drawing from state matrices. For these classes of jump linear systems, we seek to investigate the role of m on moment and almost sure stability.

This study is motivated by our previous work on the synchronization of coupled systems, which are intermittently coupled by a dynamic network that rewires without memory of its past at a constant switching period. Through the study of scalar chaotic discrete maps [61, 77] and chaotic continuous-time oscillators [79], we have unveiled a rich and often counterintuitive dependence of the stochastic stability of the synchronous solution on the switching period. More specifically, for chaotic tent maps, we have analytically demonstrated the existence of multiple, disconnected intervals of the switching period where the synchronous solution is mean-square stable [61]. For Rössler chaotic oscillators, we have com-

putationally studied almost sure stability and uncovered an equivalently rich dependence on the switching period, where synchronization in the switching network becomes stable even though it is unstable in the averaged/fast-switching network [79].

We use the name "windows of opportunity" to describe these intervals of the switching period where stochastic stability is attained. The characterization of these windows of opportunity for jump linear systems is the main objective of this appendix. By focusing on linear stochastic systems, we seek to gain insight into the determining factors for the occurrence of windows of opportunity, without potential confounds associated with nonlinearities. We focus on both moment and almost sure stability, bringing to light key differences between them for scalar and higher-dimensional jump linear systems.

The rest of this appendix is organized as follows. In Sec. D.2, we review key findings on the stochastic stability of jump linear systems, drawing upon the work of Fang, Feng, and Loparo [56, 53, 55]. In Sec. D.3, we present the main claims of this appendix by first focusing on scalar systems and then higher-dimensional problems. We study in detail a two-dimensional problem that allows for the derivation of closed-form results. The main conclusions of the study are summarized in Sec. D.4, together with an outlook of open research areas and potential lines of further inquiry.

D.2 Mathematical preliminaries

Here, we briefly review key concepts on the stability of jump linear systems from the classical work of Fang, Feng, and Loparo [53]. Consider a linear discrete-time system of the following form:

$$x_{k+1} = H(\sigma_k)x_k \tag{D.1}$$

where $k \in \mathbb{N}$ is the discrete time variable, $x_k \in \mathbb{R}^n$ is the state variable with n being a positive integer defining the dimension of the system, H is a real valued matrix function in $\mathbb{R}^{n\times n}$, and σ_k is a finite-state independent i.i.d. random process taking values in $\{1, \ldots, N\}$ with N being the number of state matrices and $p_1 \ldots, p_N$ their respective probability to occur.

For simplicity, we assume that the initial condition x_0 is a constant vector. This setup is a specialization of the general framework considered in [53], where σ_k could be a finite state, homogeneous Markov process.

Definition 2.1 in [53] can be restated as follows:

Definition D.1 *Let* $\Pr(\cdot)$ *and* $\mathsf{E}(\cdot)$ *indicate, respectively, probability and expectation with regard to the sigma-algebra induced by the i.i.d. process, and let* $\|\cdot\|$ *be a norm in* $\mathbb{R}^n$ *(for example, the Euclidean norm). The jump linear system in* (D.1) *is said to be*

1. *Asymptotically* δ*-moment stable, if for any* $x_0 \in \mathbb{R}^n$

$$\lim_{k\to\infty} \mathsf{E}(\|x_k\|^\delta) = 0 \tag{D.2}$$

   We speak of mean-square stability if $\delta = 2$*.*

2. *Exponentially* δ*-moment stable (*$\delta > 0$*), if for any* $x_0 \in \mathbb{R}^n$*, there exist* $\alpha, \beta > 0$ *such that*

$$\mathsf{E}(\|x_k\|^\delta) < \alpha\|x_0\|^\delta e^{-\beta k}, \quad k \in \mathbb{N} \tag{D.3}$$

   Similar to asymptotic stability, for $\delta = 2$*, we say that the system is mean-square exponentially stable.*

3. *Almost sure asymptotically stable, if for any* $x_o \in \mathbb{R}^n$*,*

$$\mathsf{P}(\lim_{k\to\infty} \|x_k\| = 0) = 1 \tag{D.4}$$

By adapting the claims in Theorem 4.1, Proposition 4.3, and Lemma 4.8 in [53][a], we formulate the following set of relationships between these notions of stability.

Proposition D.1 *Given the jump linear system in* (D.1) *and the stability notions in Definition D.1, the following relationships hold:*

1. *(Theorem 4.1) Asymptotic and exponential* δ*-moment stability are equivalent.*

[a]Some of these claims can also be found in [56], albeit in a less general form.

2. *(Proposition 4.3) Exponential δ-moment implies almost sure stability.*

3. *(Lemma 4.8) For any $0 < \delta_1 \leq \delta_2$, asymptotic δ_2-moment stability implies δ_1-moment stability*[b].

This Proposition supports our intuition that exponential and asymptotic moment stabilities are equivalent for jump linear systems, similar to classical time-invariant systems. Also, it clarifies that almost sure stability is the least conservative notion of stability and that the higher is the value of δ, the more conservative stability criteria are formulated.

To assess the stability of (D.1), we may examine the sign of the top Lyapunov exponent associated with the δ-moment or sample-path evolution. More specifically, if the limit exists [55], we define the following:

Definition D.2 *The top (or largest) sample-path Lyapunov exponent and the top δ-moment Lyapunov exponent of* (D.1) *are defined, respectively, as*

$$\lambda = \max_{x_0 \neq 0} \lim_{k\to\infty} \frac{1}{k} \log \|x_k\| = \lim_{k\to\infty} \frac{1}{k} \log \|H(\sigma_{k-1}) \cdots H(\sigma_0)\| \tag{D.5a}$$

$$g(\delta) = \max_{x_0 \neq 0} \lim_{k\to\infty} \frac{1}{k} \log \mathsf{E}\|x_k\|^\delta = \lim_{k\to\infty} \frac{1}{k} \log \mathsf{E}\|H(\sigma_{k-1}) \cdots H(\sigma_0)\|^\delta \tag{D.5b}$$

where the computation is independent of the norms used for vectors or matrices. If λ ($g(\delta)$) is negative, the system is almost sure (δ-moment) asymptotically stable and it is unstable otherwise – these claims also include infinitely large values of the Lyapunov exponents that would imply convergence in one time step.

Computing the top δ-moment Lyapunov exponents for $\delta \in \mathbb{R}^+$ can be undertaken by using the notion of generalized spectral radius studied in a general setting in [103]. For the more common case of mean-square stability, it is easy to verify the following:

$$g(2) = \log[\rho(\mathsf{E}(H(\sigma) \otimes H(\sigma)))] = \log \left[\rho \left(\sum_{j=1}^{N} p_j H(j) \otimes H(j) \right) \right] \tag{D.6}$$

[b] *Lemma 4.8 is an implementation of Jensen's inequality, and it specifically states that for any random variable ξ, the function $F(y) = \mathsf{E}(\|\xi\|^y)^{\frac{1}{y}}$ is nondecreasing in $\mathbb{R}^+$ whenever it is well defined. This is sufficient to prove our claim, which appears in a more general form as Theorem in 4.7 in [53].*

where $\rho(\cdot)$ is the spectral radius of a matrix and $\otimes$ is the Kronecker product [c].

Evaluating the top sample-path Lyapunov exponent is a much more challenging task [153]. If a closed-form result is available for $g(\delta)$ and all the state matrices are invertible, then one may consider applying Proposition 2.3 in [55], which posits that $\lambda = g'(0+)$ – corresponding to the derivative of $g(\delta)$ from above. Alternatively, one may advocate the law of large numbers to compute

$$\lambda = \lim_{k\to\infty} \frac{1}{k} \mathsf{E} \log \|H(\sigma_{k-1}) \cdots H(\sigma_0)\| \tag{D.7}$$

almost surely, from Lemma 4.5 in [53].

Very few closed-form results are presently available for nontrivial higher dimensional systems, whereby exact computations are typically restricted to scalar systems or commuting matrices. The seminal paper by Pincus [113] and later refinements in [94] have put forward analytical results for the case of binary switching between two 2×2 matrices with one of them being singular. More recently, tight bounds for binary switching between 2×2 "shear" hyperbolic matrices have been presented by [149], which also offer a meticulous overview of the state-of-the-art in the computation of Lyapunov exponents associated with random matrix products.

D.3 Windows of opportunity

Rather than switching between state matrices at every time step as in (D.1), we consider the more general case in which the same state matrix is retained for m consecutive time steps. By scaling the time variable, our problem becomes

$$x_{k+1} = \underbrace{H(\sigma_k) \cdots H(\sigma_k)}_{m} x_k = H^m(\sigma_k) x_k \tag{D.8}$$

[c] Equation (D.6) can be found by writing the Lyapunov equation for the second moment matrix $\mathsf{E}\left[x_k x_k^{\mathrm{T}}\right]$ where T indicates matrix transposition, see, for example, [**?**]

where we take the m-th power of each individual state matrix in one "scaled" time step. When $m = 1$, the problem is equivalent to (D.1).

D.3.1 Scalar systems

For a scalar system ($n = 1$), we can compute in closed-form the δ-moment Lyapunov exponent in (D.5b), which is simply given by

$$g(m, \delta) = \log \left[\sum_{j=1}^{N} p_j |H(j)|^{\delta m} \right] \tag{D.9}$$

with an explicit dependence on our control parameter m. δ-moment stability depends on the sign of $g(m, \delta)$, which is determined by the values of $|H(1)|, \ldots, |H(N)|$, the choice of δ, and the value of m. To examine this complex interplay, we evaluate the exponential of both sides of the previous equation, such that,

$$e^{g(m,\delta)} = \left[\sum_{j=1}^{N} p_j |H(j)|^{\delta m} \right] \tag{D.10}$$

Extending the analysis in [**?**] for $\delta = 2$ to an arbitrary, positive, value of δ, we define the right-hand-side of (D.10) as $q(\mu)$ where the nonnegative real variable μ takes the place of the integer m. It is easy to verify that $q(0) = 1$ and $q''(\mu) \geq 0$ in $\mathbb{R}^+$, where a prime indicates derivative with respect to the argument.

Therefore, $q(\mu)$ is a concave function which can attain values below 1 only if $q'(0) < 0$, that is,

$$\sum_{j=1}^{N} p_j \log |H(j)| < 0 \tag{D.11}$$

which requires that at least one of the individual realization $H(1), \ldots, H(N)$ is Schur-stable, that is, less than one in magnitude. If this condition is not verified, then no choice of m can ensure the asymptotic stability of the system.

On the other hand, if condition (D.11) is verified, we may have a window of δ-moment asymptotic stability. Specifically, if all the individual realization $H(1), \ldots, H(N)$ are Schur-

stable, then $\lim_{\mu\to\infty} q(\mu) = 0$ and (D.8) is asymptotically δ-moment stable for any value of m. If at least one of the individual realizations $H(1), \ldots, H(N)$ is unstable, then $\lim_{\mu\to\infty} q(\mu) = \infty$ and (D.8) is δ-moment asymptotically stable for m between 1 and $\overline{m} = \lfloor\overline{\mu}\rfloor$, such that $q(\overline{\mu}) = 1$ with $\overline{\mu} > 0$. This set might be empty if $\overline{m}$ is zero or one, however, for sufficiently small values of δ, we should expect to always identify a window of opportunity for weak stochastic stability. If the system is not δ-moment asymptotically stable for $m = 1$, there is no value of m that can ensure δ-moment asymptotic stability.

With respect to almost sure stability, we can compute the derivative of (D.9) with respect to δ, such that

$$\lambda(m) = m \sum_{j=1}^{N} p_j \log |H(j)| \tag{D.12}$$

which poses a condition analogous to (D.11). This result indicates that almost sure stability is independent of m, in contrast with δ-moment stability that can be hampered or improved by increasing the value of m. This surprising result is unique to the scalar case and one should not attempt at generalizing it to higher-dimensional systems, as we will make clear in what follows. Through the detailed study of an exemplary system, we will in fact demonstrate the existence of nontrivial windows of opportunity for both almost sure and mean-square stability.

We can summarize the previous analysis in the following proposition.

Proposition D.2 *Consider the scalar jump linear system in* (D.8)*. The sign of the sample path Lyapunov exponent is independent of m, such that sample path stability is not influenced by the switching period. If the system is almost sure asymptotically stable, then it is δ-moment asymptotically stable for any value of m if the individual realizations $H(1), \ldots, H(N)$ are all Schur-stable* [d]*. If one of the realizations is unstable, then for sufficiently large values of m, δ-moment asymptotic stability is lost. Specifically, the system is δ-moment asymptotically stable for $m \in \mathcal{W}_{\text{as}} = \{1, \ldots, \lfloor\overline{\mu}\rfloor\}$, with $\overline{\mu}$ being the nonzero solution of $g(\overline{\mu}, \delta) = 0$ given by* (D.9) *for $\mu \in \mathbb{R}^+$.*

[d] This claim is true even if some of the realization have unitary magnitude, provided there is at least one which is Schur-stable.

As an example, consider the two-state process ($N = 2$) with $H(1) = \frac{5}{8}$ and $H(2) = \frac{9}{8}$ of equal probability $p_1 = p_2 = \frac{1}{2}$. The sample-path Lyapunov exponent in (D.12) is $\lambda \simeq -0.176m$, such that the system is almost sure asymptotically stable for any switching period, that is, $\mathcal{W}_{\text{as}} = \mathbb{Z}^+$. The δ-moment Lyapunov exponent in (D.9) is $\log\left(2^{-3\delta m-1}5^{\delta m} + 2^{-3\delta m-1}9^{\delta m}\right)$, such that the system is mean-square asymptotically stable only in the narrow window $\mathcal{W}_{\text{ms}} = \{1, 2\}$.

Based on prior literature on fast-switching stability of continuous systems [**? ? ?**], one may be tempted to infer the stability of the jump linear system for $m = 1$ from the average system, whose state-matrix is $\mathsf{E}[H(\sigma_k)]$. However, this is incorrect, as pointed out in [**?**] in the context of mean-square stability of scalar maps.

First, stability of the average system does not imply stability of the jump linear system. As an example, consider the two-state process with $H(1) = 2$ and $H(2) = -2$ of equal probability $p_1 = p_2 = \frac{1}{2}$. The average system allows to reach the origin in a single time step, while the sample-path Lyapunov exponent in (D.12) is $\log 2$, such that the system is not almost sure (or δ-moment) asymptotically stable. Second, lack of stability of the average system does not prevent the jump system to be stable. As an example, consider again a two-state process with $H(1) = \frac{15}{8}$ and $H(2) = \frac{3}{8}$ of equal probability $p_1 = p_2 = \frac{1}{2}$. The average system is unstable with Lyapunov exponent of $\log \frac{9}{8}$, while the system is almost sure asymptotically stable with sample-path Lyapunov exponent in (D.12) equal to $\frac{1}{2}\log \frac{45}{64}$ and δ-moment asymptotically stable for $\delta < 0.562$ with δ-moment Lyapunov exponent in (D.9) equal to $\log\left[\frac{1}{2}\left(\frac{15}{8}\right)^{\delta} + \frac{1}{2}\left(\frac{3}{8}\right)^{\delta}\right]$.

D.3.2 Higher-dimensional systems

For n larger than one and state matrices that do not commute, we cannot expect an equivalent case to the scalar system analyzed above. More specifically, the notions that almost sure asymptotic stability is independent of m and that δ-moment stability is restricted to a single window in m that must start from $m = 1$ are both invalid.

We illustrate the highly nontrivial nature of the problem through the analysis of a

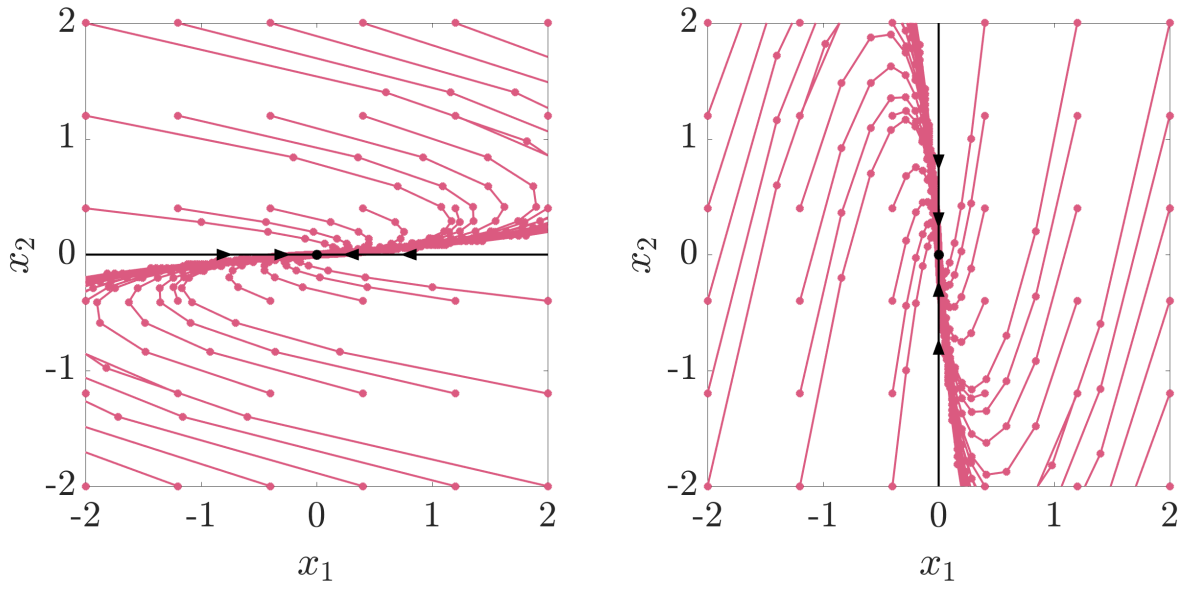

Figure D.1 Phase portraits for the state matrices $H(1)$ (left) and $H(2)$ (right) in (D.13) for $a = \frac{7}{10}$. Temporally-adjacent states are connected for ease of illustration. Trajectories converge to the stable fixed point at the origin along the eigenvector (black line in each panel) in the direction of the black arrows.

two-dimensional ($n = 2$) example. Specifically, we consider a two-state process

$$H(1) = \begin{bmatrix} a & 1 \\ 0 & a \end{bmatrix}, \quad H(2) = \begin{bmatrix} a & 0 \\ -1 & a \end{bmatrix} \tag{D.13}$$

where $0 < a < 1$ and $p_1 = p_2 = \frac{1}{2}$. In this case, each of the realization is Schur-stable as the spectral radius of each matrix is $a < 1$, but the coupled stochastic dynamics will reveal a complex dependence on m. Figure D.1 illustrates the evolution associated with each of the state matrices for a selected value of a.

We start the analysis by examining mean-square stability through the top second-moment Lyapunov exponent in (D.6), which is equivalent to the computation of the spectral

m	1	2	3	4	5	6	7	8	9	10
$g(m,2)$	-0.010	0.199	0.181	-0.001	-0.289	-0.649	-1.062	-1.512	-1.993	-2.498
Prop. D.3 - 1 norm	N/A	N/A	N/A	N/A	N/A	N/A	N/A	Yes	Yes	Yes
Prop. D.3 - 2 norm	N/A	N/A	N/A	N/A	N/A	N/A	N/A	Yes	Yes	Yes
Prop. D.3 - ∞ norm	N/A	N/A	N/A	N/A	N/A	N/A	N/A	Yes	Yes	Yes
$\lambda(m)$	-0.111	0.036	-0.080	-0.332	-0.529	-0.789	-1.049	-1.420	-1.702	-1.947
Prop. D.4 - 1 norm	N/A	N/A	N/A	N/A	N/A	N/A	Yes	Yes	Yes	Yes
Prop. D.4 - 2 norm	N/A	N/A	N/A	N/A	N/A	N/A	Yes	Yes	Yes	Yes
Prop. D.4 - ∞ norm	N/A	N/A	N/A	N/A	N/A	N/A	Yes	Yes	Yes	Yes

Table D.1 Analysis of the problem in (D.13) with $p_1 = p_2 = \frac{1}{2}$, $a = \frac{7}{10}$. Each column shows results for a different value of the switching period m and each row depicts predictions of the top mean-square and sample path Lyapunov exponents, along with the claims about stability from the proposed sufficient conditions. "N/A" indicates that the sufficient condition is not applicable, while "Yes" means that asymptotic stability can be inferred from the sufficient condition.

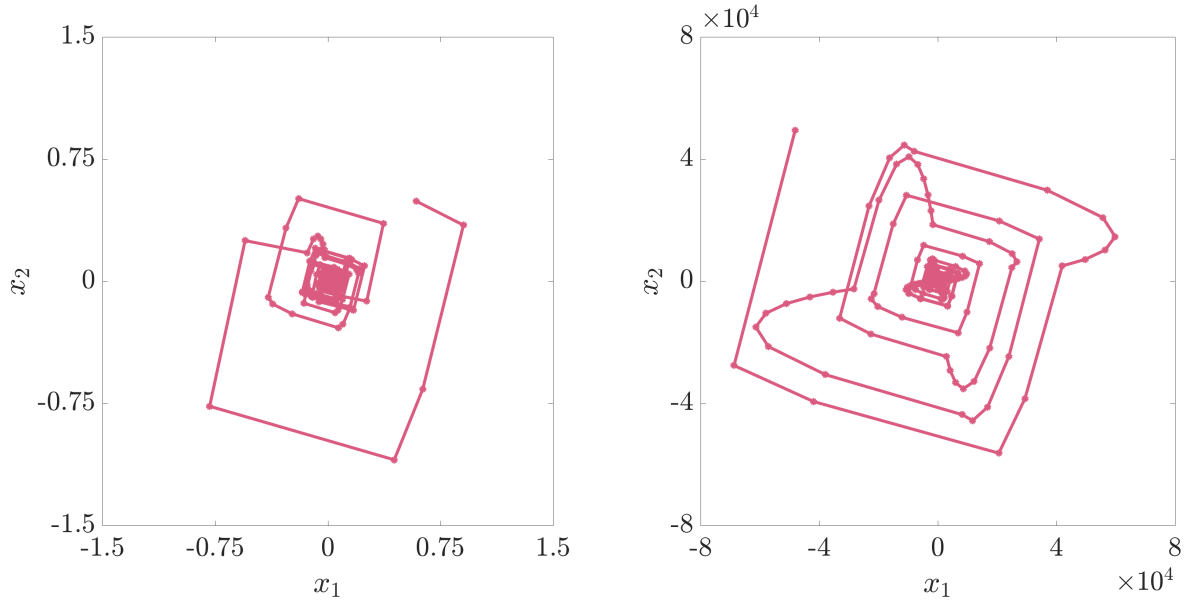

Figure D.2 Trajectories of the switching system (D.1) with state matrices $H(1)$ and $H(2)$ as in (D.13) with parameter $a = \frac{7}{10}$ for switching periods $m = 1$ (left) and $m = 2$ (right). The switching system converges to the fixed point at the origin when switching is fast (left) and diverges to infinity for intermediate switching periods (right).

radius of the following 4×4 matrix:

$$\frac{1}{2}(H(1) \otimes H(1) + H(2) \otimes H(2)) = a^{2m} \begin{bmatrix} 1 & \frac{1}{2}\frac{m}{a} & \frac{1}{2}\frac{m}{a} & \frac{1}{2}\frac{m^2}{a^2} \\ -\frac{1}{2}\frac{m}{a} & 1 & 0 & \frac{1}{2}\frac{m}{a} \\ -\frac{1}{2}\frac{m}{a} & 0 & 1 & \frac{1}{2}\frac{m}{a} \\ \frac{1}{2}\frac{m^2}{a^2} & -\frac{1}{2}\frac{m}{a} & -\frac{1}{2}\frac{m}{a} & 1 \end{bmatrix} \tag{D.14}$$

Through simple algebra, we can calculate the four eigenvalues of this matrix and determine a general form for the spectral radius, such that the top mean-square Lyapunov exponent is

$$g(m, 2) = \log \left[a^{2m} \left(1 + \frac{1}{2}\frac{m^2}{a^2} \right) \right] \tag{D.15}$$

For $m = 1$, the spectral radius of the matrix is simply $a^2 + \frac{1}{2}$, which indicates the possibility of attaining unstable mean-square dynamics for $a > \frac{1}{\sqrt{2}}$, albeit each of the individual matrices is asymptotically stable. For very large values of m the matrix approaches the zero matrix, such that the large switching periods will lead to mean-square asymptotic stability. For intermediate values of m, depending on the value of a, the system may be stable or unstable. More specifically, from the analysis of the function, we discover that for $a > \frac{1}{\sqrt{2}}$, the system is unstable for m ranging from 1 to a given value $\overline{m}$ (determined by searching for nonzero roots of (D.15)) and asymptotically stable for larger values of m. On the other hand, for $a < \frac{1}{\sqrt{2}}$, we have a richer landscape, whereby: for $a < 0.642$, the system is asymptotically stable for every choice of m; for $0.642 < a < 0.670$, the system is asymptotically stable for every value of m except for $m = 2$; for $0.670 < a < 0.700$, the system is asymptotically stable for every value of m except for $m = 2$ and 3; and for $0.700 < a < \frac{1}{\sqrt{2}}$, the system is asymptotically stable for every value of m except for $m = 2$, 3, and 4 (see Fig. D.2). In Tab. D.1, we report the numerical values of the top mean-square Lyapunov exponent for $a = \frac{7}{10}$, for which we have a window of opportunity equal to $\mathcal{W}_{\text{ms}} = \mathbb{Z}^+ / \{2, 3\}$.

Next, we evaluate the top sample path Lyapunov exponent for the same two-dimensional system (Fig. D.3). The computation is performed numerically by drawing $\left\lfloor \frac{5000}{m} \right\rfloor$ realizations

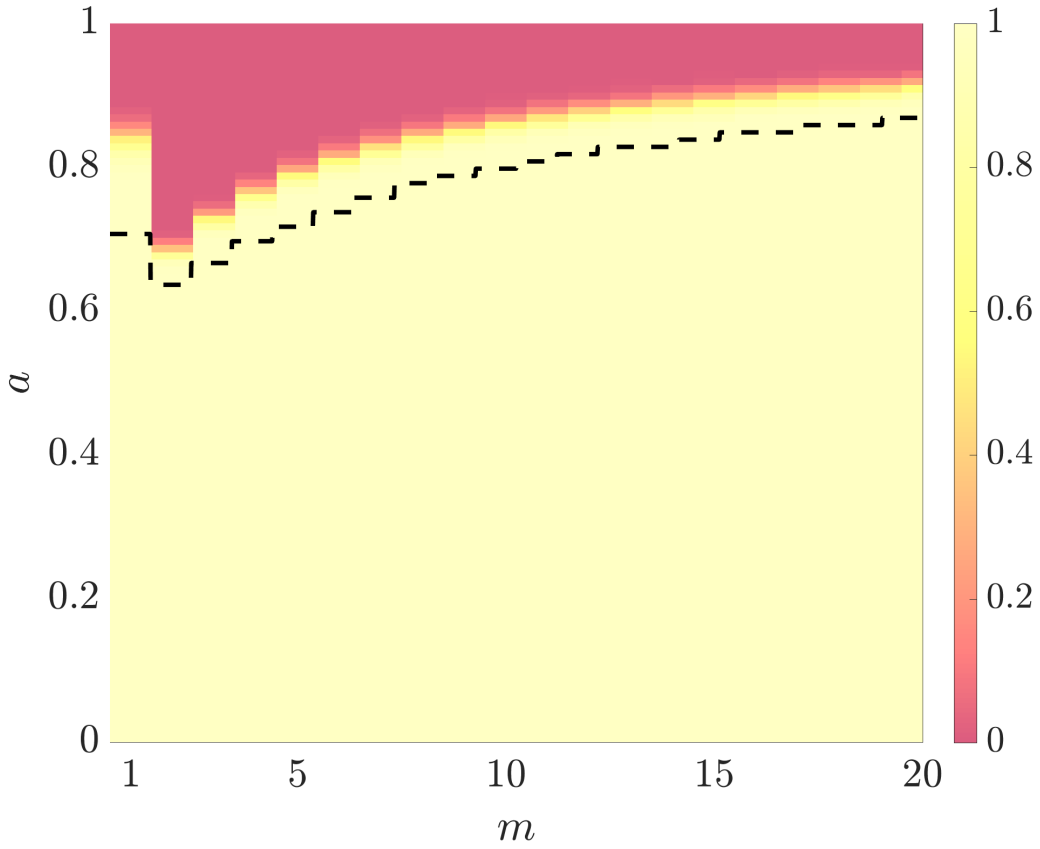

Figure D.3 Probability that the sample path Lyapunov exponent, λ, is negative as a function of the parameter a and switching period m. Probability is based on 1000 trials, with light yellow indicating a probability of stability (negative Lyapunov exponent) of 1 and pink indicating a probability of 0. The dashed black curve gives the boundary for which the Lyapunov exponent for mean square stability changes sign. Each realization is 500 iterates long.

of the state matrix, taking their product, and evaluating the Lyapunov exponent through (D.7) using the Euclidean norm. We average the last 10% of the samples to mitigate the effect of the initial transient. For $a = \frac{7}{10}$, we find that the system is almost sure asymptotically stable for every value of m, except of $m = 2$ when it loses stability, as shown in Tab. D.1, such that $\mathcal{W}_{\text{as}} = \mathbb{Z}^+/\{2\}$. This finding is in agreement with Proposition D.2, in that almost sure stability is a less conservative criterion than mean square stability. While the form of the matrices considered herein is similar to [149], their bounds are only applicable to the case $a < \frac{1}{2}$, which does not seem to lead to interesting landscape for almost sure stability.

In our example, the system switches between two stable degenerate nodes with a repeated eigenvalue a and one linearly independent eigenvector. As a result, the trajectories of either system determined by $H(1)$ or $H(2)$ are tangent to the eigenvector and curve around to the opposite direction (see Fig. D.1). Therefore, each trajectory can increase its relative distance from the origin before reaching the turning point where it starts approaching the stable fixed point. This property suggests a mechanism for the trajectory of the switching system to escape to infinity, provided that the switching frequency lies within the window of opportunity. More specifically, when switching is slow, the trajectories converge to the fixed point along the paths of either of the state matrices. When switching is fast, the trajectories converge along the path of the average system (obtained by replacing the switching state matrices with their expectation), see Fig. D.2 (left). Lastly, when switching is intermediate, the trajectories tend to evolve along the paths in either state that move *away* from the fixed point, by virtue of the single eigenvector in the system. This enables the system to spiral away from the origin toward infinity, see Fig. D.2 (right). A similar phenomenon was observed in a switching continuous-time linear system in a different setting where the system switches at exponential times between a collection of different matrices [91].

In general, it is difficult to provide necessary and sufficient conditions for stochastic stability of higher dimensional systems due to the complexity of evaluating the spectrum of a large matrix associated with mean-square stability or the application of the law of large numbers for almost sure stability. A trivial result is obtained if all the individual

state matrices are Schur-stable. In this case, for sufficiently large values of m, each of the summands in (D.6) will asymptotically approach zero and the spectral radius of the matrix will tend to zero accordingly. As a consequence, the system will be mean-square stable for large switching periods m. In general, stability may also be possible for unstable state matrices and a number of sufficient conditions might be established from the application of classical spectral bounding techniques.

For example, a sufficient condition for mean square stability can be derived by bounding the spectral radius of the matrix in (D.6) using classical norm bounds. More specifically, for a p-norm, we have that $\rho(A) \leq \| A \|$ for any matrix $A \in \mathbb{R}^{n \times n}$. By applying the triangular inequality and recalling that the norm of the Kronecker product of two matrices is equal to the product of the norms, we establish the following result.

Proposition D.3 *The jump linear system in* (D.8) *is mean-square asymptotically stable if for some p-norm, the following inequality holds*

$$\sum_{j=1}^{N} p_j \| H^m(j) \|^2 < 1 \tag{D.16}$$

Note that for $m = 1$ and the Euclidean norm, this is equivalent to the second statement in Theorem 2.5 of [56]. Also, the power m could be brought out of the norm leading to a more conservative bound, which is, however, simpler to implement.

For almost sure asymptotic stability, we can directly apply Theorem 2.2 of [56], which for the case at hand will read as follows.

Proposition D.4 *The jump linear system in* (D.8) *is almost sure asymptotically stable if for some matrix norm, satisfying the submultiplicative property, the following inequality holds*

$$\prod_{j=1}^{N} \| H^m(j) \|^{p_j} < 1 \tag{D.17}$$

The Theorem is a direct application of Young's inequality to the right hand side of (D.7).

Tab. D.1 illustrates the application of these conservative bounds for our exemplary problem, for which all of these bounds take a compact form that is easy to check for different

values of m. In this example, varying the norm does not influence the tightness of the lower bound, whereby for the three considered norms, we find that mean-square asymptotic stability is attained for m larger than 7, while almost sure asymptotic stability is reached for m larger than 6. While these predictions are on the same order of magnitude of exact computations, they do not assist in identifying the instability region for lower values of m, thereby challenging the identification of disjoint windows of opportunity.

D.4 Conclusions

In this appendix, we have studied the stochastic stability of a class of jump linear system, where the state matrix retains the same value for m consecutive time steps, before switching according to a finite-state i.i.d. process. Through a detailed analytical treatment of the problem, we have demonstrated a complex dependence of stochastic stability on the switching period m. Changing the dimension of the system and the lens through which stability is examined has a remarkable effect on the existence, extent, and topology of windows of opportunity for the stability of the stability of the system.

The causes for the rich dependence of stochastic stability on the switching period are yet to be fully understood. Particularly elusive and intriguing is the effect of the switching period on almost sure asymptotic stability. Our intuition suggests that increasing the switching period would automatically enhance almost sure stability, by reducing the range of matrix products on which we should enforce the top Lyapunov exponent to be negative. In other words, one may expect that if the system is almost sure asymptotically stable for a given m, then it should remain almost sure asymptotically stable for any larger, multiple, value of m.

However, this is not the case of higher-dimensional systems, where we have shown that a system may be asymptotically stable for $m = 1$ but not for $m = 2$ and again be asymptotically stable for any larger switching period. While we have offered a qualitative explanation of this phenomenon, its rigorous, quantitative justification remains a subject of future study. It is likely that this phenomenon is grounded in the same rationale that underlies the almost sure stability of a jump system switching between matrices that may

not be stable. Specifically, in our two-dimensional example, it is tenable to hypothesize that for m larger than 2, the repetitive occurrence of multiple product of the same state matrices will cause a stabilizing countereffect, against the destabilizing effect elicited by the second order powers of the state matrices.

To further exacerbate the complexity of the problem, we have found that for scalar systems almost sure asymptotically stability is independent of the switching period, suggesting that windows of opportunity do not exist in an almost sure sense for scalar systems. An equivalent claim could be formulated for higher-dimensional systems with a commuting structure, suggesting that the existence of windows of opportunity in an almost sure sense is associated with switching between different modes of the system.

Beyond the need for further research to illuminate the causes of windows of opportunity, especially in an almost sure sense, we envision future work along two main thrusts. On the one hand, we should seek to expand on the theoretical framework to expand on its practical significance toward the analysis and design of switched systems. For example, it is viable to incorporate memory effects through a Markovian switching process, contemplate the possibility of time-varying dynamics, and include stochastic perturbations. On the other hand, future endeavor may attempt at refining the mathematical basis of the present appendix, by extending the bounds for the top Lyapunov exponent of [149] to non-hyperbolic matrices and establishing tight bounds that can be used for the determination of windows of opportunity for arbitrary jump linear systems.